DEVELOPMENT OF NOVEL THERMAL ANALYSIS TECHNIQUES FOR CHARACTERIZATION OF SALT BASED PHASE CHANGE MATERIALS FOR THERMAL ENERGY STORAGE APPLICATIONS

Thesis

Submitted in partial fulfillment of the requirements for the degree of

DOCTOR OF PHILOSOPHY

by

SWATI AGARWALA
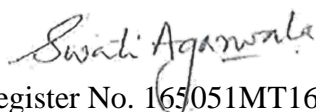

DEPARTMENT OF METALLURGICAL AND MATERIALS ENGINEERING

NATIONAL INSTITUTE OF TECHNOLOGY KARNATAKA,

SURATHKAL, MANGALORE – 575025

DECEMBER, 2021

D E C L A R A T I O N

By the Ph.D. Research Scholar

I hereby *declare* that the Research Thesis titled **"DEVELOPMENT OF NOVEL THERMAL ANALYSIS TECHNIQUES FOR CHARACTERIZATION OF SALT BASED PHASE CHANGE MATERIALS FOR THERMAL ENERGY STORAGE APPLICATIONS"** which is being submitted to the National Institute of Technology Karnataka, Surathkal in partial fulfilment of the requirements for the award of the Degree of **Doctor of Philosophy** in **Metallurgical and Materials Engineering** is a *bonafide report of the research work carried out by me*. The material contained in this Research Thesis has not been submitted to any University or Institution for the award of any degree.

Register No. 165051MT16F08,

SWATI AGARWALA

Department of Metallurgical and Materials Engineering

Place: NITK-Surathkal

Date:07/12/2021

CERTIFICATE

This is to *certify* that the Research Thesis titled **"DEVELOPMENT OF NOVEL THERMAL ANALYSIS TECHNIQUES FOR CHARACTERIZATION OF SALT BASED PHASE CHANGE MATERIALS FOR THERMAL ENERGY STORAGE APPLICATIONS"** submitted by **Ms. SWATI AGARWALA, (Register Number: 165051MT16F08)** as the record of the research work carried out by her, is *accepted as the Research Thesis submission* in partial fulfillment of the requirements for the award of the degree of **Doctor of Philosophy.**

Dr. K. Narayan Prabhu

Research Guide

(Signature with Date and Seal)

Chairman - DRPC

(Signature with Date and Seal)

ACKNOWLEDGEMENTS

ABSTRACT

Solar energy storage technologies have proved to be promising in terms of providing an uninterrupted power supply. Latent heat thermal energy storage systems in the form of salt phase change materials have been successfully used in concentrated solar plants for energy storage applications due to their superior energy storage parameters and functionalities.

In the present work, to characterize the salt phase change materials, the development, suitability, and reliability of a characterization method devoid of the limitations of the conventional thermal characterization techniques have been researched and proposed. A new approach based on the solution to inverse heat conduction problem for assessing solidification parameters of phase change materials (PCMs) salts in steel mold with furnace cooling has been proposed. The method estimates the steel mold -salt interfacial heat flux, and it is used to calculate the latent heat and phase change parameters of salt PCMs using calorimetry-based energy balance equations. This method is more accurate than the conventional Computer-Aided Cooling Curve Analysis (CACCA) techniques. It eliminates the drawbacks of baseline fitting calculations and errors introduced due to the improper selection of solidification points. Pure Salt PCMs such as potassium nitrate (KNO_3) and solar salt mixture of 60 wt% $NaNO_3$ and 40 wt% KNO_3 were used for the validation of this technique in the work. The solidification parameters such as rate of cooling, time taken for solidification and latent heat of the PCMs were determined and were found to be in close accordance with the reported literature data. A quantitative method for this determination of phase change parameters of salt-based PCMs has also been proposed. This technique involves estimating mold-salt interfacial heat flux by solving Fourier's law of heat conduction within the salt and using it to calculate the phase change enthalpy of salt PCMs. Pure salt PCMs such as potassium nitrate (KNO_3), sodium nitrate ($NaNO_3$)), and solar salt mixture (60wt.%$NaNO_3$+40wt.%KNO_3) were used for validation of this technique

Further, the effects of the addition of MWCNT carbon-based nanostructures on thermal energy storage (TES) parameters of lithium-based eutectic binary, ternary and quaternary salts were investigated. The addition of nanoparticles showed no effect on the solidification time and temperatures of the PCMs. In binary and ternary salts, lower concentrations of nanoparticles showed a positive impact on the TES parameters. LiK and LiT with 0.1% MWCNT showed an enhancement in the latent heat values of 27.6% and 19.28% respectively. However, the effects were limited at higher MWCNT weight concentrations.

It was observed that the addition of nanoparticles had no significant effect on the TES parameters of the quaternary salts.

In addition, the micrographic studies to analyze the agglomeration at higher concentrations of nanoparticles and wettability studies were also performed.

Contents:

List of Figures:

List of Tables:

Abbreviations:

TES	Thermal Energy Storage
CSP	Concentrated solar plants
HTF	Heat transfer fluid
SHC	Specific heat capacity
LHS	Latent heat storage
PCM	Phase change materials
LHTES	Latent heat thermal energy storage systems
SHTES	Sensible heat thermal energy storage systems
CFLR	Compact linear Fresnel reflector
MTSA	Multi tower solar array
SEM	Scanning electron microscopy
DSC	Differential scanning calorimetry
TGA	Thermogravimetric analysis
NePCM	Nanoenhanced phase change materials
MWCNT	Multi-walled carbon nanotubes
CNT	Carbon nanotubes
CNF	Carbon nanofibers
SWCNT	Single-walled carbon nanotubes
FTIR	Fourier transform infrared spectroscopy
EG	Expanded graphite
NG	Nano Graphite
EDAX	Energy dispersive X ray analysis
Hf-DSC	Heat flux differential scanning calorimetry
m-DSC	Modulated differential scanning calorimetry
CACCA	Computer-aided cooling curve analysis
FDC	First derivative curve
Z_C	Zero curve or baseline
BL_f	Fourier baseline
LCOE	Levelised cost of electricity
IHCP	Inverse heat conduction problem
SS	Stainless steel

Nomenclature:

A   Heat transfer area (m^2)

B(t)   Temperature distribution at the outer surface of the mold

c_v Specific heat at constant volume

c_p Specific heat capacity (J/kg K)

c_{ps} Specific heat capacity in solid-state (J/kg K)

c_{pl} Specific heat capacity in liquid state (J/kg K)

c_{pavg} Average Specific heat capacity (J/kg K)

c_{peff} Effective Specific heat capacity (J/kg K)

dT /dt   Cooling rate (°C/s)

dT /dr   Thermal gradient in the radial direction

D   Diameter of the mold (m)

e   Thermal effusivity

E1   Liquidus point

E2   Solidus point

f_s Fraction solidified

h   Heat transfer coefficient (W/m^2K)

H'   Height of the mold (m)

k   Thermal conductivity (W/m K)

k_{avg} Average Thermal conductivity (W/m K)

l   Iteration number

L   Thickness of the mold (m)

L'	Length of the mold (m)
L_1	Position of the T3 thermocouple (m)
m	Mass of the sample (kg)
Mo	Mold
nf	Nanofluid
np	Nanoparticle
ns	Nanolayer region
q	Heat flux (W/m^2)
q_{M+1}	Heat flux at any future time step (W/m^2)
Q	Net heat liberated from the sample into the mold
Q'	Heat released during solidification
Q_{inst}	The rate of heat liberated during solidification
Q_{total}	Total heat liberated during the phase change
$\Delta Q_{sensible}$	Sensible heat stored
ΔQ_{PCM}, H, H_f	Phase change enthalpy/latent heat
R1 and R2	Thermocouple position at two different radii (m)
r	Radius of the mold (m)
r	Number of future time temperature +1
s	Base salt
S	Sample
t	Time (s)
t_s	Time corresponding to the start of solidification (s)
t_e	Time corresponding to the end of solidification(s)

ts'	Time corresponding to the start of solidification temperature +5 (s)
te'	Time corresponding to the end of solidification temperature -5 (s)
T	Sample temperature (°C)
T_i	Initial temperature (°C)
T_{n+i}	Calculated temperature at a particular time step
T_2, T_s	Temperature corresponding to the end of solidification (°C)
T_1, T_l	Temperature corresponding to the start of solidification (°C)
T1	Temperature of the centre thermocouple (°C)
T2	Temperature of the thermocouple at 2mm from outer surface of the mold (°C)
T3	Temperature of the thermocouple at 2mm from inner surface of the mold (°C)
T_0	Ambient temperature (°C)
T_m	Melting temperature (°C)
ΔT	Small temperature interval
U	Overall heat transfer coefficient
W	Mass fraction
Y(t)	Measured thermocouple temperature at L1 position
Y_{n+i}	Measured temperature at a particular time step
α	Thermal diffusivity (W/m^2)
αl	Thermal diffusivity in liquid state (W/m^2)
αs	Thermal diffusivity in solid state (W/m^2)
α_{avg}	Average Thermal diffusivity (W/m^2)
$\Delta \theta$	Time step for heat flux
Δt	Time step for temperature

ρ	Density (kg/m^3)
ϵ	A very small value
φ	Sensitivity coefficient

Chapter 1 INTRODUCTION

Significant progress and achievements have been made in science, engineering, and technology since the industrial revolution of the 18th century. This growth has been accelerated by using fossil-based energy resources; however, there is a minimal supply of these resources. Due to this growth and excess demand, fossil energy resources are depleted at a rapid rate. The by-product of the combustion of these fossil fuels is let into the atmosphere resulting in environmental problems like air pollution and global warming.

Environmental pollution and the shortage of energy are the major global issues that need to be sorted out urgently. This can only be achieved by developing renewable energy sources, conservation of energy, and reduction of exhaust emissions. Renewable energy resources include solar energy, hydro energy, wind energy, and many others. These energy sources will completely take over the energy sector soon by replacing fossil fuels due to their unlimited energy supply and environmentally safe nature. Renewable energy sources are intermittent. Once these energy resources take over the energy sector, this limitation will adversely affect the efficiency and stability of the energy system. Therefore, sources with continuous energy supply which meet the growing energy demand are required. However, the wastage of energy from these renewable sources due to their surplus supply at a particular time also needs to be looked into while designing the thermal energy storage (TES) system.

TES technology is an effective way to increase the energy flexibility and efficiency of the energy system by regulating the energy supply and demand. It is just like creating a new energy resource. TES system is a fast-growing field of innovation and research in recent times. TES technology has been the center of attraction for many research studies due to its remarkable behavior of heat storage for a later period which will reduce the mismatch between the energy demand and supply. The TES is a highly efficient heat storage method. It serves as an intermediate step in the concentrated solar plants (CSP) by which the stored energy can be utilized during non-solar hours. TES systems can store excess energy when it is abundant and provide the same at the hour of need. The intermittent nature of renewable energy sources can be taken care of by installing the TES system in the energy system. The installation of TES will reduce the imbalance in energy dispatchability, which will, in turn, enhance the performance and reduce the cost of energy production. (Lin et al. 2018)

(Sharma et al. 2009)(Zalba et al. 2003) (Alva et al. 2018)(Liu et al. 2016) (Rathod and Banerjee 2013)

A schematic representation of a CSP plant integrated with a TES system is shown in Figure 1.1.
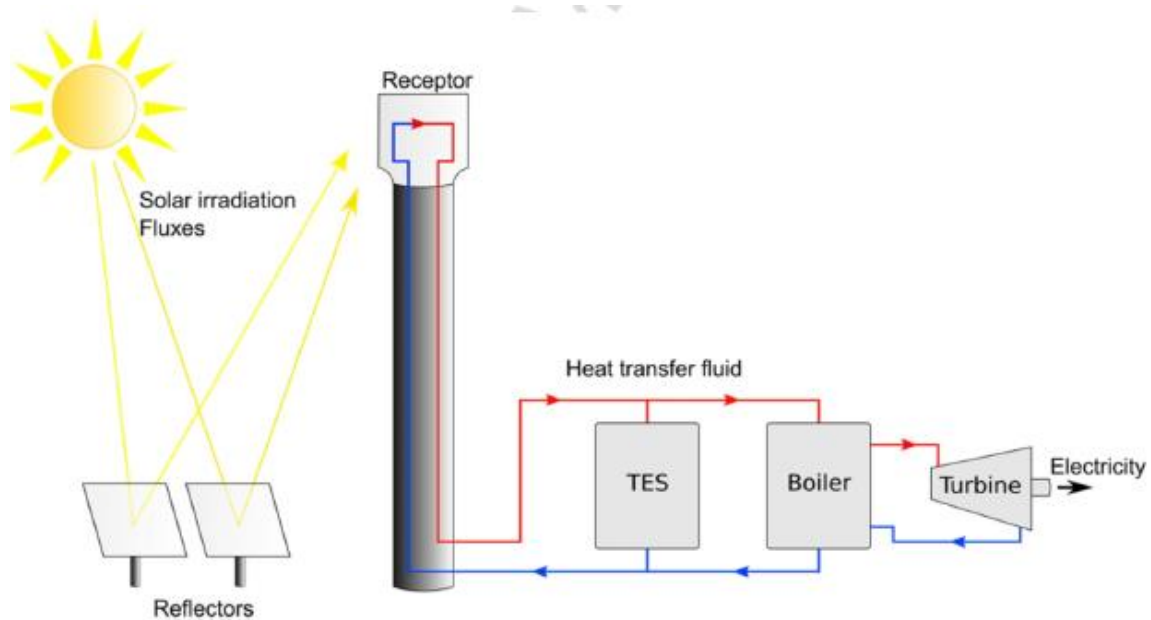
Figure 1.1: Schematic representation of a concentrated solar plant integrated with the thermal energy storage unit (Yang et al. 2020)

Depending on the variation in solar radiations and electricity demand, CSP with TES units can have the following functions:

1. To overcome the small fluctuations during transient weather conditions
2. Provide electricity during the non-solar hours
3. Improves the annual capacity factor

The CSP technology is classified into four types based on the focusing of the sun's rays and whether the receiver is fixed or mobile.

1. Parabolic trough
2. Linear Fresnel
3. Parabolic tower
4. Parabolic Dish

In the case of parabolic trough and linear Fresnel, the mirror tracks the sun along one axis; therefore, it is line focus, whereas, in tower and dish, the mirror follows the sun along two axes which are point focus. In linear Fresnel and parabolic tower, the receiver is fixed, while in the other two, it is mobile.

Less than half of the installed CSP capacity is integrated with the thermal storage units. Some examples of CSPs integrated with TES systems are Adnasol-1 CSP projects in Spain with 2 tank indirect TES storage systems with a storage duration of 7.5 hrs. Crescent Dunes solar energy project with 2 tank direct system with storage duration of 10 hrs in Nevada, United states. Another project called Nevada solar one is also operational with working hours of 0.5 hrs.(Bauer et al. 2021)

There are two types of CSP and TES storage systems:

1. Direct storage
2. Indirect storage

In direct storage, the heat transfer fluid (HTF) and the storage materials are the same, while in indirect storage, they are different, which makes use of an extra heat exchanger for heat transfer between HTF and the storage materials. (Liu et al. 2016). A schematic diagram showing the direct and the indirect thermal energy systems is shown in Figure 1.2.
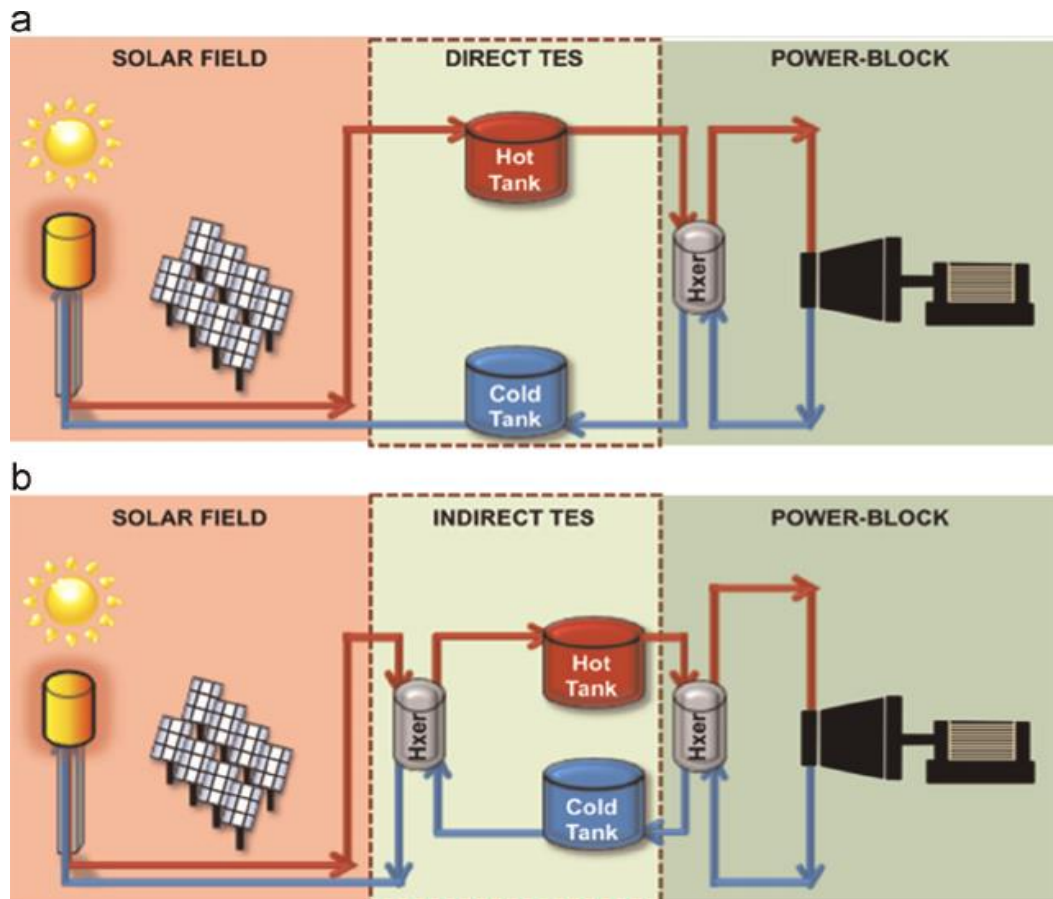
Figure 1.2: Direct and Indirect thermal energy storage systems (Liu et al. 2016)

1.1. State of the art in the field

1.1.1. Thermal Energy Storage:

Storage of solar energy is as good as developing a new source of energy. This will reduce the mismatch between the supply and the demand. It will also improve the performance of the energy system and play an essential role in conserving energy.

Thermal energy can be stored as sensible heat, latent heat, and through a chemical reaction, and the classification of the TES systems is shown in Figure 1.3.

Thermal Energy Storage

Sensible heat storage

Latent Heat storage

Chemical Reaction Heat Storage

Solid

Liquid

Solid-Liquid

Liquid-Gas

Solid-Solid

Thermochemical Reactions

Thermochemical Pipeline energy transport

Chemical Heat pump Storage
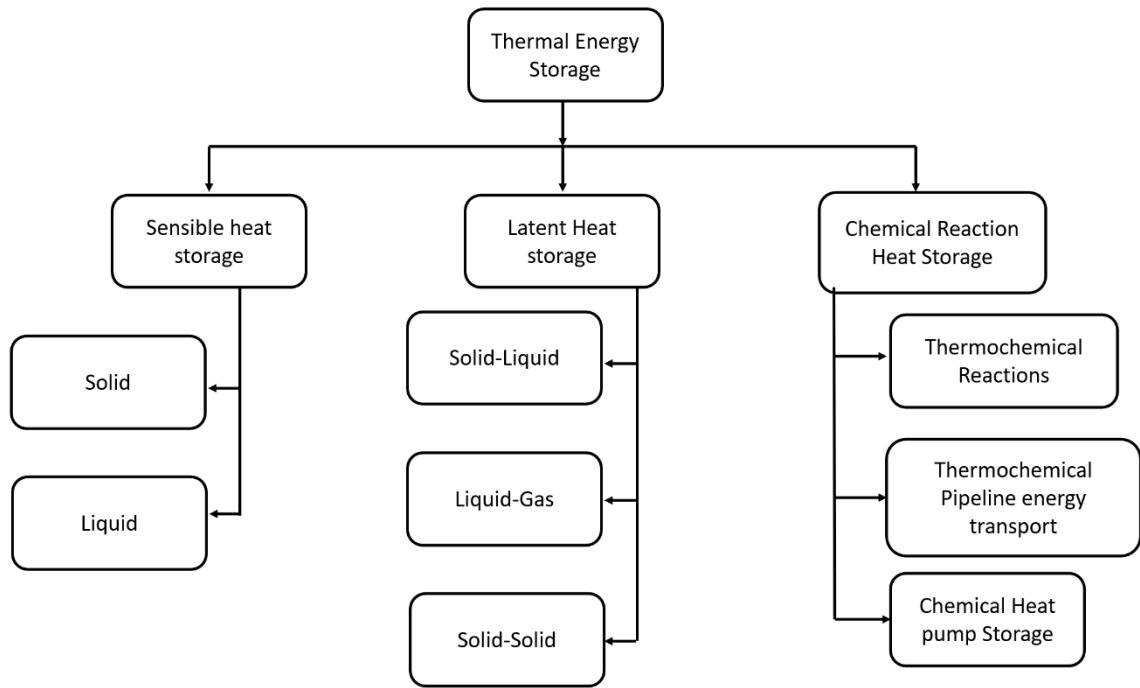
Figure 1.3: Classification of the thermal energy storage system redrawn (Raam Dheep and Sreekumar 2014)

1.1.1.1. Sensible heat storage:

In this, the thermal energy is stored when the temperature of the solid or liquid is increased. It depends on the specific heat capacity and change in temperature during charging and discharging. Here, the energy stored is strictly by its temperature. Heat capacity and thermal diffusivity are the only factors determining the energy density and the rate of energy release in the TES system. The amount of heat stored due to sensible heat ($Q_{sensible}$) is given by the formula:

$$Q_{sensible} = m \int_{t_s}^{t_e} c_p \ \frac{dT}{dt} \tag{1.1}$$

Where m is the mass of the sample used (kg), t_s and t_e are the time corresponding to the start and end of solidification respectively (s), c_p is the specific heat capacity (SHC) of the material (J/kgK), and dT/dt is the cooling rate (°C/s).

1.1.1.2. Latent heat storage (LHS):

LHS is the heat absorbed or released when a material undergoes a phase transformation given by the latent heat of fusion or enthalpy of fusion. The phase transformation can be solid to liquid and vice versa or liquid to gas and vice versa. The latent heat storage materials are called phase change materials (PCM). The amount of heat stored due to the phase change (Q_{latent}) is given by the formula:

$$Q_{latent} = m \int_{t_s}^{t_e} H_f \frac{df_s}{dt} \qquad (1.2)$$

Where m is the mass of the sample used (kg), t_s and t_e are the time corresponding to the start and end of solidification respectively (s), df_s/dt is the rate of fraction solidified, and H_f is the latent heat value of the material (J/kg).

1.1.1.3. Chemical reaction or Thermo-chemical energy storage:

Such systems involve the energy absorbed or released when a chemical reaction occurs (endothermic or exothermic reactions). Basically, during a completely reversible chemical reaction, energy is released or absorbed when molecular bonds are broken or reformed. The stored heat in this system depends on the amount of material, the heat of reaction, and the extent of a reaction at a particular time. Challenges in controlling reaction kinetics make the design of TES systems a very complex affair.

1.2. Latent heat thermal energy storage systems (LHTES):

As per the studies, latent heat storage systems have attracted many researchers as they can provide high energy storage density. It also possesses the property of storing heat at a constant temperature, i.e., phase change temperature. The phase transformations can be solid-solid, solid-liquid, solid-gas, liquid-gas, and vice versa.

In solid-solid transformations, the stored heat is due to the change in the crystalline form of the material. Such transitions are accompanied by low latent heat and small volume change, making it easy to store. These PCMs also offer design flexibility. In the case of solid-gas and liquid-gas transition, we have high latent heat and significant volume change. This leads to a problem of containment and makes the system very complex and infeasible. Thus, these materials cannot be used as storage materials.

In solid-liquid transitions, the heat of transformation is lesser and is accompanied by small volume changes of 10% or less. This brings down the problem of containment. Therefore, these materials are attractive among researchers as energy storage materials. The container should be appropriately designed to take care of the volume changes and be compatible with the PCMs.

These solid-liquid latent heat storage systems also behave like conventional storage systems by absorbing heat like sensible heat due to its temperature rise. After reaching its phase transformation temperature, these PCMs absorb heat in the form of latent heat at a constant temperature. The design parameters for a LHTES are latent heat of fusion and coefficient of thermal expansion along with other thermophysical parameters. Latent heat storage is nearly an isothermal process that can significantly enhance energy storage quantities compared to sensible heat thermal energy storage systems (SHTES) of the same temperature range. Storage density in LHTES systems is 5-14 times higher than that stored in SHTES systems. As the storage capacity of LHTES systems is governed not only by the heat of fusion but also by specific heat capacity, this can enable a compact, more efficient, and lower-cost alternative to SHTES systems.

This high storage capacity of LHTES as compared to SHTES is shown in Figure 1.4 where Q is the energy storage capacity, T_m is the phase change temperature, ΔT is the small temperature interval, $\Delta Q_{sensible}$ is the sensible heat stored, and ΔQ_{PCM} is the latent heat stored.
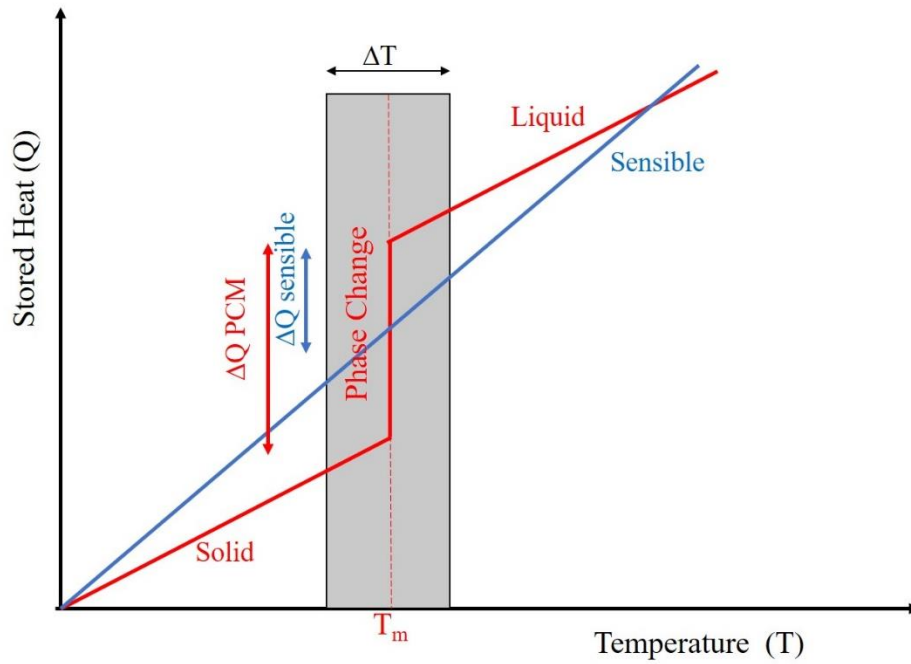
Figure 1.4: Energy storage capacity (Q) of latent heat storage materials compared to sensible heat storage materials when used in small temperature intervals ΔT redrawn (Günther et al. 2009)

PCMs can be used in building applications to enhance the energy storage capacity, hot and cold storage for heating and cooling plants, hot storage for solar cooling and heating and can also be used for cold chain logistics and medical applications.(Sarbu and Sebarchievici 2018)

To be used as thermal energy storage materials, the PCMs should possess specific desired properties and consider the availability of materials and economic cost. (Sharma et al. 2009)(Zalba et al. 2003)

The thermophysical, kinetics and chemical properties that these PCMs should possess are as follows:

1. Thermal properties:
   - A suitable phase transformation temperature
   - High latent heat of phase transformation
   - Good heat transfer properties such as high thermal conductivity

2. Physical properties:
   - Phase stability
   - High density
   - Volume change should be small
   - Low vapor pressure
3. Kinetic properties:
   - No or low super cooling
   - Sufficient crystallization rate
4. Chemical properties:
   - Chemical stability
   - Compatibility with the container material
   - Nontoxic and non-hazardous
5. Economic
   - Low cost
   - High availability

These selection criteria for PCMs are shown in Figure 1.5.
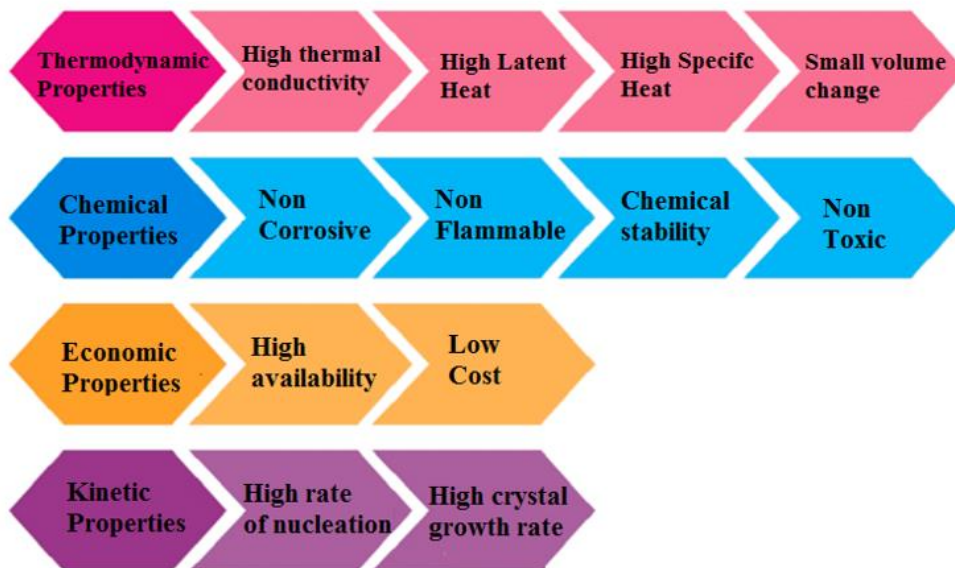
Figure 1.5: Selection criteria for the phase change materials redrawn (Yang et al. 2020)

PCMs also possess some disadvantages such as phase separation, low thermal conductivity, supercooling and thermal and chemical stability. Lot of research has been performed to eliminate or reduce these disadvantages and produce improved PCMs.(Thakare and Bhave 2015)

1.3. Organization of the thesis:

The thesis is divided into six chapters. Chapter 1 presents the introduction, Chapter 2 provides the literature review on phase change materials, nano-enhanced phase change materials, the mechanisms involved in thermal performance enhancement, and the various characterization methods and techniques used for the thermal characterization of phase change materials followed by the scope and objectives of the present research work. Chapter 3 describes the theoretical background of the inverse heat conduction problem, which was used in the research work. Chapter 4 describes the experimental details, materials used, and the methodology adopted for the investigation. Chapter 5 presents the results of the experiments and gives a detailed analysis of these results, interpretation, and related discussion. Chapter 6 lists the conclusions drawn based on experimental findings and the discussion.

Chapter 2 LITERATURE SURVEY

A detailed literature survey on various aspects of latent heat thermal energy storage using salt PCMs and nano-enhanced PCMs and different thermal characterization techniques was carried out. The phase change materials that store thermal energy as latent heat are superior compared to various other sensible heat storage materials due to their higher energy storage capacity.

PCMs can be classified into organic PCMs, Inorganic PCMs, and their Eutectics. The classification of the phase change materials and their respective advantages and limitations are discussed in the following section.

2.1. Classification of phase change materials

Many phase change materials are available depending upon the melting temperature and their latent heat of fusion. (Raam Dheep and Sreekumar 2014) (Sharma et al. 2009) (Zalba et al. 2003). The classification of the phase change materials is shown in Figure 2.1.
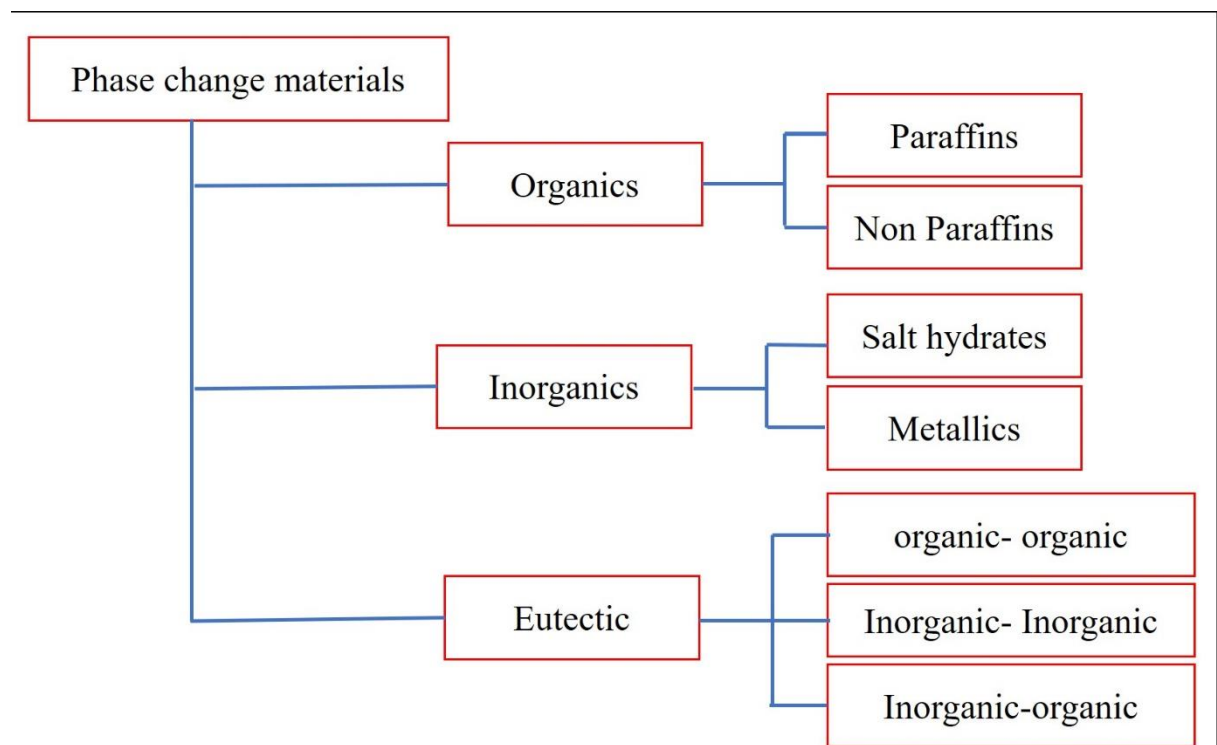
Figure 2.1. Classification of the phase change materials redrawn (Zalba et al. 2003)

Phase Change Materials (PCMs) can be classified as follows:

2.1.1. Organic phase change materials:

Various organic PCMs which are reported to be suitable for the usage in TES systems are fatty acids, glycols, paraffin, esters, and eutectics of these compounds. These materials melt and repeatedly freeze on thermal cycling with no phase separation or deterioration in latent heat of fusion. They are non-corrosive and possess self-nucleating properties. All these organic PCMs have a low thermal conductivity, resulting in a longer thermal cycle of the materials.

Organics are suitable for low-temperature applications, due to which they are not suitable for thermal energy storage in CSP plants with higher temperature requirements. TES systems in low-temperature applications utilize organic PCMs and are successfully commercialized. These PCMs are further classified as paraffin and non-paraffins:

2.1.1.1. Paraffins:

These are primarily linear chains of n-alkanes. The melting point and the latent heat of fusion increases with an increase in the number of carbon atoms. These are available over an extensive temperature range. It is safe, non-corrosive with low volume change and low vapor pressure. These materials have low thermal conductivity, flammability and have containment problems.

2.1.1.2. Non-paraffins:

These materials are flammable and unstable at high temperatures, have a high enthalpy of fusion, low thermal conductivity, are combustible and toxic. Some examples of non-paraffins are oil based PCMs, fatty acids and glycols.

2.1.2. Inorganic phase change materials:

Inorganic PCMs work over an extensive range of temperatures. For lower temperature applications, PCMs with phase transition temperature below 150 °C can be considered. The operating range of inorganic phase change materials is up to 1500 °C. Thus they find a place for its usage in CSPs.

The PCMs which fall under this category are salt hydrates, salts, metals, and eutectics. These materials are superior to other materials as they possess ideal properties to be used for energy storage. As compared to organic, inorganic PCMs have higher thermal conductivity and heat of fusion. This makes them an appropriate choice for thermal energy storage applications. These inorganic PCMs also have demerits such as supercooling, phase segregation, degradation of materials on thermal cycling, and low thermal conductivity in the case of salt PCMs. (Sharma et al. 2009)

2.1.2.1.   Salt Hydrate PCMs

Salt hydrates are crystalline solids made up of inorganic salts and water that form AB.nH$_2$O. The phase transition of these salt hydrates is the dehydration of the water of crystallization of the salt. Salt hydrates melt down to give salt a lower degree of hydration or its anhydrous form. This is very different as compared to the actual phase change that the inorganic salt present in them undergoes. Therefore, the value of latent heat of fusion is low in salt hydrates as compared to their corresponding salt PCMs.

The salt hydrates have the problem of incongruent melting. The lower hydrate salt or anhydrous salt, due to lower density, settles down, and the released water of crystallization is not sufficient to dissolve the remaining salt. This leads to phase segregation and a decrease in the melt-freeze of salt hydrate with every thermal cycle.

Salt hydrates result in supercooling as it has poor nucleating properties. It can be sorted out by the addition of thickening gels and nucleating agents.

Salt hydrates have high latent heat of fusion per unit volume, higher thermal conductivity, and small volume changes. They are also non-corrosive, slightly toxic, and compatible with the container materials, i.e., plastics. (Sharma et al. 2009)

2.1.3. Eutectics:

When two or more compounds at a fixed composition percentage are mixed, they form eutectic PCMs with a minimum melting point. These PCMs melt and freeze congruently without any segregation.

A mind map of the available PCMs is shown in Figure 2.2.
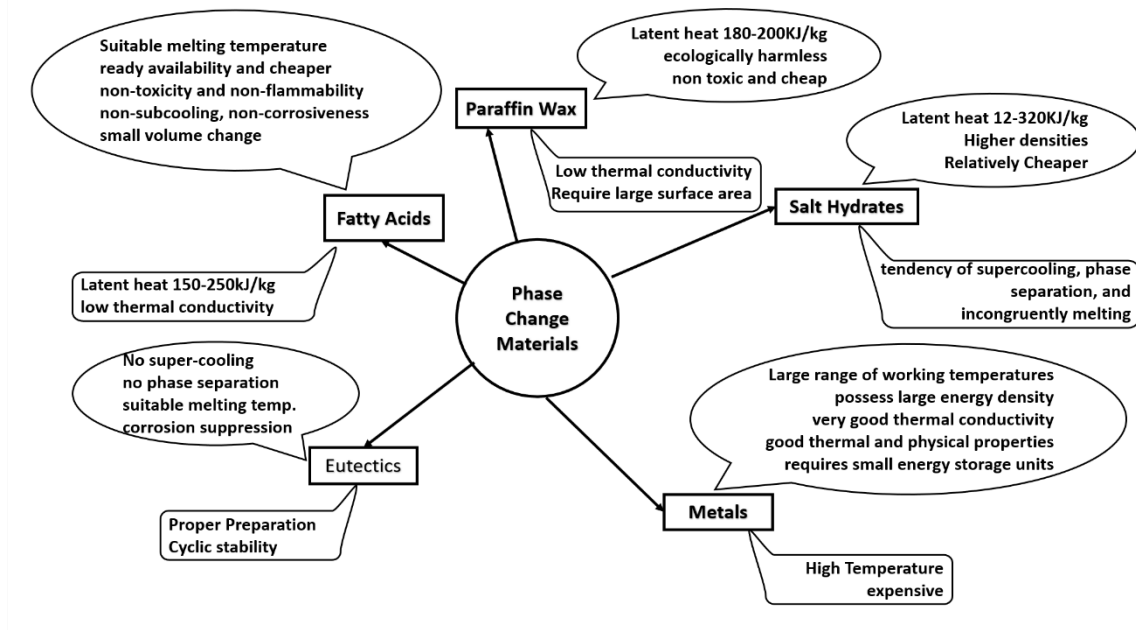
Figure 2.2: A mind map of PCMs redrawn (Shukla 2018)

2.2. Inorganic salt phase change materials

Inorganic PCMs are preferred over organic PCMs because of various advantages like a wide range of melting temperatures, high latent heat, and higher thermal conductivity. The inorganic PCMs have some limitations, that they are corrosive, undergo subcooling, and the phase separation of salt hydrates during the phase transition process.

Inorganic PCMs have a wide range of phase change temperatures and have a high operating temperature range. This will expand the overall operating range of the CSP plants and thus increase their efficiency. The salt-based PCMs are cheaper than other conventional PCMs, which reduces the system cost of the TES systems. These PCMs are environment friendly, and thus the cost incurred on the remedial measures for the environment is also reduced. (Lin et al. 2018)(Alva et al. 2018)(Wong-Pinto et al. 2020)(Pedrosa et al. 2018)(Farid et al. 2004). The energy change that occurs within the PCM during melting or solidification is depicted in Figure 2.3.
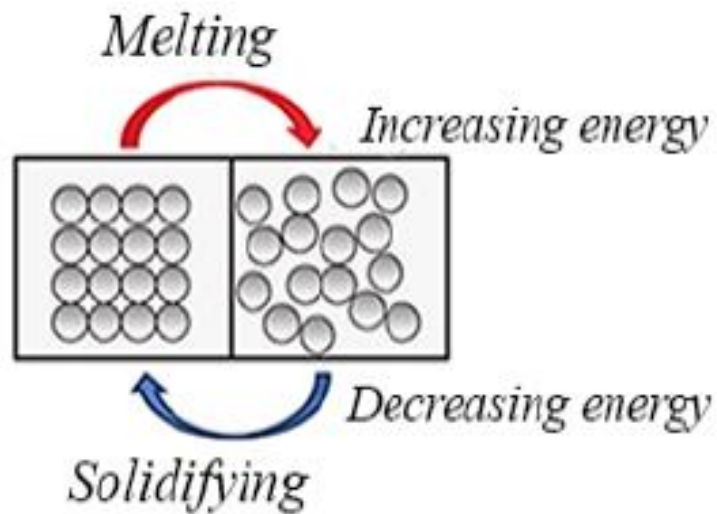
Figure 2.3: The solidification and the melting process of the PCMs (Kaviarasu and Prakash 2016)

(Glatzmaier 2011) conducted an intensive study of suitable inorganic salt mixtures for cascaded PCM devices in solar power plants for a temperature range of 300-400 °C. Homogeneous samples of KNO_3-KCl-KBr, $NaCl$-KCl-$LiCl$ and $MgCl_2$-KCl-$NaCl$ were produced and their thermal properties and thermal stability were studied. The chemical stability of the container material was analyzed in a controlled atmosphere furnace with N_2 gas.

(Michels and Pitz-Paal 2007) investigated the suitability of PCMs like $NaNO_3$, KNO_3 and eutectic of KNO_3-KCl experimentally to be used in cascaded latent thermal energy storage systems. It was observed that $NaNO_3$ showed superior characteristics by virtue of latent heat and corrosive power. Simulation studies also compared the effectiveness of cascaded systems over non cascaded systems.

The melting and freezing cycles of various salt-based PCMs suitable for Compact linear Fresnel reflector (CFLR), Multi tower solar array (MTSA), and parabolic trough collector systems were investigated and modeled with a working temperature range of 500-1300°C by (Hoshi et al. 2005). The cost-efficiency of these systems was also studied.

(Morisson et al. 2008) through numerical simulations, the transfer of heat and fluid flow parameters in the latent thermal heat storage systems adapted to direct steam generation technology.

(Herrmann et al. 2004) conducted a study to assess the concept in which a different (cheaper) liquid medium such as molten salt was used as a medium to store thermal energy instead of heat transfer fluid used in solar thermal power plant incorporated in a 2-tank storage system. In this, the heat transfer fluid and the storage medium was the same). The salts used for the above study were Hitec and Hitec XL ternary salt mixtures, solar salt. Detailed analysis of their performance and cost-effectiveness of these salts were also carried out, and it was observed that the realization of this concept is quite possible.

A comparative study of six gaseous and liquid HTFs was performed by (Liu et al. 2014). This study was to investigate their suitability for high-temperature TES applications which utilize flat slabs of PCMs. In terms of capacity rates, liquid sodium (99.4%) was recognized as the best HTF. The electrical energy output to the grid was highest with liquid sodium. The value achieved by solar salt was 93.6%. The values achieved by gaseous fluids like atmospheric air, air, and steam at 10 bar all ranged between 87.9 % and 91.3 % of the ideal energy delivered. This study concluded that the performance of gaseous fluids and liquid HTFs were comparable in terms of energy storage.

A list of various inorganic eutectics with their thermal parameters is given in Table 2.1.

Table 2.1: List of inorganic eutectics with melting temperature and heat of fusion.
(Zalba et al. 2003)

Compound	Melting temperature (°C)	Heat of fusion (kJ/kg)	Thermal conductivity (W/m K)
66.6% $CaCl_2 \cdot 6H_2O$ + 33.3% $MgCl_2 \cdot 6H_2O$	25 [6]	127 [6]	n.a.
48% $CaCl_2$ + 4.3% NaCl + 0.4% KCl + 47.3% H_2O	26.8 [1,6]	188.0 [6]	n.a.
47% $Ca(NO_3)_2 \cdot 4H_2O$ + 33% $Mg(NO_3)_2 \cdot 6H_2O$	30 [1]	136 [1]	n.a.
60% $Na(CH_3COO) \cdot 3H_2O$ + 40% $CO(NH_2)_2$	31.5 [24] 30 [25]	226 [24] 200.5 [25]	n.a.
61.5% $Mg(NO_3)_2 \cdot 6H_2O$ + 38.5% NH_4NO_3	52 [11]	125.5 [11]	0.494 (liquid, 65.0 °C) [11] 0.515 (liquid, 88.0 °C) [11] 0.552 (solid, 36.0 °C) [11]
58.7% $Mg(NO_3) \cdot 6H_2O$ + 41.3% $MgCl_2 \cdot 6H_2O$	59 [11] 58 [6]	132.2 [11] 132 [6]	0.510 (liquid, 65.0 °C) [11] 0.565 (liquid, 85.0 °C) [11] 0.678 (solid, 38.0 °C) [11] 0.678 (solid, 53.0 °C) [11]
53% $Mg(NO_3)_2 \cdot 6H_2O$ + 47% $Al(NO_3)_2 \cdot 9H_2O$	61 [1]	148 [1]	n.a.
14% $LiNO_3$ + 86% $Mg(NO_3)_2 \cdot 6H_2O$	72 [6]	>180 [6]	n.a.
66.6% urea + 33.4% NH_4Br	76 [11]	161.0 [11]	0.331 (liquid, 79.8 °C) [11] 0.324 (liquid, 92.5 °C) [11] 0.649 (solid, 39.0 °C) [11] 0.682 (solid, 65 °C) [11]
11.8% NaF + 54.3% KF + 26.6% LiF + 7.3% MgF_2	449 [26]	n.a.	n.a.
35.1% LiF + 38.4% NaF + 26.5% CaF_2	615 [26]	n.a.	n.a.
32.5% LiF + 50.5% NaF + 17.0% MgF_2	632 [26]	n.a.	n.a.

The major drawback in using molten salts in solar power plants as HTFs is that salts tend to freeze in the flow pipes and equipment. The issue can be resolved using a recovery plan which is cold filling. Simulation studies of cold filling of molten salts into the receiver tube using the volume of fluid method and enthalpy method were done by (Liao et al. 2014).

In an elaborative study based on the mechanism of phase change, the release of pressure drop along the tube was demonstrated. The effect of cold filling on the temperature distribution along the flow tube was also investigated. This research provides a practical reference for the application of cold filling.

The concept of a three-part storage system using a PCM ($NaNO_3$) for the two-phase evaporation was proposed by (Laing et al. 2011). The concrete material was used for

sensible heat storage. It was detected that after 172 thermal cycles, there was no degradation, and the melting temperature was maintained at 306 °C.

(Zhou and Eames 2016) studied the thermal characterization of binary $NaNO_3$ and $LiNO_3$ salts with compositions 46-54% and 60-40% and measured the thermophysical properties of the salts. They found that the salts showed good thermal stability and chemical stability as PCM at medium temperatures. (<200°C) The thermal properties were studied using differential scanning calorimetry (DSC) and chemical stability using a thermo-gravimetric analyzer (TGA). Both the salts showed high latent heat values (more than 220KJ/Kg).

Thermophysical properties of the binary nitrate salt of sodium, potassium and lithium were studied i.e. $NaNO_3$-KNO_3, $NaNO_3$-$LiNO_3$, and KNO_3-$LiNO_3$. The distribution of parameters like melting temperature, specific heat capacity, latent heat and viscosity as a function of shear rate and temperature were studied. They observed a maximum increase in the specific heat of the system with $LiNO_3$. All these nitrates had exceptional thermal properties with low cost. $LiNO_3$ made the salt more viscous and enhanced the specific heat and latent heat of the system. The salt system still showed an issue of supercooling. (Coscia et al. 2011)

(Fernández et al. 2014) studied the effect of $LiNO_3$ and $Ca (NO_3)_2$ on the solar salt ($NaNO_3$-KNO_3). They concluded that $LiNO_3$ increased the thermal stability of the salts and reduced the corrosivity of the salt because of the vast concentration of oxide ions. The addition of $Ca(NO_3)_2$ led to the reduction in melting point and effectively reduced the cost of these mixtures.

On thermal cycling, organic materials showed a slight change in melting point and latent heat after 1000 cycles, whereas inorganic materials showed degradation in their thermal properties after the thermal cycling. (Shukla et al. 2008)

The thermophysical properties of the various salt combinations of chlorides, nitrates, fluorides and hydroxides for high-temperature applications were presented. (Kenisarin 2010)

Analysis of thermophysical properties and stability tests was performed on some high-temperature PCMs comprising chlorides and carbonates of sodium, potassium, and lithium.

It was concluded that chlorides salts did not show any subcooling while carbonate salt showed high subcooling in the initial stages, decreasing with subsequent stages. (Liu et al. 2015)

2.3. Nano salt phase change materials

The rapid advancement in nanotechnology has led to an innovative concept of using nanosized particles of various carbon-based, metal, or metal oxides having a nominal diameter in the range of 10 to 50 nm in energy storage systems. These high conductivity nanoparticles can be used with the base inorganic salt PCMs to develop a highly conductive fluid as compared to the base salt called nano salts or nanoenhanced salts. The impregnation of salt PCM with nano-sized particles well dispersed in the salt has brought remarkable improvements in several TES parameters. Usually, solid-state particles are introduced in the base liquids as they conduct heat faster than the fluid. Particle precipitation is a significant limitation of such systems.

Due to the Van der walls force existing between the nanoparticles; they have a strong affinity for adhesion. Therefore, a large number of nanoparticles adhere together to form clusters. These clusters merge to form agglomerated nanoparticles leading to their deposition. This agglomeration and deposition are not desirable in the case of Nano-enhanced PCMs (NePCMs). Nanoparticles are effective only when they are well dispersed in the base PCM. This can be attained by the use of sonication, surface modification, and use of surfactants. These methods enhance nanoparticle stability in the PCM. The usage of surfactants reduces the adhesion tendency of the nanoparticles but also decreases their positive influence. The most commonly used method to obtain evenly dispersed nanoparticles is sonication. The sonication time used also affects the thermal parameters of the NePCMs.

Nano-sized particles tend to stay suspended for a longer time as compared to micro-sized particles. This is because the nanoparticles possess a higher surface area to volume ratio than micro-sized particles (1000 times). Due to this reason, nanofluids offer a higher rate of heat transfer.

Nanoparticles have a high surface area to volume ratio, owing to which they have certain specific properties. The thermal conductivity of multi-walled carbon nanotubes (MWCNT)

and graphene nanoparticles is about 3000 W/mK and 5300 W/mK, respectively while salts have quite low thermal conductivity. Therefore, it is expected that the thermal conductivity of the salt would increase with the addition of nanoparticles with high thermal conductivity values. Studies showed that NePCMs have better phase change parameters and improved energy storage properties. (Yang et al. 2020)

Using nanoparticles has opened up a gateway of opportunity for new innovative research in this area. The doping of nanoparticles to the PCM intensively alters their thermophysical parameters such as thermal conductivity, phase change enthalpy, viscosity, subcooling, etc. A lot of work has been done to study the effect of dispersion of nanoparticles on the thermal parameters of the NePCMs. The thermal properties of the salt-based PCM were effectively enhanced by doping nanoparticles into the base PCMs.(Pielichowska and Pielichowski 2014)(Kaviarasu and Prakash 2016)(Kibria et al. 2015)(Wei et al. 2018)

PCMs have high energy storage capacity because of the latent heat involved in their phase change. A minimal study has been done to investigate the effect of nanoparticles on the phase change enthalpy of the salt PCMs. Some studies have observed that the doping of nanoparticles had a positive impact on the phase change enthalpy, while some researchers reported that the addition of nanoparticles leads to a reduction in the volume of the base salt PCM, therefore, reducing the latent heat values. However, in some studies, it was found that when a low volume fraction of nanoparticles was added, latent heat of the NePCM increased but a high-volume fraction of nanoparticles led to the decrease in the value of the latent heat obtained. (Yang et al. 2020)(Hamdy et al. 2017)(Huang et al. 2014)(Tao et al. 2015)(Xiao et al. 2014)

The nanoparticle addition to the PCMs also affects the phase change temperature. In some studies, it has been observed that the presence of nanoparticles did not have any significant or has negligible effect on the phase change temperature of the NePCM. Some researchers observed a desirable outcome of reduced melting temperature in the NePCM. This decrease was not significant enough to improve the TES efficiency. (Yang et al. 2020)(Romanin and Fereres 2017)(Xie et al. 2016)

The energy storage density of the PCM is governed by two forms of heat, namely sensible heat and latent heat. For sensible heat, the SHC is a significant parameter. The addition of nanoparticles affects the SHC values and, in turn, affects the energy storage capacity of the

material. Research studies have revealed that the addition of nanoparticles greatly enhances the SHC values. The increase observed was directly proportional to the weight fraction of the nanoparticles added to the salt PCMs.

Salt PCMs sometimes undergo subcooling before the start of solidification where the PCM is still in the liquid state even below the liquidus point. This subcooling helps to initiate the nucleation of the solid-state and thus delays the phase change process. Usually, materials with low or no subcooling are preferred for energy storage applications. Some researchers have reported a significant decrease in the degree of subcooling (89-92%) due to the nanoparticle addition to salt PCMs. (Wu et al. 2020)(Jin et al. 2018)

It is believed that thermal cycling reduces the stability of the nanoparticles and leads to agglomeration. These agglomerated nanoparticles get deposited and negatively affect the thermophysical parameters of the PCM. Enhanced thermal and chemical stability was observed in NePCMs by many researchers. Improved thermal stability of up to 400 cycles has been reported in the literature. (Ge et al. 2014) (Wu et al. 2020)

Nanofluids preparation can be done by two methods. A single-step method in which the production and dispersion of nanoparticles into the base salt occur simultaneously. Another method is a two-step method in which nano powders are prepared in the first step and in the next step it is physically dispersed into the base salt. In both cases, it has to be ensured that the nanoparticles are well mixed and the dispersion is uniform in the base fluid. This will help in the enhancement of the energy storage parameters of the nanofluid.

The addition of nanoparticles to the base fluid has a remarkable effect on the thermophysical parameters of the base salt. The effect on the thermal parameters such as thermal conductivity and SHC has been the primary topic of research in literature. It was reported in many of the research studies that the addition of nanoparticles significantly enhanced the thermal conductivity of the base salt. Later many related research areas were also studied where the effect of the concentration of nanoparticles added to the base salt was analyzed. The effect of nanoparticle size and their stability in the base medium was also assessed. Their effect on the thermophysical properties was the focus of all research studies. An improvement in the thermal conductivity was seen in the nanofluids of water and other organic liquids. A decrease in the SHC accompanied it.(Zhou and Ni 2008) (Hentschke 2016)

However, it was observed by (Lasfargues et al. 2015) that in nanofluids prepared with salt as the base liquid, the thermal conductivity of the base fluid decreased while the SHC increased. A similar result of enhanced SHC was observed by (Jo and Banerjee 2015) (Hentschke 2016), where he cleared that the addition of any nanoparticle to salts led to an increase in the SHC.

The anomalous behavior and effect observed by the addition of the nanoparticles on the thermal parameters was also studied and observed by (Khanafer et al. 2015). It was concluded that the enhancement of the thermal properties, especially SHC and thermal conductivity depended not only on the nanoparticles but also on the nanoparticle's concentration and the base PCMs used.

Research studies based on the effects obtained in salt-based PCMs doping them with various carbon-based and other nanoparticles are discussed below.

2.3.1. Carbon-based nanoparticles:

Nanoparticles exhibit certain thermal, magnetic, and optical properties. With the decrease in the size of the particle, the surface area to volume ratio of the particle increases. This means that the ability of the nanoparticles to transfer heat increases. (Sudheer and Prabhu 2017a). The dispersion of nanoparticles improves the thermal conductivity of the PCM and also alters its thermal parameters.

2.3.1.1. Carbon nanotubes (CNT)/ carbon nanofibers (CNF)

Among different nanoparticles, CNT/CNF possesses certain exclusive physical properties, due to which they are considered to be a potential candidate in the field of PCM-based storage systems. Schematic sketches depicting the CNTs and CNFs are shown in Figure 2.4.
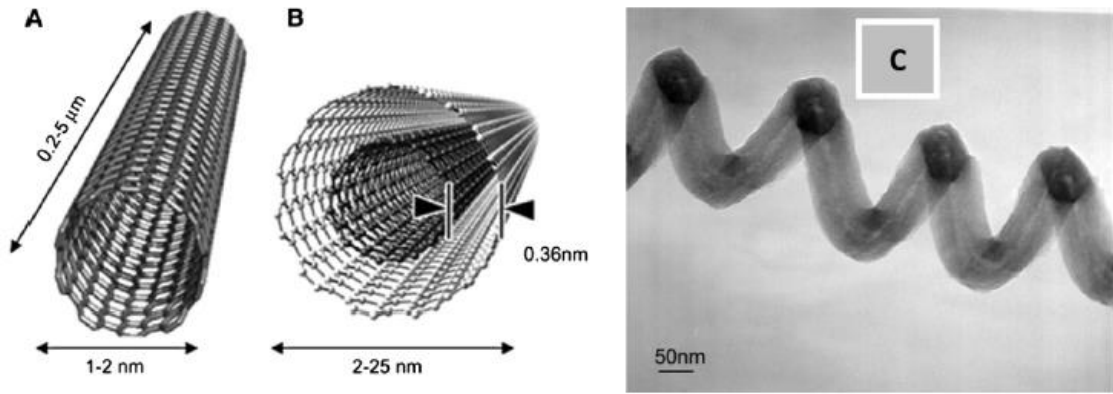
Figure 2.4 A transmission electron micrograph of (A). Single-walled carbon nanotubes (B). MWCNT (C) Carbon nanofiber (Kibria et al. 2015)

To study the effect on TES parameters, carbon nanoparticles were dispersed in salt PCMs. (Jo and Banerjee 2015) studied the effect of the addition of MWCNT into a eutectic salt mixture of lithium carbonate and potassium carbonate. They observed an enhancement in the SHC values in both solid and liquid states. This increment was in proportion with the weight percentage of nanoparticles added. This was against the common notion of an optimum weight percentage of nanoparticle addition for SHC enhancement. (Hentschke 2016; Sudheer and Prabhu 2017a). In this case, the increment of SHC was, however, very small, 5% in the liquid state and 12 % in the solid-state.

The preparation and thermal characterization of the carbonate salts using different forms of carbon nanoparticles with varying microstructures as nanoparticles were studied. The microstructural studies after the addition of nanoparticles were also done. The results showed that nanoparticle microstructures also affected the thermal performance of the NePCMs. The sheet structure, graphene, proved to be the best additive for the increase in SHC by 18.57%. Single-walled carbon nanotube (SWCNT) with columnar structure proved to be the best additive for increasing thermal conductivity by 56.98%. With an increase in the specific area of the nanoparticles, the phase change point also increases but the enthalpy of phase change decreases. In contrast, with an increase in the mass fraction of nanoparticles, melting point and latent heat decreases in the range of 1 to 2 °C and 4.6% to 9.8% respectively. (Tao et al. 2015)

Modification of nano-enhanced salt PCMs has been done by preparation of composite with the addition of support material. Nanoparticles improve the thermophysical parameters of

the PCM, while the support material provides an improvement in the shape and stability of the structure of the PCM. (Ge et al. 2014) studied a composite made up of Li- Na carbonate eutectic as base salt, support material being MgO, and nanoparticles such as graphite flakes and CNT were used. Uniaxially compressed green pellets of this composite were prepared and sintered at a temperature of 550 °C. Thermal cycling stability of up to 28 thermal cycles was performed on the above composite, and it was concluded that the material showed good thermal and chemical stability.

Solar salt has been a very popular choice in the salt-based energy storage domain, but low thermal conductivity has been a significant setback for using this salt. (Wu et al. 2018) added different amounts of MWCNT to solar salt and observed an enhancement in the thermal parameters of the nano-enhanced salt. An addition of 0.3 wt. % of MWCNT with uniform dispersion as per the scanning electron microscope (SEM) micrograph increased the thermal conductivity by 256%. It was concluded that uniform dispersion and the formation of high thermal conductivity channels were the main contributors to the improved thermal properties of the NePCMs.

(Romanin and Fereres 2017) studied various nanofluids of solar salt and 1% CNT prepared using different synthesis methods and various sonication times. They observed that this did not affect the phase change enthalpy of the nanofluids. However, a desirable effect of 2-3 degrees decrease in melting temperature was observed. This decrease was significantly low and thus had no remarkable effect on the efficiency of the TES systems.

This study (Hamdy et al. 2017) prepared various nano-enhanced salt composites of MWCNT using solar salt $NaNO_3$- KNO_3 (60:40 ratio). Various thermophysical properties such as morphology, phase change enthalpy, melting temperature, SHC, and thermal conductivity were investigated. They observed that when 0.1 %, 0.5%, and 1 % of MWCNT by weight of the salt was added, the increase in the value of latent heat was 36.11%, 33.3%, and 10.11% respectively. The thermal conductivity enhancement was 21.93%, 33.33%, 43.86% and 50.88% for 0.1 %, 0.5%, 1% and 1.5 % addition of MWCNT respectively.

Similarly, (Ye et al. 2014) studied a composite material with base salt as sodium carbonate, MWCNT nanoparticles, and MgO as support material. It was observed that the weight concentration of nanoparticles 0.1%, 0.2%, 0.3%, and 0.5% by weight of the sample led to an increase in the thermal conductivity from 0.75 to 0.901, 0.976, 1.048, and 1.127W/mK,

respectively. They also observed that the thermal conductivity of the composite material increases with the increase in temperature. This increment was attributed to the fact that the support material being porous led to convective and radiative heat transfer.

It was also observed that these support materials used would reframe themselves inside the composite, which led to an increase in the bulk density due to the higher wettability of the support material with the base salt. The low wettability of the nano additives led to the formation of a network of chain-like structures, which would, in turn, reduce the bulk density. Both the effect cancels each other leading to no or minimal change in the bulk density of the composite. With carbon addition of 10% and 20 %, the enhancement in the thermal conductivity was observed as 5 W/mK and 4.3 W/mK, respectively.

(Shin et al. 2010) observed an increment in SHC value by 5-20% when nanoparticles of silica, alumina, and CNT with a weight percentage of 0.05% and 2% was added to eutectics of salt carbonate and conventionally used HTF (Therminol VP-1)

(Munyalo et al. 2018) observed a 6% increase in thermal conductivity when 0.2-1% MWCNT was added to $BaCl_2.H_2O$ with MgO as support material.

The effect of MWCNT on 23 wt. % $MgCl_2$ –H_2O was studied by (Wu et al. 2020). It was observed that there was an improvement in the thermal conductivity values. The degree of subcooling was also reduced. The usage of thickener xanthan gum prevented agglomeration and phase separation. With 1 % MWCNT, 89 % reduction in subcooling was observed and a 400 thermal cycle's stability was also obtained. By the addition of nanoparticles, latent heat was improved, increased thermal conductivity, reduction in subcooling, and enhanced thermal stability was observed. The cooling curves, differential scanning calorimetry (DSC) curves, and Fourier-transform infrared spectroscopy (FTIR) for the nano-enhanced PCMs over various thermal cycles are given in Figure 2.5 below.
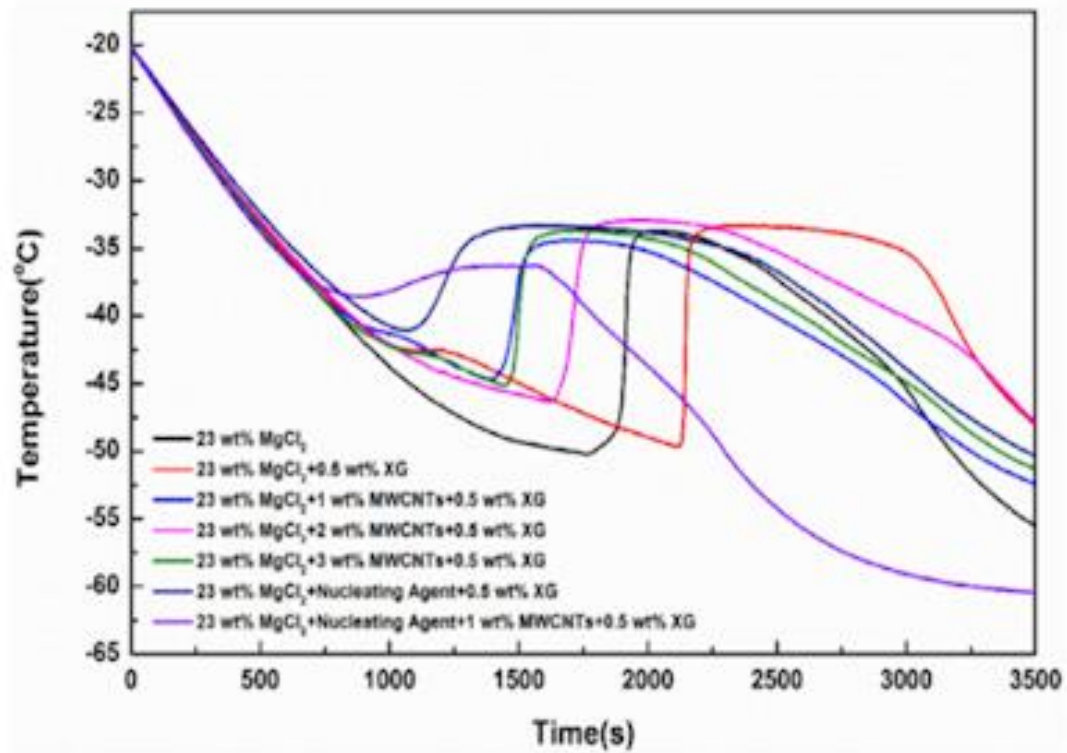
Figure 2.5: Cooling curves of base salt and nano-enhanced salts (Wu et al. 2020)
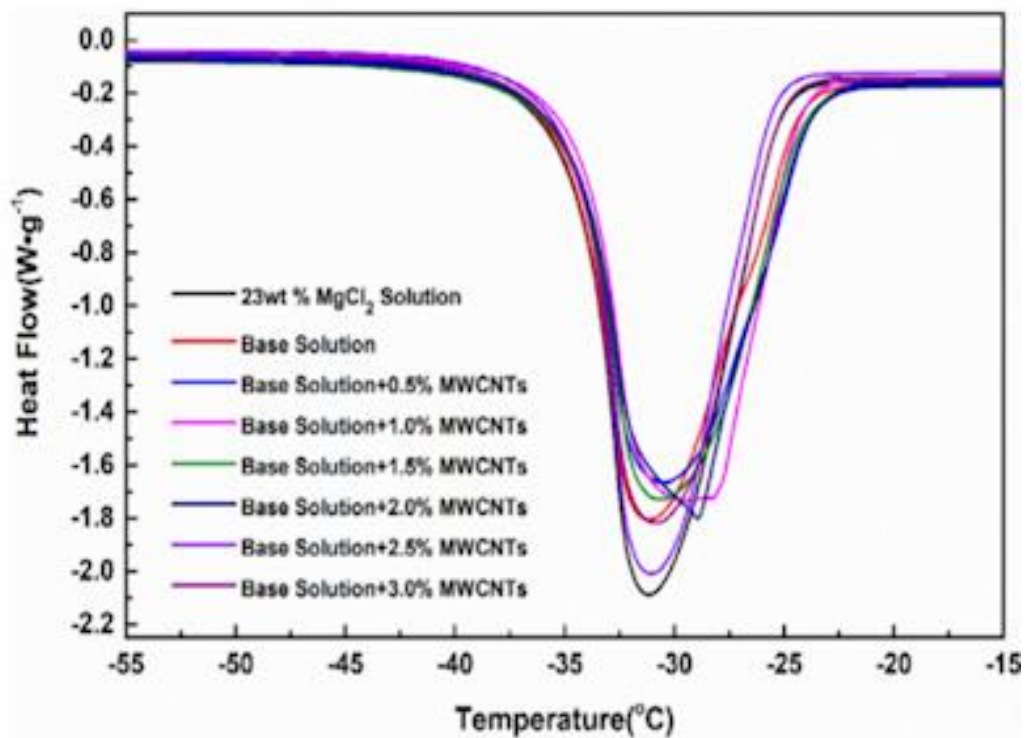
Figure 2.6: DSC curves of base salt and nano-enhanced salts (Wu et al. 2020)

The cooling curves of base salt and nano-enhanced salts shown in Figure 2.5 shows the effect on subcooling. The degree of subcooling reduced from 16.29 °C to 10-13 °C with the addition of nanoparticles. The DSC curves in Figure 2.6 revealed that the latent heat values decreased from 153.3 KJ/kg to a reduced value of 139.8 KJ/kg with the addition of MWCNT. The effect of nanoparticles on thermal conductivity can be observed in Figure 2.7 which shows an enhancement from a value of 0.51 W/mK to 0.56 W/mK with the increase in mass fraction of MWCNT. Figure 2.8 shows the FTIR analysis of 1 % nano-enhanced salts after 400 cycles, showing that there is not much significant change in the chemical composition of the salt after 400 cycles, and the salt has good thermal and chemical stability.
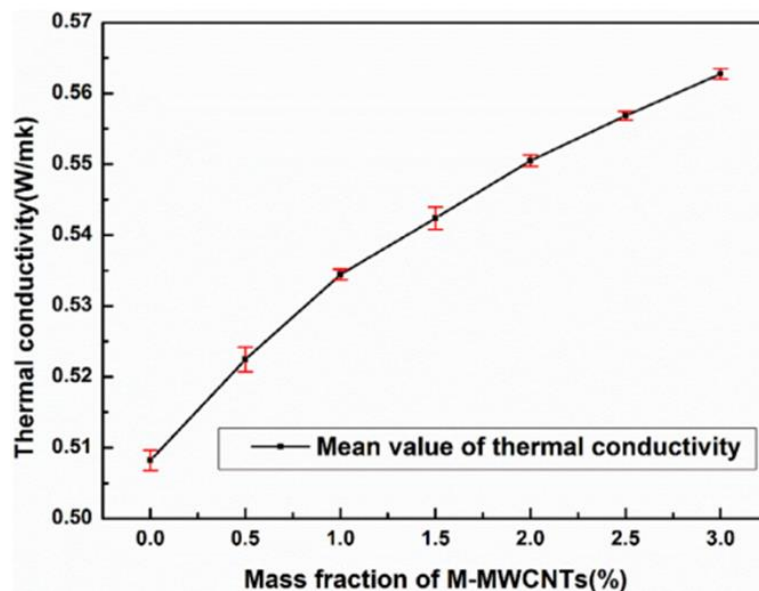
Figure 2.7: Effect of nanoparticles on the mean value of thermal conductivity (Wu et al. 2020)
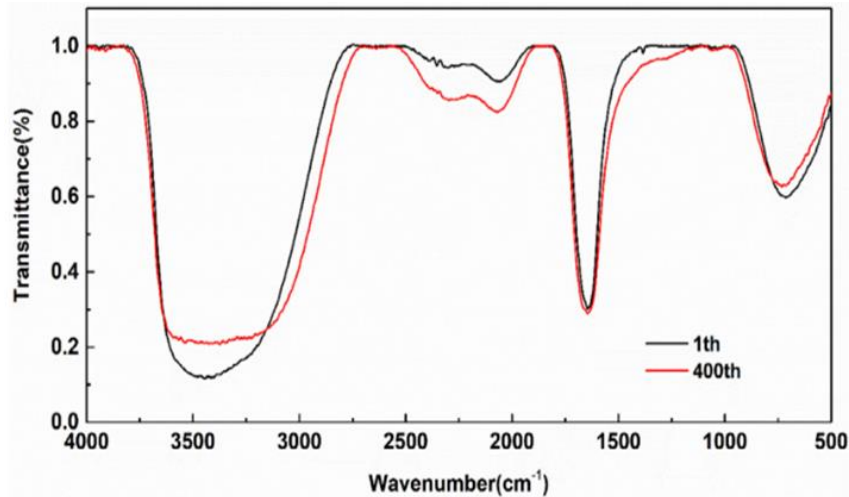
Figure 2.8: FTIR analysis of the 1% nano-enhanced PCMs after 400 thermal cycles (Wu et al. 2020)

2.3.1.2. Graphite/Graphene

(Xie et al. 2016) studied that the concentration of nanoparticles added to the molten salt also affected the thermal storage parameters of the salt. In their experimentation, the molten salt used was the solar salt eutectic mixture of KNO_3 and $NaNO_3$ (40%-60%). The nanoparticles used were the graphene nanoplatelets. They observed an increase of 16.7 % in specific heat with one wt.% of graphene. The onset temperature and end temperature decreased by 10.4 °C and 4.7°C, respectively. The startup heat also reduced by 9%.

Composite PCM was prepared by adding different mass rates of expanded graphite (EG) to the eutectic mixture of KNO_3 and $NaNO_3$ (40%-60%) by ultrasonic method. This addition of EG enhanced the thermal conductivity but reduced the latent heat by 11%. As the mass rate of EG increases, the specific heat, thermal conductivity, and thermal diffusivity also increase. (Xiao et al. 2014)

The addition of expanded graphite had a positive influence on the storage systems of salts like sodium nitrate and potassium nitrate. This effect on binary mixtures of the mentioned salts was studied by (Xiao et al. 2013), and ternary mixtures were analyzed by (Bauer et al. 2006). In both cases, an improvement in the thermal conductivity was observed.

28

(Kardam et al. 2015) investigated the thermophysical parameters of the nano-enhanced salt hydrate-based PCM. The base salt used here was magnesium nitrate hexahydrate ($Mg(NO_3)_2 \cdot 6 H_2O$). The nanoparticles used were nano graphite (NG) (0.1-0.6 wt.%) and MWCNT (0.1-0.2 wt.%). The stabilizing agent used was nano-cellulose. It was observed that thermal conductivity was improved and the rate of heating was fast. The melting and solidification rate was enhanced by 48 % and 77%, respectively. With 0.6 wt. % nano graphite, the increment was 24% and 15%, respectively.

(Tian et al. 2016) prepared a nanocomposite PCM with binary eutectic chloride (NaCl–$CaCl_2$) using EG. It was observed that with the increase of the EG content, the SHC and the latent heat of the nanocomposite decreased. With 0.5-20% of EG, the decrease of latent heat was 2.98%. to 19.25%. However, with the increase in the EG content and density, the thermal conductivity value increased linearly. With the addition of 20% expanded graphite, the thermal conductivity value of the composite was 4.937 W/mK which was 700% more as compared to the base salt.

(Sudheer and Prabhu 2017a) hand-mixed graphite nanoparticles into pure KNO_3. A 40% increase in thermal conductivity was observed. Ball milling was also employed for the nano-PCM preparation. It was observed that the ball milling method had no significant effect on the time for solidification. However, the discharging rate was high over 10 thermal cycles compared to the hand-mixed nano salt.

Reduction in subcooling by 92-98 % was observed when graphene oxide nanosheets were added to $CaCl_2.6H_2O$.(Jin et al. 2018)

(Xiao et al. 2015) studied the effect of the addition of expanded graphite to pure $NaNO_3$ and binary nitrates (50% $NaNO_3$-50% KNO_3). They observed that the composite PCMs resulted in a remarkable increase in thermal conductivity. With 5%, 10%, and 20%, the thermal conductivity was two times, four times, and seven times respectively. The thermal conductivity values decreased with the temperature rise.

(Kant et al. 2017) studied the addition of 1%, 3%, and 5% graphene nanoparticles to organic, inorganic, and paraffin PCMs. The inorganic PCM used in this work was $CaCl_2.H_2O$. An enhancement in the thermal conductivity of the NePCM was observed. Phase change properties were also improved. The melting rate was observed to improve

but the increase was not much significant. The addition of nanoparticles leads to a rise in both viscosity and conductivity. At higher concentrations, the negative effect of the increase in viscosity is comparable to the positive impact of thermal conductivity enhancement.

The addition of expanded graphite to salts systems of $LiNO_3$-KCl, $LiNO_3$-KNO_3, and $LiNO_3$-NaCl by solution impregnation method was studied by (Zhong et al. 2014). The thermal conductivity was 4.9-6.9 times higher than the base salt. Higher thermal stability was also observed.

(Huang et al. 2014) added expanded graphite (EG) to $LiNO_3$-KCl. No significant effect was seen in the melting temperature of the salt. The thermal conductivity was 1.85-7.56 times higher than the base salt, and its values varied with the mass fraction of the EG added. The phase change enthalpy values obtained were in the range of 142.41-178.10 J/g and were dependent on the mass fraction of EG.

0-5% of EG was added to the salt system of NaCl-$CaCl_2$-$MgCl_2$, and the effect was studied by (Tian et al. 2015). The value of SHC decreased with the mass fraction of EG added and temperature. A reduction in latent heat in the range of 17.5% to 0.97% was observed with the mass fraction of EG. The thermal conductivity obtained was 1.35-1.78 times higher than the base salt.

(Acem et al. 2010) physically mixed EG particles to the salt eutectic system of KNO_3-$NaNO_3$. The thermal conductivity of the NePCM was 20 times higher than the base salt with 15-20 wt. % of EG.

2.3.2. Other nanoparticles

The solar salt, when dispersed with nanoparticles of SiO_2, Al_2O_3, TiO_2, SiO_2+Al_2O_3 showed an improved specific heat capacity and enhanced thermal properties. The dispersion of these nanoparticles played an essential role in this improvement. The nanoparticles were added with the volume fraction of 0.5, 1, 1.5 wt.%. It was observed that SiO_2+Al_2O_3 had a more significant effect in enhancing the thermal storage characteristics of the salt (specific heat capacity). The increment reported was 57 % in the solid phase and 22 % in the liquid phase. A high amount of interaction was seen between the salt and the

nanoparticles, which is the reason for the enhanced heat capacity, which will cut down the cost of electricity. (Chieruzzi et al. 2013)

The effect of the addition of SiO_2 nanoparticles only was studied by (Andreu-Cabedo et al. 2014). It was observed that with 1% addition of nanoparticles by weight, the specific heat capacity of the PCM increased by 25 %. In many research studies, it was suggested that there has to be an optimum weight percentage of the nanoparticles that could be added to the salts to obtain improved thermal parameters. Any addition beyond this optimum value will lead to a decrement in the properties. The thermal cycling stability of the nano-enhanced salts was also investigated. The thermal cycles employed in the study were eight successive cycles. The increment of specific heat capacity of the nano-enhanced PCM was attributed to the theory of the formation of nanolayers. According to the theoretical model, the ions of the base salt PCM orient themselves around the nanoparticle forming fractal-like structures called nanostructures. This was due to the electrostatic interactions between the nanoparticle and the salt ions.(Lasfargues et al. 2015) (Andreu-Cabedo et al. 2014).

(Lasfargues et al. 2015) studied that the mechanical dispersion of the nanoparticles also affects the thermal properties of the salt, like the specific heat capacity. The salt considered was the eutectic mixture of KNO_3 and $NaNO_3$. The nanoparticles considered were CuO and TiO_2. The results showed improved specific heat capacity in both conditions. Agglomeration of the nanoparticles was visualized in CuO but not in TiO_2. This clustering was responsible for the enhancement of the specific heat capacity. The size and shape of the nanostructures formed impacted the energy storage density of the salts.   CuO impact on SHC was concentration-dependent where only 0.1% addition led to an increase in SHC, but as the concentration increased to 1.5% the SHC value decreased. No such dependency was seen in TiO_2.

It was also observed that with a higher concentration of nanoparticles, the heat of fusion value decreased. This is due to the dispersion of nanoparticles and size and the presence of clusters of nanoparticles which changed the entropy of the system. The dispersion of nanoparticles was observed by the Energy dispersive X ray analysis (EDAX) mapping and the clustering in CuO by SEM images. With TiO_2, large interconnected layers were observed rather than agglomeration. Clustering holds the key to the thermal conductivity enhancement in NePCM. This was experimentally investigated. (Gao et al. 2009)

The thermophysical properties of the NePCM of KNO_3 and the dispersion of the nanoparticles in the salt were studied. The nanoparticles added were silica and alumina of concentration 1wt% but of different sizes, i.e., 7, 13, 20-200 nm, respectively. They observed an enhancement in specific heat values, out of which silica was recognized to have significant potential for improving the TES characteristics of KNO_3.

The phase transformation temperature was also lowered by 3°C with an increase in latent heat value by 12% with the addition of silica particles. SEM and EDAX tests showed that the silicon particles were uniformly distributed, and clustering was seen in the case of silicon addition. (Chieruzzi et al. 2013)

(Myers et al. 2016) studied the thermophysical properties, chemical stability, and thermal performance of the Nano-enhanced salt nitrate salts. Here CuO was taken as the nanoparticles and the salts were KNO_3, $NaNO_3$, and the eutectic of KNO_3 and $NaNO_3$. With the addition of 2% by volume of CuO, they observed enhanced thermal diffusivity and thermal conductivity. It was also observed that the addition of nanoparticles' chemical stability and thermal performance was improved.

The thermal properties and thermal performance of the quaternary molten salt KNO_3-$NaNO_3$-$NaNO_2$ with three different combinations of additives and weight was studied for use as Heat transfer fluid. (Peng et al. 2009)

(Lasfargues et al. 2016) studied that when a simple primary precursor of $TiOSO_4$ with a different concentration is added to the solar salt, then in-situ TiO_2 nanoparticles of size 16 nm are produced, which improves the thermophysical properties of the salt. The production of TiO_2 was ensured using EDAX.

An enhancement in specific heat was seen in the ternary salt mixture of $LiNO_3$ +$NaNO_3$+KNO_3 when doped with 1% SiO_2 nanoparticles of size 60nm. The thermal characterization of the sample was done with DSC. A 13% increase in specific heat was observed. This increase was due to the fractal-like nanostructures of eutectic formed near the embedded SiO_2 particles. These structures have a large specific surface area as a result of high surface energy. This leads to an increase in specific heat and in turn thermal energy storage capacity.

When these nanoparticles were added to ethylene glycol and water anomalous behavior of nanoparticles addition was seen where thermal conductivity increased but specific heat decreased. But in the case of molten salts, both the parameters increased. This anomalous behavior was also reported by other researchers. SiO_2 nanoparticles were preferred as they are thermally stable, cheap, and less toxic. This ternary salt has the highest specific heat and low melting point among all other ternary systems, so this salt was considered. (Seo and Shin 2014)

(Tiznobaik and Shin 2013a) The specific heat capacity of the Nano-enhanced high-temperature molten salts was enhanced by the addition of SiO_2 particles in the eutectic mixture of $LiCO_3$ and KCO_3. The studies were done with nanoparticles of different sizes of 5, 10, 30, and 60nm. These nanoparticles in the salt system form needle-like structures with an increased surface area, increasing their specific surface energies. Due to this, an enhancement of nearly 25% in specific heat capacity is seen for all sizes of nanoparticles.

2.4. The mechanism involved in the enhancement of thermal parameters in nano-enhanced salt phase change materials

The particle size of the nanoparticles and the temperature affected the SHC value of the nano-enhanced salt PCM. This effect was studied and investigated by (Wang et al. 2006). They reported that the SHC value increased with an increase in temperature and decreased with the increase in the size of the dispersed nanoparticles, i.e., the smaller size of the nanoparticles led to higher enhancement in the SHC value.

It is believed that the salt ions form a semisolid ordered network around the nanoparticle which is called a nanolayer. The anomalous increase in the SHC value is due to this nanolayer formation. Another reason for the rise in SHC value is the latent heat of the salt entrapped in this nanolayer. This ordering of the salt ions around the nanoparticle surface has been a subject of interest. (Oh et al. 2016) proved this nanolayer formation theory in his work which makes this theory entirely accurate and reliable.

A strange chain-like layered structure(nanolayer) in nano-enhanced salts after a thermal cycle was observed in SEM by (Shin and Banerjee 2014). Such arrangements were not present in the base salt structure. They proposed a modified model to estimate the SHC value of the nanofluid, as shown in equation 2.1.

$$C_{P_{nf}} = W_{np} \cdot C_{P_{np}} + W_{ns} \cdot C_{P_{ns}} + (W_s - W_{ns}) \cdot C_{P_s} \qquad (2.1)$$

where, nf= nanofluid, np= nanoparticle, ns = nanolayer region, s = base salt, W= mass fraction.

(Hentschke 2016) proposed a theory based on the meso layer. In this, it was assumed that the nanoparticles influenced the surrounding base liquid in the long range. This layer of ordered atoms in the liquid also led to a slight increase in the SHC value. This was possible only when the nanoparticles were capable of having a long-range influence. With the rise in the concentrations of nanoparticles, these layers can overlap each other. This explains the optimum weight percentage of nanoparticles up to which the SHC values increase, as reported by many researchers.

Nanoparticles themselves can also be a reason for the increased SHC value of the NePCM, (Lasfargues et al. 2015). Nanoparticles themselves possess a higher SHC value than the larger grained particles of the same material. The value of SHC is also material structure-dependent. The vibrational entropy and configurational entropy which is affected by the surrounding or the neighbor configurations, also affect the SHC value of the material. In nano-grained particles, the no of atoms exposed to the surface is more because nanoparticles have a higher surface-to-volume ratio. The atoms at the surface are always less restricted as compared to the center atoms. Due to this, the nanoparticle structure possesses higher energy when compared to large-grained particles. The surface atoms of the nanoparticles have more volume to expand; therefore, nanoparticles have twice the value of thermal expansion compared to larger grained particles.

The nanoparticles morphology also affects the SHC of the nano salts. The SHC of the nano salts sample was measured as a function of morphology and sonification power. An 18% enhancement in the SHC of the nano salts was seen by controlling these two factors. (Riazi et al. 2016)

The increment of SHC in certain metal oxides, metal, and zeolite nanomaterials was investigated and compared with their corresponding larger grained materials (Tan et al. 2009). It was concluded that the nanoparticles showed higher SHC due to the high surface area to volume ratio. Many parameters such as density, thermal expansion, purity of the sample, particle size, and surface absorption led to the enhancement of SHC. The thermal

resistance offered by the interface also leads to the enhancement in the SHC value. The nanoparticles possess higher surface energy, so a system with well-dispersed particles would have a higher energy density than the agglomerated systems.

(Tiznobaik et al. 2015) in their study inferred that when nanoparticles are added to the salt, the nanoparticles induce preferred surface adsorption of different chemical species of the base salt. This creates local segregation among various chemical components. This adsorbed layer has superior thermal and chemical properties. This layer grows to form long-range secondary dendritic nano-structures originating from the nanoparticle surface, increasing the SHC of the salt-based nanoparticles.

The process of these dendrite formations is depicted in Figure 2.9 below.
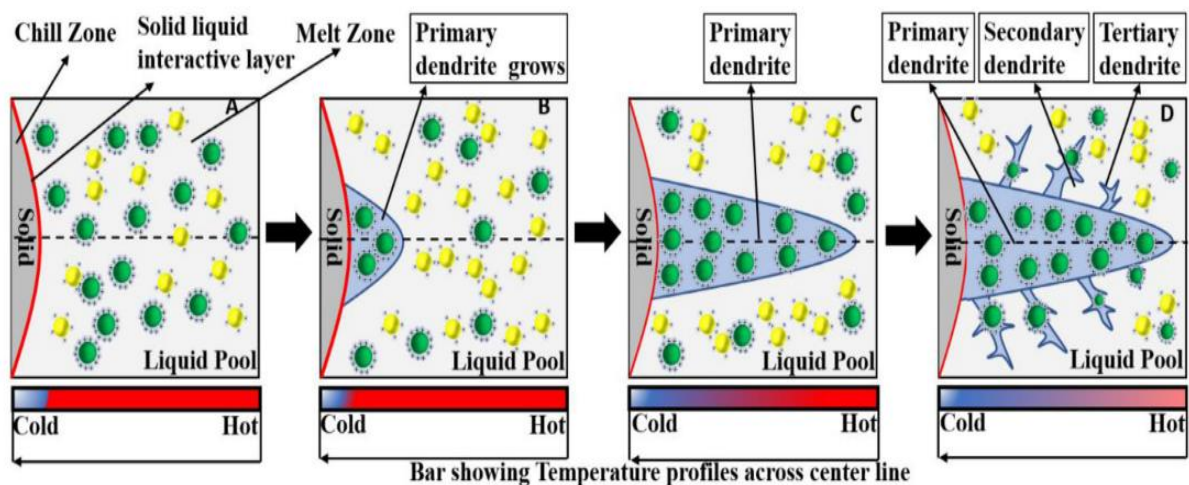
Figure 2.9: A schematic representation of the formation of primary, secondary, and tertiary dendritic nanostructures (Rizvi and Shin 2020)

(Shin and Banerjee 2010) did a study on the agglomerated and non-agglomerated salt-based nanofluids. They observed that the rise in the SHC values was more in non-agglomerated samples than the agglomerated ones. The degree of agglomeration of nanoparticles and the compressed phase formation affected the SHC values.

The anomalous behavior of the SHC values and the various mechanisms behind it was studied by (Shin et al. 2014). They observed that SHC values that decreased in the case of

organic nanofluids increased in salt NePCM. This observation was studied and explained in detail in this work.

(Tiznobaik and Shin 2013b) in his study experimentally validated the mechanism responsible for the increment in the SHC value.

(Tiznobaik and Shin 2013a) observed needle-like structures of nanoparticles with a higher surface area. Due to this, the specific surface energy increased. This led to an enhancement in the SHC value of the nanofluids.

In this work, the dispersion and the stability of the nanoparticles in the base fluid were confirmed using SEM. Nanoparticles formed a percolation network due to their high specific surface energy. This network was suggested to be the reason for the SHC value enhancement. (Shin and Banerjee 2011a)

The formation of percolation network, nanostructures, and presence of additional TES due to the interfacial resistance developed in between the surface of the nanoparticles and the surrounding base salt particles called Kapitza resistance was attributed for the increment in the SHC values. (Shin and Banerjee 2011b)

(Zhang et al. 2016) suggested the formation of a high-density lamellar structure at the nanoparticle surface to be the reason for the increment in the thermal parameters of the nano-enhanced salt.

(Mondragón et al. 2018) in his study proposed that the increment in the SHC value of the NePCM has a relationship with the ionic exchange capacity of the nanoparticles. Nanoparticles possess high specific surface, reactivity, and ionic exchange capacity due to which they are used as an adsorbent in many chemical applications to remove the nitrate ions. The adsorption of nitrate ions on the surface of the nanoparticle is based on the ionic exchange capacity mechanism and was confirmed in this work using FTIR.

In NePCMs, the strong intimate inclusion of nanoparticles in salt PCMs can change the van der walls forces when the concentration of nanoparticles is high. If the salt-nanoparticle interaction potential is higher than that between the salt molecules themselves, an increase in the latent heat is expected. (Shaikh et al. 2008)

The same mechanism was supported by (Hamdy et al. 2017) for the rise in the latent heat values. The decrease in the latent heat in some studies was attributed to the reason that when a high concentration of nanoparticles is added, nanoparticles get trapped and form agglomerates, which affect the latent heat by altering the system's entropy. The presence of nanoparticles in salt PCMs leads to the formation of fractal-like nanostructures which serve as the heat conduction links in the NePCM, leading to an increase in the thermal conductivity values.

From all the above research studies and discussions, it is evident that the improvement in the SHC value was majorly due to the nanolayer formations and the grain structure of the nanomaterial. There are many other factors too that have a positive influence on the property, as already discussed. The intermolecular attraction between the nanoparticles and the salt and conduction links due to the fractal nanostructures are responsible for the increment in the latent heat and thermal conductivity, respectively. Detailed research is needed, and further studies are required to evaluate and estimate each variable's influence on the PCM's thermal parameters. It should be noted that the reliability of the estimations would depend upon the chosen characterization or measurement technique.

2.5. Characterization of phase change materials

Thermal characterization of the PCMs is the main factor while designing proper and final constructive TES systems. Most of the PCMs used in the TES systems are not pure materials, and they change their phase over a temperature range, unlike pure materials, which melt at a fixed temperature. To incorporate the material in the TES systems, the temperature-dependent stored thermal energy is an essential parameter, as discussed by (Mehling and Cabeza 2008).

To choose a PCM and incorporate it into the TES systems, one should know the properties of the materials used. The most important property to be known is the phase change temperature of the materials. The energy storage density of the material is well-determined majorly by four parameters which are the SHC in solid-state (c_{ps}), SHC in a liquid state (c_{pl}), melting temperature (T_m), and the phase change enthalpy or the latent heat (Δh). Thermal conductivity is also one parameter that is very important for the PCM selection for TES applications. Many PCMs do not undergo phase change at a particular temperature rather, they melt over a range called a melting range, so the phase change enthalpy in such

PCMs is attributed to the entire melting range which is given by temperature-dependent (h (T)). This is depicted in Figure 2.10.
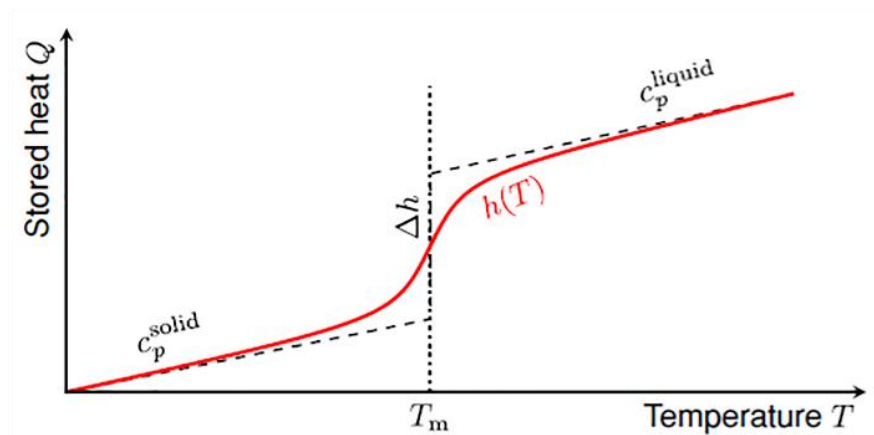
Figure 2.10: The storage density (Q(T)) of a pure PCM (dashed) with latent heat (∆h) and PCM melting over a range of temperatures with latent heat as h(T). (Günther et al. 2009)

Calorimetric methods

The most commonly and widely used calorimetric method for the thermal characterization of the TES materials is Differential Scanning Calorimetry (DSC) in step mode and dynamic mode and the T-history method.

2.5.1. Differential scanning calorimetry (DSC):

 The most conventionally and widely used method for the thermal analysis of the PCMs is the DSC. The parameters that can be estimated from DSC are the phase change temperature, phase change enthalpy, and SHC. DSC can be of two types, namely power compensating and heat exchanging calorimeters based on the working principle involved. The power compensating calorimeter utilizes an electric heater to compensate for the temperature difference developed between the reference material and the TES sample. The heat exchanging calorimeter also called the heat-flux DSC (hf- DSC) is the most commonly used type of DSC. This calorimeter measures the difference in heat exchanged between the sample and the environment and between the reference material and the environment.

The hf-DSC can operate in two different modes 1. Dynamic mode 2. Step mode.

In dynamic mode, the temperature of the sample is made to vary from an initial value to a final value keeping the rate constant. To measure specific heat, the heating rate is maintained at 2-10 K/min. The signal obtained is proportional to the temperature difference between the reference and the sample. The temperature-dependent SHC is measured using reference material. The accuracy of the estimated values depends on the rate of heating and the size of the sample used.

In step mode for the determination of SHC, stepwise heating of the furnace in a given interval of temperature is adopted. In this, the sample follows the step with a slight delay, and then a signal is detected. After this, the next step comes, and the furnace heats up. The area enclosed under the peak is directly proportional to the heat taken up by the sample in that particular step. This heat is calculated stepwise over the entire temperature range and then added, giving us the heat storage capacity values. A better accuracy and temperature resolution can be obtained by reducing the step size. (E. Günther, S. Hiebler 2004) (Günther et al. 2009)

A simplified diagram of the experimental setup of DSC and a DSC thermogram is represented in Figure 2.11 and Figure 2.12, respectively. In Figure 2.12, the T1 and T2 are the temperatures corresponding to start and end of solidification points, and Tm is the phase change temperature. ΔH is the latent heat.
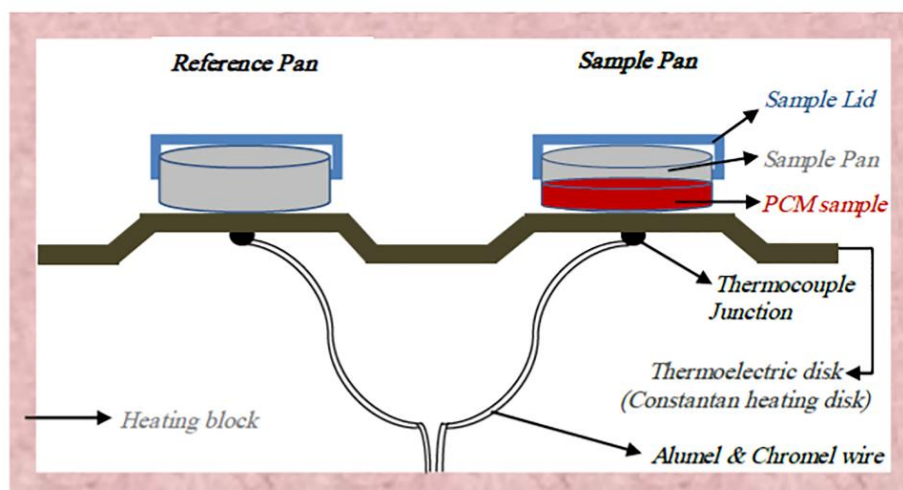
Figure 2.11: A Schematic diagram of a typical DSC chamber (Mohammad and Saeed 2016)
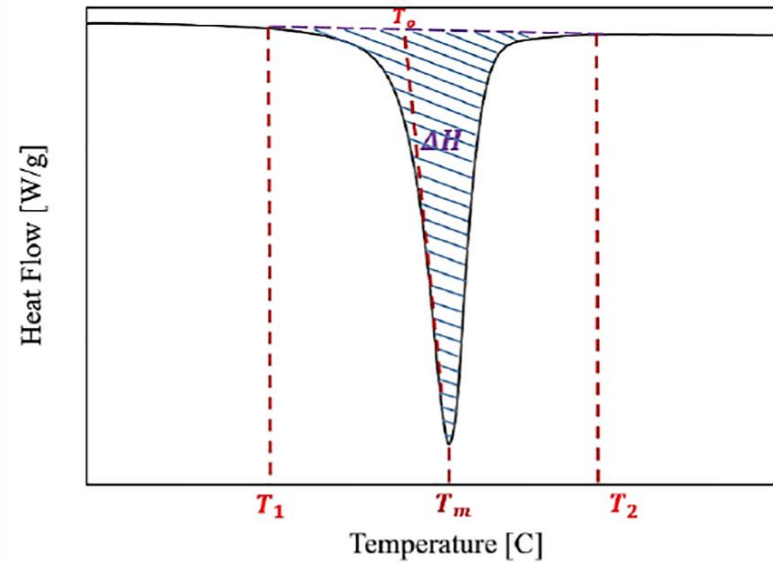
Figure 2.12: Typical characteristics of a DSC thermogram (Mohammad and Saeed 2016)

(Barreneche et al. 2013) investigated the effect of two DSC operation modes i.e. dynamic and step mode, on common PCM material (paraffin and salt hydrates). In the case of paraffin, no significant difference was observed, but with salt hydrates, a slow dynamic mode was recommended over the step mode in DSC.

Other than this hf-DSC there is one more type of DSC called the temperature modulated DSC (m-DSC). In this, the temperature of the sample is modulated to achieve a signal which is used to measure the heat flux. This obtained signal is not dominant enough to affect the already investigated thermal characteristics. (Mehling and Cabeza 2008)

SHC measurements are done in DSC using three different methods. i.e., Dynamic method, Isostep method, and Areas method (Frazzica and Cabeza 2019), and it is represented in Figure 2.13.
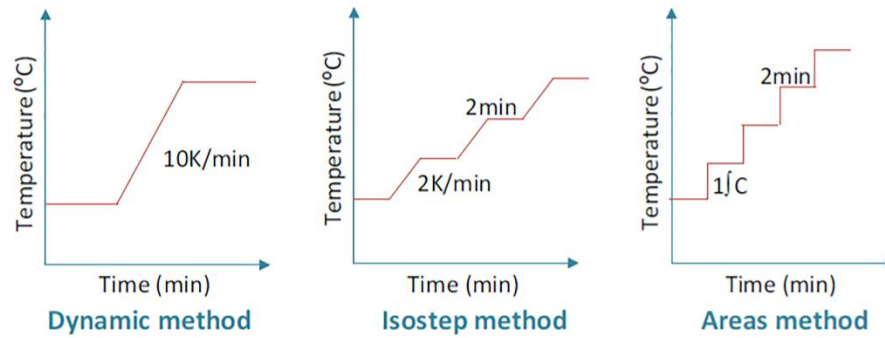
Figure 2.13: DSC methods for SHC measurements (Frazzica and Cabeza 2019)

- **Dynamic method:** In this method, a temperature range is chosen and a constant and high value of heating rate is used for a small sample size.

- **Isostep method:** In this method, the temperature is increased 1 K by 1 K by 120 s isothermal steps. The heating rate value used in this method is 2 K/min.

- **Areas method:** In this method, the increase in temperature is 1 K by 1 K without applying any value of heating rate between them.

(Ferrer et al. 2017) presented a new methodology for the estimation of SHC values of PCMs using DSC. Three different DSC methods were employed, and their results were compared to assess their suitability. Materials used in this study were salts, water, and potassium nitrate. It was observed that by using the areas method, the error value was lower than 3 %. Dynamic and isostep methods gave error values of 6% and 16%, respectively. This was due to the sensitivity issue during the measurements.

Lots of researchers have used this DSC technique for the thermal characterization of salt-based PCMs and nano-enhanced salt-based PCMs to date.

The major drawback in the usage of DSC is the limitation on the sample size used, which is in order of milligrams (=30). In the case of inhomogeneous materials, the DSC results obtained reflect the thermal characteristics of the sample used only, not of the entire amount of material used. Thermal response from DSC also gets influenced by the small sample size. In DSC, the supercooling is overestimated which leads to a reduced latent heat value data. This is another drawback associated with the DSC method. The results obtained from DSC are very much affected by the rates of heating and cooling used during measurement

and in turn, also affect the measured values. This effect of size of the sample and rate of heating was studied by (Günther et al. 2009) and is represented in Figure 2.14.
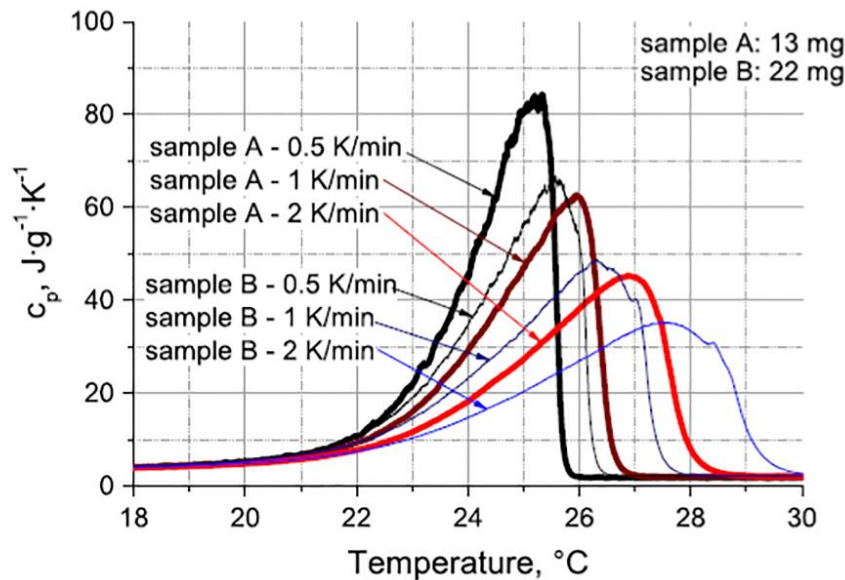
Figure 2.14: Effect of sample size and rate of heating on a substance using DSC measurements. (Günther et al. 2009)

The estimated values are not very much repeatable while analyzing inhomogeneous samples. For example, in inhomogeneous composite materials, the main constituent of composite interferes with the thermal response DSC signals. The phase change happening during the analysis cannot be visually observed. The study of instrumentation is also very complex and expensive. (Yinping et al. 1999)

In CSP installations, TES units utilize TES material in bulk (in tonnes), which underscores the need to develop new and novel characterization techniques for determining the SHC and phase change enthalpy of the material. Due to these shortcomings, researchers are looking for alternative characterization techniques involving larger samples to investigate inhomogeneous materials. One such technique is the temperature history method, also called as T-history method. (Solé et al. 2013) (Sudheer and Prabhu 2016)

2.5.2. T-history method

This method was first used and suggested by (Yinping et al. 1999). It is a simple and inexpensive method to determine the heat stored in PCM as a function of temperature. In

this method, the sample material and a reference material whose properties are known are heated above the PCM phase change temperature and then subjected to air cooling. The thermal history during this process is recorded. The thermal history curves obtained are compared and analyzed, assuming that the heat transfer coefficients between the sample and the ambient and the reference material and the ambient are the same. Thus, the heat stored within the material is estimated. The values of the SHC, phase change enthalpy, and the melting temperature are taken as constant in this method.

This technique was improvised by (Marín et al. 2003), in which the SHC and enthalpy as a function of temperature were calculated, unlike Yinping's method following the same experimental procedure. The samples were kept in an environment where the temperature was controlled. This helped in improvement in data accuracy and also allowed the thermal characterization during both the heating and cooling process. These temperature-dependent properties are important to estimate the storage capacity of the PCMs. The advantages observed by using Marin's setup were that the SHC as a function of temperature was taken into account, error value was reduced as the convection coefficient was not taken to be constant, unlike Yinping's method, SHC in both the solid and liquid states could be estimated. The disadvantages observed were that the accuracy of the temperature sensors was not up to mark. Due to low diameter, thermocouples were used, which can lead to some errors. The significant radiation effect was not taken into account. This effect of radiation could be minimized by coating the external walls of the tube with metallic materials. (Marín et al. 2003)(Badenhorst and Cabeza 2017).

Later (Solé et al. 2013) reviewed the evolution of the temperature history method and explained the experimental arrangements and various modifications done to date. The T-history experimental setup used by (Yinping et al. 1999) and (Marín et al. 2003) is shown below in Figures 2.15 and 2.16.
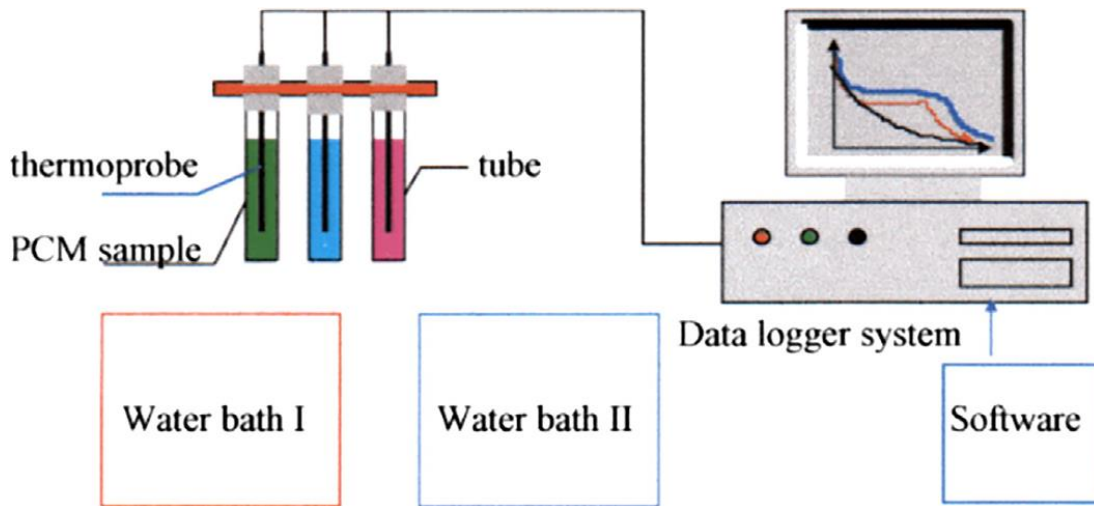
Figure 2.15: Experimental set up of T-history method (Yinping et al. 1999)
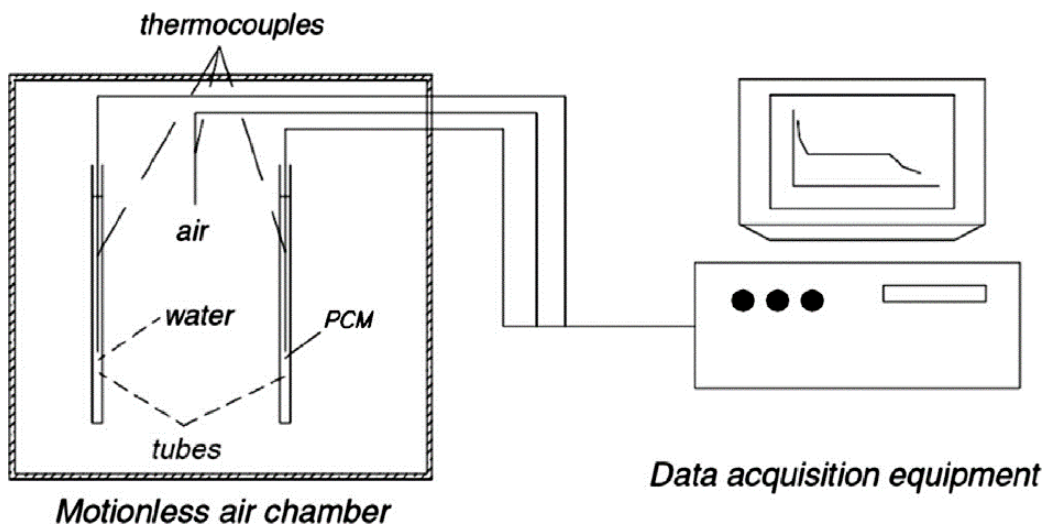
Figure 2.16: Experimental set up of the modified T-history method (Marín et al. 2003)

The thermal performance of salt mixtures based on Glauber's salt was performed using the Temperature history method. The reference material used here was water. (De Paola et al. 2017)

(Jansone et al. 2018) studied four PCM samples using the T-history method. Out of these four samples, two were organic PCMs and two were inorganic salt PCMs. The reference material used was water.

Some serious limitations are also associated with this method due to which the method could not be of much help for high-temperature PCMs. In this method, the choice of reference material to be used is also a drawback. The T –history method uses a reference material whose properties such as SHC, thermal coefficient of expansion, thermal conductivity, etc. are known in the concerned temperature range. In the case of high-temperature research, reference material such as water or low carbon organic materials cannot be used as they may vaporize easily when the temperature is above 423 K. Low temperature melting metals, alloys such as alloys of Ga, In and heat transfer fluids such as liquid Na, NaK cannot be used as they are very costly. Organic compounds with high carbon are a suitable choice, but these compounds are highly inflammable, and their melting point increases as you increase the number of carbon atoms. In this method, even the container material has to be chosen carefully. Any kind of chemical interaction between the sample PCM material and the container must be studied over a broad range of temperatures. At present, such a detailed and elaborate dataset is not available. To avoid such chemical interactions, borosilicate and quartz can be used, but due to their brittle nature and susceptibility to breakage/failure at elevated temperatures, they are not an appropriate option.

Containers made of ceramics can be a good choice for such conditions, but unfortunately, a cylindrical container with L'/D >16 is required in this method. The production of ceramic cylinders of such dimensions seems impossible. Thus the development of a reference material suitable for a wide range of temperatures, for example, 473-1273 K does not appear feasible. (Sudheer and Prabhu 2016) (Mehling and Cabeza 2008)

Due to these limitations, a new technique called Computer-Aided Cooling Curve Analysis (CACCA), based on the thermal analysis and cooling rate curves for PCM thermal characterization, has been investigated by researchers.

2.5.3. Computer-aided cooling curve analysis

Computer-aided cooling curve analysis (CACCA) is a technique of thermal analysis that is very effective in the rapid evaluation of several temperature-dependent thermal characteristics of the PCMs. The thermal events of heating or cooling are directly related to the phase change happening within the sample forms the basis of this technique. The

thermal analysis technique monitors the temperature change in the sample as it cools during the phase change range.

With CACCA thermal analysis technique, databases can be created for PCMs with various chemical compositions. This method is quite simple, cheap, and provides consistent results. Owing to these reasons this method can be used for multiple commercial applications.

The information that can be obtained using this thermal analysis technique is the alloy composition, the phase change enthalpy, the solidifying phases, and the dendritic coherency. The distance between the dendrite arm, the degree of granular modification and refinement, the start and end of solidification temperatures, and the characteristic temperatures associated with the eutectic region and intermetallic phase changes can also be determined using CACCA thermal analysis technique as described by (Malekan and Shabestari 2011).

Newtonian and the Fourier methods are the two methods that have been successfully used to analyze and calculate the thermal characteristics of the PCMs using the CACCA thermal analysis technique as its basis. The local temperature gradient developed in the sample is not considered in the Newtonian technique during the phase change. Meanwhile, the Fourier technique takes into consideration the thermal gradient effect that develops during the cooling process. This indicates that the estimations of Fourier and Newtonian methods are considerably different. One thermocouple at the center of the sample is employed in the Newtonian method, while the Fourier technique uses at least two thermocouples, one in the middle and the other at a distance from the center. (Carlson and Beckermann 2012)(Gibbs and Mendez 2008)(Barlow and Stefanescu 2002)(Stefanescu 2015) (Palkowski and Günther 2005)

The thermocouples record the thermal behavior of the sample PCM, and thus the cooling curve is obtained. The information attained from the cooling curves is the phase change temperatures. The first derivative curve (FDC) or the rate of cooling curve is the most important tool in CACCA thermal analysis technique. In the cooling rate curve, the transition temperatures appear as a kink accompanied by a significant slope change. Nucleation is the reason for the rise in the slope, while a drop in slope indicates cooling or remelting of the PCM. Loops in the curve are indicative of the undercooling, whereas eutectic transitions appear as straight lines. (Sudheer and Prabhu 2016).

2.5.3.1.   Newtonian Technique

The Newtonian technique is a simple CACCA method that uses a thermocouple at the center of the sample to obtain a thermal history or PCMs cooling curve. The assumptions involved in the Newtonian technique are listed below, as described by (Djurdjevic et al. 2011):

- The sample under consideration is assumed to be a lumped thermal system whose Biot number is less than 0.1. The lumped thermal system assumes an even distribution of temperature in the test sample during cooling.

- The SHC of the sample is assumed to be temperature-independent and maintains a constant value during the solidification of the PCM.

- The heat transfer coefficient from the PCM sample to the environment can be characterized using temperature under certain experimental conditions.

From the experiment, the thermal history or the cooling curve can be obtained. The FDC of the cooling curve obtained is an essential aspect of the thermal performance of PCM. The start and end of the phase transformation appear as sharp peaks at FDC, while the area enclosed in the FDC can be utilized to estimate the net heat loss from the sample into the mold.

In this Newtonian technique, another curve is required apart from the FDC of the sample which is called Zero Curve (Z_C) or the base-line. This baseline is essential for the determination of the latent heat of the sample PCM. This Z_C, is imaginary and in principle, is the cooling rate curve wherein it is assumed that the sample did not undergo any phase transition between the solidification temperature ranges. The calculation of this baseline is a very critical subject in CACCA. The difference in area between the cooling curve and Z_C rate is used to calculate the enthalpy of the phase change/heat evolved during the phase change. (Sudheer and Prabhu 2015)

The energy balance equation for the sample-mold system during solidification can be given as:

$$\frac{dQ}{dt} - mc_p \frac{dT}{dt} = UA(T - T_o) \qquad (2.2)$$

where m is the sample mass, c_p is the SHC of the material, T is the sample temperature, U is the overall heat transfer coefficient, t is time, T_0 is ambient temperature, A is sample surface area, and Q is the rate of heat released during phase change.

When no phase change is involved, then the heat of fusion evolved is 0, i.e. *dQ/dt* = 0, then the cooling rate of the PCM can be written as equation 2.3, which represents the "**Newtonian zero curve**" or the **Baseline** (Z_C).

$$\frac{dT}{dt} = \frac{-UA(T - T_o)}{mc_p} = Z_C \qquad (2.3)$$

To obtain the Z_C, the first derivative curve (FDC) has to be fitted, which is generally done by three methods; (i) Polynomial Fitting, (ii) Experimental Fitting, (iii) Curve Fitting. (Ihsan-ul-haq et al. 2004) in their work have discussed that, results obtained by modes of exponential fitting and second-order polynomial fitting are quite inaccurate and inconsistent. On the other hand, by linearly fitting the FDC, the results obtained were accurate and reproducible.

The Baseline and the FDC of the base PCM trace the same path for temperatures before the start of the solidification/liquidus point and after the end of the solidification/solidus point. The integral area difference between the FDC and Z_c curves represents the phase change enthalpy of fusion of the PCM sample as given in equation (2.4). The fraction solidified (f_s) can also be obtained from equation (2.5).

$$H = c_p \int_{t_s}^{t_e} \left(\frac{dT}{dt} - Z_C\right) dt \qquad (2.4)$$

$$f_s = \frac{c_p \int_{t_s}^{t_e} \left(\frac{dT}{dt} - Z_C\right) dt.}{H} \qquad (2.5)$$

A schematic diagram of the experimental setup used for the Newtonian and Fourier technique is shown in Figure 2.17.
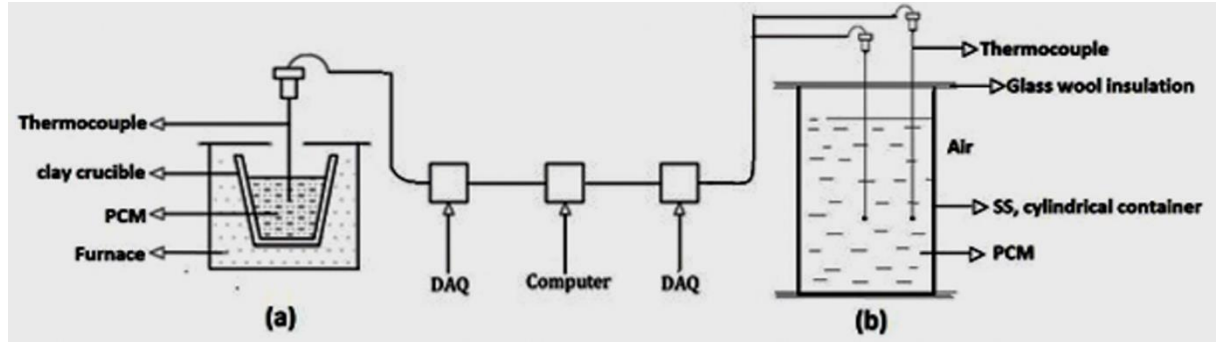
Figure 2.17: Schematic diagram of (a) Newtonian Technique, (b) Fourier Technique setups. (Sudheer and Prabhu 2016)

2.5.3.2.   Fourier Technique

The theory of the Fourier thermal analysis technique was initially proposed by (Fras et al. 1993). The Fourier equation with heat generation from the heat source can be written as equation (2.6), which can be rearranged as equation (2.7) where α is the thermal diffusivity, C_v is the specific heat capacity at constant volume of the material, BL_F stands for Fourier baseline in equation 2.7.

$$\frac{\partial T}{\partial t} = \alpha \nabla^2 T + \frac{1}{C_v} \frac{\partial Q}{\partial t} \tag{2.6}$$

$$\frac{\partial Q}{\partial t} = C_v \left(\frac{\partial T}{\partial t} - BL_F \right) \text{ where } BL_F = \alpha \nabla^2 T \tag{2.7}$$

A baseline or zero curve is an imaginary line that connects the start and endpoints of solidification in the sample's FDC, assuming that no latent heat has been released during solidification. The area under the FDC and its corresponding baseline curve (BL_F) is calculated, and the difference in these two areas will give the latent heat evolved during solidification.

In transient heat conduction, the thermal distribution within a mold (cylinder) with sample PCM depends on both the axial and the radial coordinates (z, r, and θ), and also on the time t. By maintaining the L'/D ratio of 4 or more of the cylindrical mold, it can be ensured that the heat transfer will take place radially (r axis). This makes the process axisymmetric and the thermal distribution independent of the angular coordinate. The sample's radial solidification is an important factor in the Fourier technique. (Sudheer and Prabhu 2017b)

49

The Transient Heat conduction equation, with no source of heat generation in a sample of cylindrical shape with a ratio of L'/D equal to 5, can be represented by Equation (2.8). In the Fourier technique, the thermal distribution at any point of time within the sample is parabolic and can be stated as $T = Ar^2 + B$, where r is the sample radius. This fact can be used in the calculation referred to in Equation (2.9).

$$\nabla^2 T = \frac{1}{r} \frac{\partial}{\partial r} \left(r \frac{dT}{dr} \right) \tag{2.8}$$

$$\nabla^2 T = \frac{4(T_2 - T_1)}{r_2^2 - r_1^2} \tag{2.9}$$

$$\alpha = \frac{\frac{\partial T}{\partial t}}{\nabla^2 T} \tag{2.10}$$

$$H = \int_{t_s}^{t_e} \frac{\partial Q}{\partial t}(t) dt \text{ where } \frac{\partial Q}{\partial t} = C_v \left(\frac{\partial T}{\partial t} - BL_F \right) \tag{2.11}$$

Using the thermal history data acquired using thermocouples placed at two different radii R_1 and R_2, the value of thermal diffusivity can be calculated from Equation (2.10). Equation 2.11 represents the latent heat calculation where the difference in the integral areas of FDC and BL_F was used. The CACCA thermal analysis technique has been studied extensively by (Sudheer and Prabhu 2016) and (Djurdjevic et al. 2011).

It was observed that the Fourier technique was more reliable and accurate for thermal characterization than the Newtonian technique as the Fourier method is independent of the experimental procedure used or the sample cup used. In Fourier analysis, the actual thermal history of the material recorded using two thermocouples is used incorporating the thermal gradient, unlike the Newtonian method.(Palkowski and Günther 2005)

Both Newton and Fourier techniques involve calculating zero curves or imaginary curves, which are also known as baselines. This baseline calculation includes linear fitting of the solidification points and their proper selection. The obtained results are strongly influenced by the fitting technique used and the selection of the start and end of solidification points, which are the primary sources of error in the calculated values.

It is evident from the literature review; researchers have used different methods and techniques for the thermal characterization of the salt PCMs. Every method has its advantages and limitations. Differential Scanning Calorimetry (DSC) is extensively used for characterization. CACCA methods have the edge over the T-history method and DSC method because it is quite simple, inexpensive, and consistent. These CACCA methods eliminate the drawbacks and are superior compared to the existing calorimetric methods of thermal characterization.

The CACCA methods include Newtonian and Fourier techniques that use a baseline or zero curve obtained by fitting the start and end of the solidification points. The results obtained were affected by the type of fitting chosen for the baseline calculations. The choice of the beginning and end of solidification points also affected the parameters obtained.

As per the factors discussed, it is clear that the choice of the characterization method depends on the PCM chosen and the applications involved.

The limitations of all the conventional characterization techniques discussed above strongly support the need for a new method for determining the SHC and latent heat of TES materials over a broad temperature range. A new and improvised characterization technique is needed that takes care of all the limitations of DSC, T-history and CACCA methods and can be suitably used for the salt PCM characterization.

Table 2.2 : Advantages and limitations of thermal characterization techniques for salt PCMs

Sl. No.	Methods/Techniques	Advantages	Limitations
1.	Differential scanning calorimetry (DSC)	• Most widely used • Can be used for all types of materials	• Sample size is small. Results of inhomogeneous salt PCMs are not accurate. • Phase change cannot be visually observed. • Results are affected by heating and cooling rates

			• Supercooling value is overestimated so reduced Latent heat values • Analysis is complex and expensive
2.	T-history method	• Larger sample size • Suitable for low temperature materials • Simple and inexpensive	• Reference material is needed. • High temperature material cannot be characterized. • Design restrictions of the container materials for reference and sample. • Errors due to temperature sensors.
3.	Newtonian method	• Simple and inexpensive • Larger sample size • Can be used for high temperature • Can be used for all types of materials	• Choice of solidification points • Baseline calculations • Results affected by Fitting techniques • Errors due to temperature sensors
4.	Fourier method	• Simple and inexpensive • More reliable and accurate than Newtonian technique as thermal gradient is considered in calculation	• Choice of solidification points • Baseline calculations • Results affected by fitting techniques • Errors due to temperature sensors

		• Larger sample size • Can be used for all types of materials.	
5.	IHCP- energy balance technique	• No baseline calculations • Solidification point errors are eliminated • No fitting techniques errors	• Errors due to temperature sensors • The method is evolving and needs more research

2.6. Scope of the present investigation:

Modern energy reforms and the depletion of conventional energy resources indicate an urge among developing economies and convincingly advocate for deploying sustainable energy technologies. Energy storage technologies have emerged to be the most convincing in our pursuit of a stable, reliable, robust, and uninterrupted energy supply. In recent years, India has reformed its energy policies by focusing more on non-conventional energy technologies, shifting our energy dependability from fossil fuels to solar power. It is encouraging to see TES systems enhancing the economic viability of concentrated solar power (CSP) plants in countries like Spain and the USA. In order to employ materials for energy storage, an estimation of their thermophysical parameters is a must which is obtained by their thermal characterization. The absence of accurate and reliable data on these properties is a significant barrier to the uptake of these technologies. Providing this information will help governments, policy-makers and investors make informed decisions. This work focuses on developing a characterization method devoid of all the limitations of the conventional way.

This proposed research work also aims at improving the TES systems by intensifying the energy storage material functionalities and producing thermal energy storage PCMs that could receive and release thermal energy at significantly higher rates. Various lithium-based mixtures of salts, extending their application over a wide temperature range will be studied. The effect of nanoparticle additives on the energy storage functionalities of these PCMs called Nano-enhanced PCMs (NePCM) will also be analyzed. The development of superior energy storage PCMs can lower the levelised cost of energy (LCOE) and extend

the working life of CSP plants. So, the indigenous development of all necessary infrastructure and technical know-how is of prime importance

2.7. Objectives of the Research work:

1. To develop thermal characterization methods devoid of limitations of the existing techniques for assessment of solidification parameters of PCM and NePCM.

2. To characterize inorganic salts and binary, ternary, and quaternary salt mixtures for thermal energy storage applications using the proposed methods.

3. To characterize lithium-based salt mixtures and study the effect of multi-walled carbon nanotubes (MWCNT) addition of varying weight concentrations (0.1 wt. %, 0.5 wt. %, and 1wt. %) on the thermophysical properties of the base PCMs.

Chapter 3 THEORETICAL BACKGROUND OF INVERSE HEAT CONDUCTION PROBLEM

Inverse heat conduction problem (IHCP) estimates the boundary conditions of a sample where the thermal history within the sample is known, unlike direct heat conduction problem where the thermal history within the sample is calculated using the known boundary conditions.

IHCP can be used in a wide range of applications in material processing, solidification, and quenching. In solidification processing, the heat removed from the casting can be estimated by knowing the heat transfer at the casting/mold interface. This interfacial heat flux can be estimated using IHCP. Another area where IHCP has been found useful is estimating the cooling characteristics of the quench medium during quench hardening. IHCP is used to estimate heat flux at the metal/quenchant surface during various stages of quenching. The estimated heat flux quantifies the cooling performance of the quench medium.

The implementation of IHCP in the thermal characterization of phase change materials is adopted in this work, where the heat flux at the salt/mold interface is estimated. The estimation of the heat flux transients at the interface of salt and the mold was done using a TmmFe Inverse solver (Thermet solutions, Pvt. Ltd., Bangalore). In the Inverse heat conduction problem, the interfacial heat flux is estimated using Beck's nonlinear estimation technique. The one-dimensional heat conduction equation (equation 3.1) in cylindrical coordinates is solved using the boundary and initial conditions.

$$\frac{1}{r}\frac{\partial}{\partial r}\left(kr\frac{\partial T}{\partial r}\right) = \rho C_p \frac{\partial T}{\partial t} \qquad (3.1)$$

The boundary and initial conditions used were:

T (L_1, t) = Y (t) (Measured thermocouple temperature (T3) at a distance of L_1=0.002 m from the interface)

T (L, t) = B (t) (Thermal boundary condition at the outer surface of the mold)

T (L, 0) = Ti (Initial temperature)

Where L is the thickness of the mold model

To determine the heat flux at L=0, i.e., at the interface, the following error function 'F (q)' must be minimum (equation 3.2).

$$F(q) = \left(\sum_{i=1}^{l=mr} (T_{n+i} - Y_{n+i})^2 \right)$$

(3.2)

Where r = number of future time temperature +1 and $m=\Delta\theta/\Delta t$ where $\Delta\theta$ and Δt are the time steps for heat flux and temperature respectively and T_{n+i} and Y_{n+i} are the calculated and measured temperatures thermocouple (T3) position.

The main objective here is to calculate q_{M+1} using present and future temperatures. The future temperatures are calculated at higher time steps than the present temperatures. The key assumption here is that the $q_{M+2} = q_{M+3} = q_{M+r} = q_{M+1}$, which means q is constant over the future time steps. For the lth iteration, the Taylor series expansion for future temperature was used and is given by:

$$T_{n+i}^l \approx T_{n+i}^{l-1} + \frac{\partial T_{n+i}^{l-1}}{\partial q_{M+1}^l} \left(q_{M+1}^l - q_{M+1}^{l-1} \right)$$

(3.3)

For the start of the 1st iteration, the q value can be assumed as unity. This partial derivative in equation 3.3 is the sensitivity coefficient ($\emptyset$) which is defined as the temperature change with respect to a small change in the heat flux at the surface.

$$\emptyset_i^{l-1} = \frac{T_{n+i}\left(q_{M+1}^{l-1}(1 + \epsilon) \right) - T_{n+i}\left(q_{M+1}^{l-1} \right)}{\epsilon q_{M+1}^{l-1}}$$

(3.4)

The numerator in the above equation corresponds to the change in temperature when the heat flux q increased by a small value which is q+εq.

To evaluate the increment in heat flux for the next iteration the error function with respect to heat flux should be minimum, therefore;

$$\frac{\partial F(q)}{\partial q} = 0 \qquad (3.5)$$

So, substituting the error function as shown in equation 3.2 in equation 3.5,

$$\frac{\partial}{\partial q}\left(\sum_{i=1}^{l=mr}(T_{n+i} - Y_{n+i})^2\right) = 0 \qquad (3.6)$$

Substituting equation 3.3 in equation 3.6,

$$\frac{\partial}{\partial q}\left(\sum_{i=1}^{l}(T_{n+i}^{l-1} + \emptyset_i^{l-1}(q_{M+1}^l - q_{M+1}^{l-1}) - Y_{n+i})^2\right) = 0 \qquad (3.7)$$

Which gives,

$$\sum_{i=1}^{l}\emptyset_i^{l-1}(T_{n+i}^{l-1} - Y_{n+i} + \emptyset_i^{l-1}(\nabla q_{M+1}^l)) = 0 \qquad (3.8)$$

After rearranging the equation 3.8,

$$\nabla q_{M+1}^l = \frac{\sum_{i=1}^{l}(Y_{n+i} - T_{n+i}^{l-1})\emptyset_i^{l-1}}{\sum_{i=1}^{l}(\emptyset_i^{l-1})^2} \qquad (3.9)$$

Where,

$$\nabla q_{M+1}^l = q_{M+1}^l - q_{M+1}^{l-1} \qquad (3.10)$$

This procedure is repeated till we get a new heat flux value and the following condition is satisfied.

$$\frac{\nabla q_{M+1}^{l}}{q_{M+1}^{l-1}} < 0.005 \qquad\qquad (3.11)$$

If the condition in equation 3.11 is satisfied then the heat flux value obtained will be taken as the heat flux for the next time step, or else it will be the input for the next iteration and the whole process will be again repeated (Prabhu and Ashish 2002) (Zhang et al. 2014).

A flowchart depicting the inverse heat conduction problem is shown below in Figure 3.1 for clear understanding.
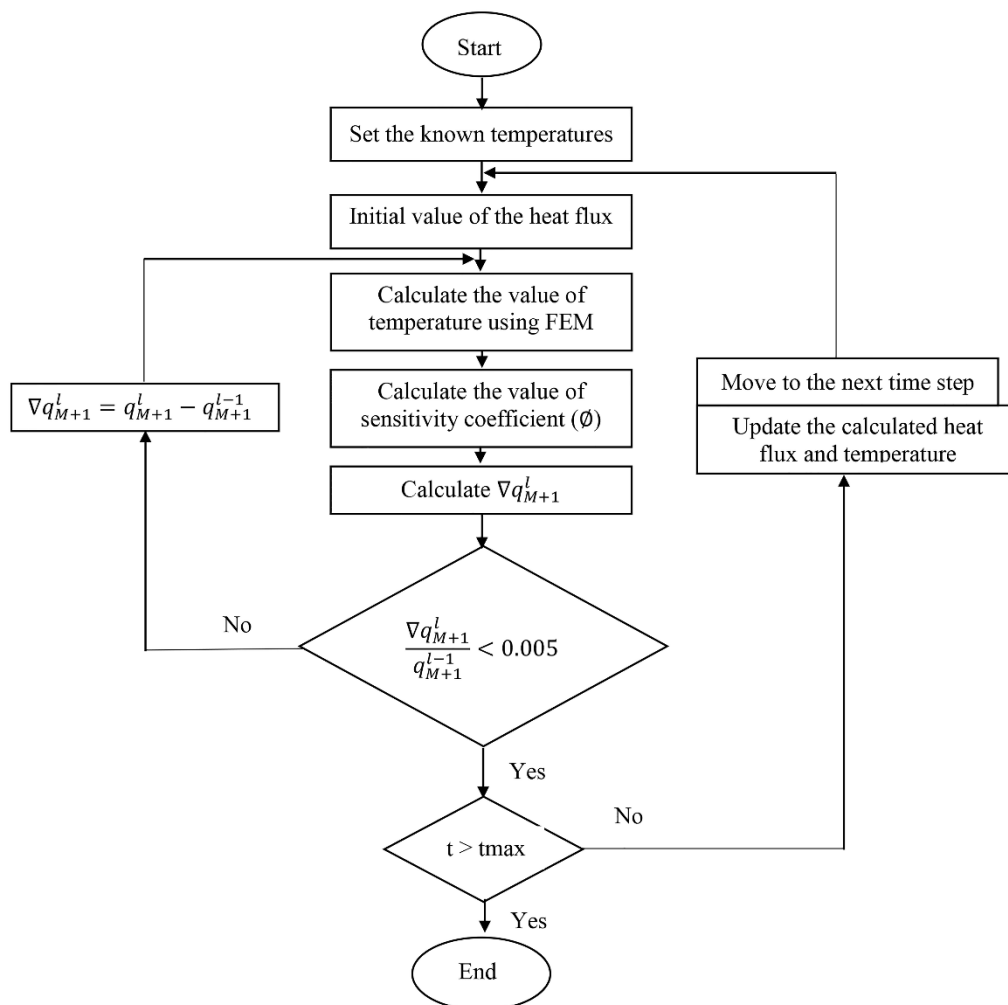
Figure 3.1 Flow chart representing the methodology of the inverse heat conduction algorithm

Chapter 4 MATERIALS AND METHODS

4.1. Energy Balance method

Energy balance technique analyzes the cooling and solidification process of the PCM samples. The samples used were tin (Sn) as pure metal and potassium nitrate (KNO₃) and sodium nitrate (NaNO₃) as salts. Salts were procured from Molychem Pvt. Ltd, Mumbai. The mass and the specific heat capacity of the samples and the steel container used in the present investigation are tabulated in Table 4.1.

Table 4.1: Mass and Specific heat capacity values of the samples

Materials / Properties	Sn	KNO₃	NaNO₃	Stainless Steel (S.S.) container
Mass (kg)	0.5	0.214	0.227	0.039
Average Specific heat capacity (kJ/kg K)	0.253 (González-Rivera et al. 2017)	1.20 (Sudheer and Prabhu 2016)	1.11 (Tooklang et al. 2014)	0.502

These samples of known weight were taken in a stainless-steel container of 0.055 m diameter and 0.075 m height. They were then heated in the temperature-controlled resistance furnace above their melting point to obtain the molten sample. The schematic representation of the simplified energy balance experimental set-up is shown in Figure 4.1.

| Heating | Air cooling |
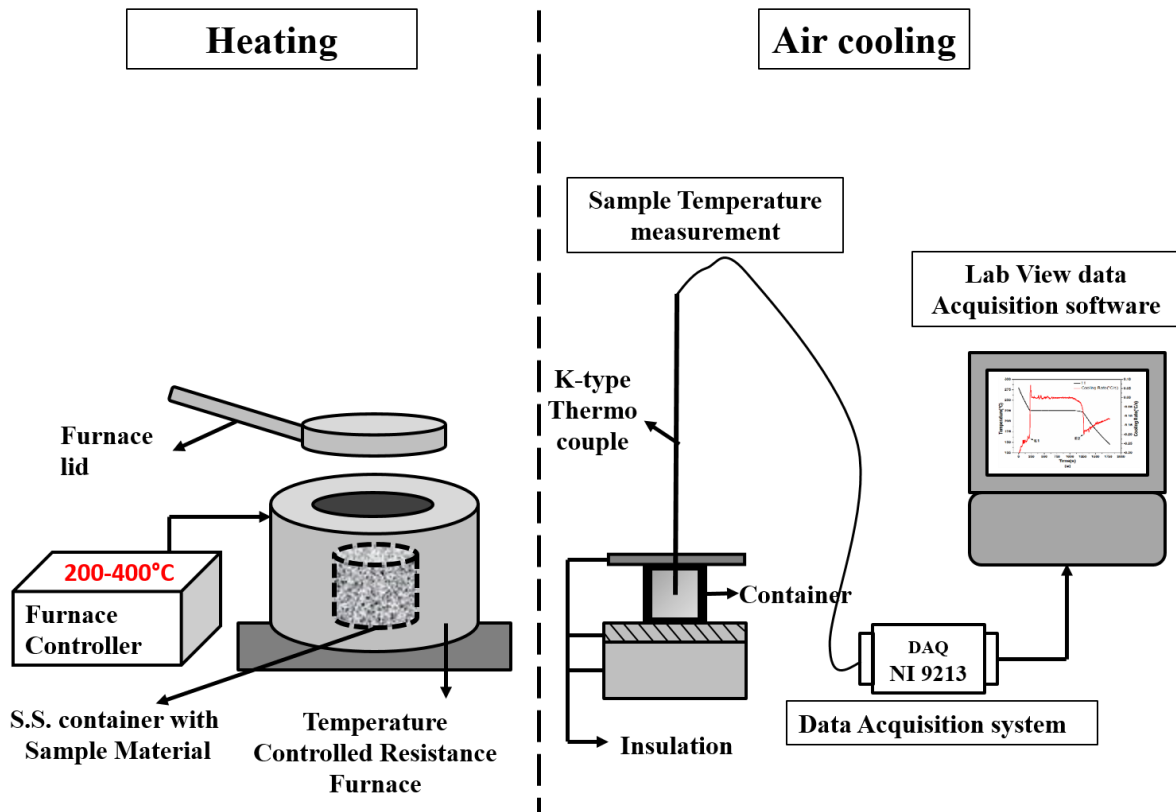
Figure 4.1: Schematic Representation of the Simplified Energy Balance
Experimental set up

The experiment's photograph, which includes the heating furnace, Stainless steel sample container, and the data acquisition system, are shown in Figure 4.2. The top and bottom surfaces of the stainless-steel container were thermally insulated. The cooling process of these samples was then analyzed.
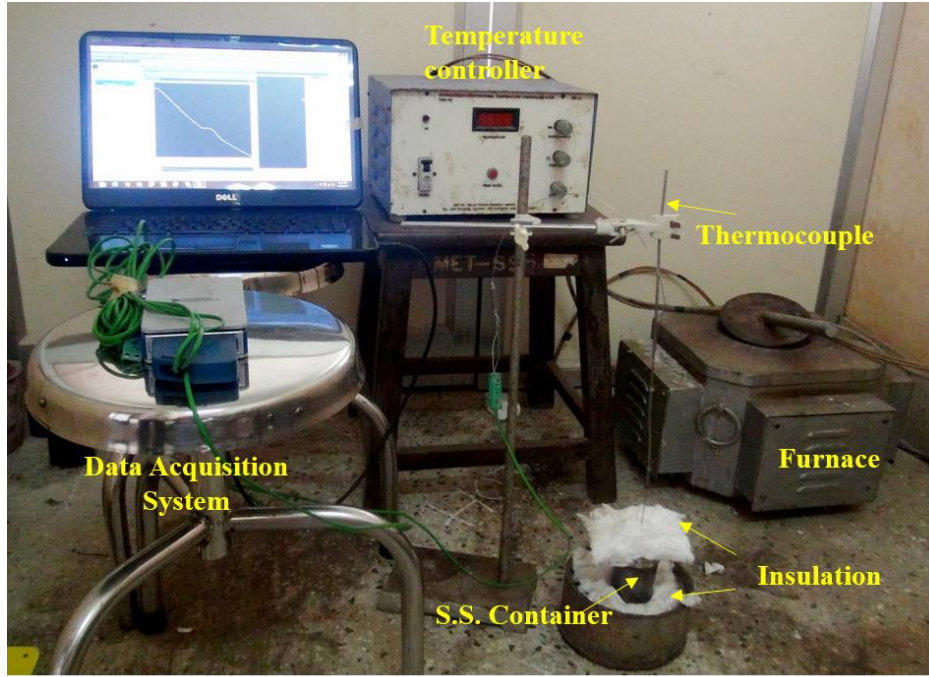
Figure 4.2: Photograph of the Experimental set-up

To record the thermal history of the cooling sample, calibrated K-type 1mm Inconel sheath thermocouple (T1) was used at the center of the molten sample. As per the specifications, the accuracy of the K type thermocouple was ±4 % of actual temperature or ±1.5 ℃. The scanning frequency selected for the temperature data acquisition was 2 Hz. NI USB 9213 data acquisition set-up was used for acquiring the temperature data. The experimentally obtained cooling curves were further analyzed and processed to determine the solidification parameters of the sample. The primary information of the phase change temperature was obtained from the cooling curves while the solidification time, liquidus and solidus points and the cooling rates were obtained from the cooling rate curves, which is nothing but the 1st derivative curve of the cooling curve.

In this method, we assume that the sample and the container start cooling at the same time and with the same cooling rate (González-Rivera et al. 2017). The energy balance equation with no phase change can be written as equation 4.1.

$$[(mCp)_S + (mCp)_{Mo}]\frac{dT}{dt} = -hA(T_1 - T_o)$$

(4.1)

$$h = \frac{[(mCp)_s + (mCp)_{Mo}]}{-A(T_1 - T_O)} \frac{dT}{dt} \qquad (4.2)$$

where m is the mass (kg), c_p is the specific heat capacity (J/kgK), dT/dt is the cooling rate (°C/s), A is the area of heat exchange (m^2), T_1 is the thermocouple temperature at the centre of the sample (°C) and T_o is the ambient temperature (°C). The subscript S refers to the sample, and M_o refers to the stainless steel mold. Using equation 4.2, the heat transfer coefficient (h) was calculated for the sample during the no phase change interval.

The mass and specific heat capacity of the sample and mold, the ambient temperature and the experimentally obtained data such as the cooling rate of the sample, the cooling temperature data of the sample were used in the above calculations to determine h as a function of temperature. This calculated heat transfer coefficient was fitted with the third order polynomial equation to estimate the 'h' values during the phase transformation period. The estimated 'h' values were then used in the energy balance equation during phase change to calculate the phase change enthalpy released at every time step (Q_{inst}) as per equations 4.3 and 4.4. The latent heat of the sample (H_f) was calculated using equation 4.5.

$$[(mCp)_S + (mCp)_{Mo}]\frac{dT}{dt} - m_S H_f \frac{df_s}{dt} = -hA(T_1 - T_O) \qquad (4.3)$$

$$Q_{inst} = m_S H_f \frac{df_s}{dt} = -hA(T_1 - T_O) - [(mCp)_S + (mCp)_{Mo}]\frac{dT}{dt} \qquad (4.4)$$

$$H_f = \frac{Q_{total}}{m_S} = \frac{1}{m_s} \int_{t_l}^{t_s} Q_{inst} dt \qquad (4.5)$$

where, f_s is the fraction solidified, Q_{total} is the net heat released by the sample (J),and t_l and t_s refer to the liquidus and solidus points respectively. The algorithmic structure of the CACCA program used in this method is shown in Figure 4.3.

Furnace heating

Air cooling and temperature acquisition

Deliverables: Melting point (Tm)

Cooling rate calculation

Deliverables: Solidification time, Start (T_l) and End (T_s) of solidification

When $T>T_l$ and $T<T_s$

When $T_l<T<T_s$

Calculation of h:
$$h = \frac{[(mCp)_S + (mCp)_{Mo}]}{-A(T_S - T_O)}\frac{dT}{dt}$$

3rd order polynomial fitting of the h versus Temperature curve

Estimation of h value from the fitted curve

Using the estimated values of h, Calculate Q_{inst}
$$Q_{inst} = m_S H_f \frac{dF_s}{dt} = -hA(T_S - T_O) - [(mCp)_S + (mCp)_{Mo}]\frac{dT}{dt}$$

Using Q_{inst}, calculate H_f
$$H_f = \frac{Q_{total}}{m_S} = \frac{1}{m_s}\int_{t_l}^{t_s} Q_{inst}\,dt$$

Experimental method

CACCA method

Figure 4.3: Algorithm structure of the CACCA program

4.2. IHCP-Energy Balance Combined Technique

The salts used in this technique were KNO_3 (Potassium nitrate) and $NaNO_3$ (Sodium nitrate). The salt sample was melted in a graphite crucible (70 mm x 70 mm) with a thickness of 11.67 mm. Once molten, the crucible with the salt was air cooled by thermally insulating the top and bottom with a layer of cerablanket. The mass of KNO_3 sample was 0.183 kg and the mass of $NaNO_3$ sample was 0.138 kg. Three thermocouples (T1 at the Centre, T2 at 2 mm from the outer surface of the crucible and another T3 at 2mm from the inner surface of the crucible) were used.

Calibrated 1 mm K-type Inconel sheathed thermocouples were used for characterizing the salts. A scanning frequency of 2 Hz was used for temperature data acquisition. NI USB 9213 Data Acquisition system was used to process the data. The experimental set-up used in this process is shown in Figure 4.4 (a).
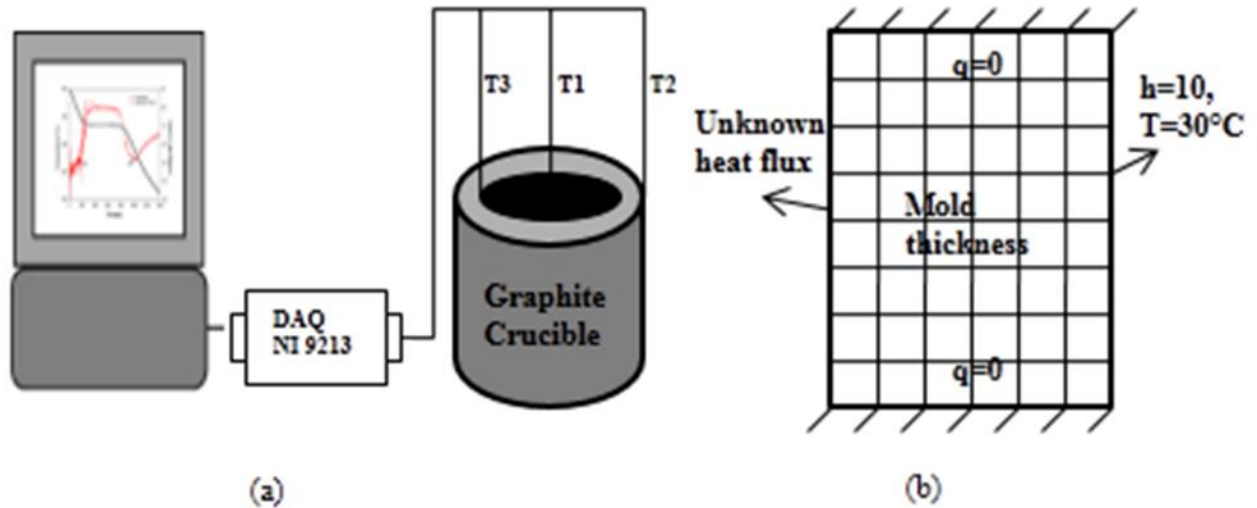
Figure 4.4: (a) Schematic sketch of the IHCP-Energy Balance Experimental set-up (b) Schematic sketch of the IHCP model used for unknown heat flux estimation

Inverse Heat Conduction problem simulation software (TmmFe Inverse Solver, Thermet solutions, Pvt. Ltd., Bangalore) was used to estimate the salt/graphite mold interfacial heat flux transients. The inputs to the solver were the thermal history of the crucible near to the inner surface (T3) and the thermophysical properties of the graphite crucible. The insulating boundary conditions with heat flux (q) =0 was applied at the top and bottom. A convective boundary condition with heat transfer coefficient (h) of 10 W/m²K was applied at the outer surface of the crucible with ambient temperature (T_0) taken as 30 °C. A four node quadrilateral element was used to represent a cylindrical axisymmetric model of the mold. The model was made with a mesh size of 70 x70 with 4900 elements. The inner surface of the crucible was taken as the unknown heat flux boundary where the heat flux has to be calculated as shown in Figure 4.4 (b). A convergence limit of 1E-6 was used during the simulation.

Using the post-processing feature, an estimated temperature data was obtained at T2 which is near to the outer surface of the crucible. The estimated temperature data was compared

with the measured thermocouple temperature data to confirm the accuracy of the model and the estimated heat flux.

From the heat flux (q) obtained, the total heat released into the crucible was calculated by multiplying it by the area of heat exchange (A). Using the energy balance equation at the inner surface of the crucible, the rate of heat released at every time step during the solidification range (Q_{inst}) can be calculated using equation 4.6. The integration of this Q_{inst} during solidification (Q_{total}) divided by the weight of the sample gives us the measured value of the latent heat of solidification per unit weight (H_f) as represented in equation 4.7.

$$Q_{inst} = q.A - m.C_p.\frac{dT}{dt} \qquad (4.6)$$

$$H_f = \frac{Q_{total}}{m}, \qquad Q_{total} = \int_{t_l}^{t_s} Q_{inst} \qquad (4.7)$$

Where, m= mass of the sample (kg), A= Area of heat exchange (m^2), C_p= Specific heat capacity of the sample (J/kgK), dT/dt= cooling rate of the sample (°C/sec), t_l and t_s are the liquidus and the solidus points and H_f = latent heat (J/kg).

4.3. Modified IHCP-energy balance combined technique using a steel mold

The IHCP-energy balance combined technique had certain limitations related to the graphite crucible used in the experimental method.

- The durability of the crucible was a concern due to frequent cracking during experiments.
- The loss of molten salt sample and absorption of moisture due to the porous nature of the crucible material were the other drawbacks.
- The literature presents a wide range of thermophysical properties for graphite. The selection of inappropriate thermophysical properties can induce errors in the results of the heat flux data obtained.
- The salt sample retained in the crucible and prevented the reuse of the crucible.

To overcome the above limitations, a steel mold, as shown in Figure 4.5, was used in this modified method.
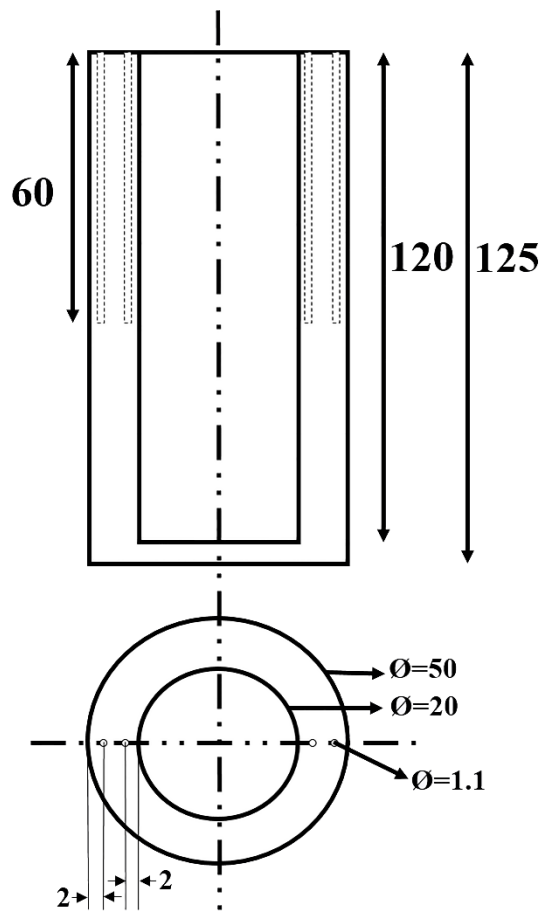
All dimensions are in mm.

Figure 4.5: Schematic model of the steel mold

The salt sample was melted in a steel mold with O.D. 50 mm, I.D. 20 mm and height 125 mm and L'/D ratio greater than 5. The top and bottom of the mold was thermally insulated by using a layer of cerablanket. The mass of the steel mold was 1.731 kg. Mass of KNO_3 and solar salt used was 0.058 kg and 0.065 kg respectively. The average specific heat capacity of salt samples used is given in Table 4.2.

Table 4.2: Average specific heat capacity values of the salts

Materials	Average specific heat capacity (kJ/kg K)
KNO_3	1.20 (Sudheer and Prabhu 2016)
60wt% $NaNO_3$ and 40wt% KNO_3 (Solar salt)	1.485 (Cáceres et al. 2017)

Three Inconel sheathed K-type thermocouples of 1 mm diameter were used in this method. One thermocouple T1 was placed at the center of the sample while two thermocouples were placed in the mold itself. T2 thermocouple was placed at a distance of 2 mm from the outer surface of the mold. Another thermocouple T3 was placed at a distance of 2 mm from the inner surface of the mold. The temperature data was acquired at a scanning frequency of 2 Hz. For data processing, NI USB 9213 data acquisition system was used. The schematic sketch of the set up used for the experimentation is shown in Figure 4.6.
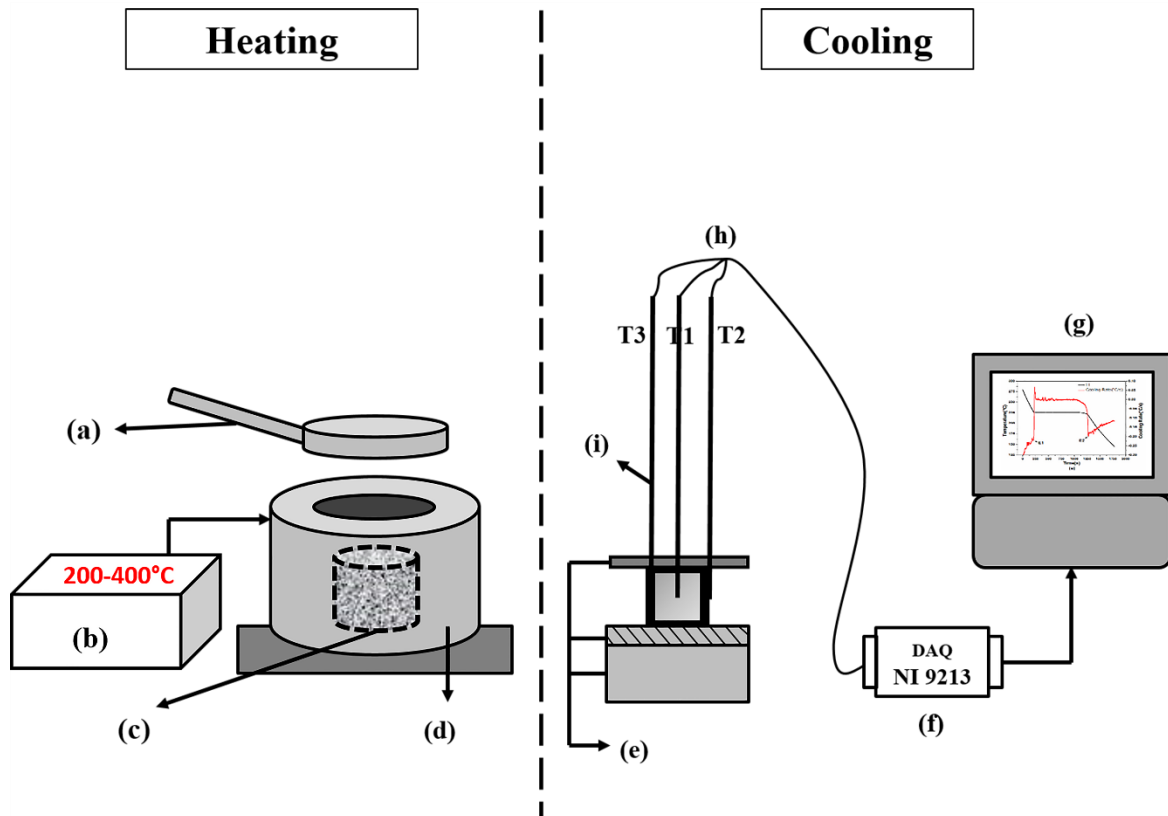
Figure 4.6: Schematic drawing illustrating the used Experimental set-up (a) Furnace lid (b) Furnace controller (c) Steel mold with the sample material (d) Temperature controlled resistance furnace (e) Insulation (f) Data acquisition system (g) PC monitor (h) Connecting cables (i) K-type thermocouples

KNO_3 was used as it is for the experiments. The solar salt was prepared by taking 60 wt. % $NaNO_3$ and 40 wt. % of KNO_3 in a stainless-steel container. It was then heated in a resistance furnace at a temperature of 300 °C to ensure the complete melting of salts. After this, the molten salt was transferred to a muffle furnace maintained at a temperature of 250 °C for two days to ensure complete homogenization of the salt mixture. The salt thus obtained was used as solar salt during experimentation.

For experiments, the salt sample was taken in a steel mold and melted using resistance furnace. For air cooling experiments, the mold with the molten salt was taken out of the furnace and kept in the ambient environment. While in the case of furnace cooling, the mold was cooled in the furnace itself. During cooling, the thermocouples were employed to record the thermal history of salt and cooling of the mold near the inner and outer surface.

68

The temperature data close to the inner surface of the mold (T3) and the thermophysical properties of the steel mold were used as input to the Tmmfe solver. To represent the steel mold, a model with cylindrical axi-symmetry was used in the inverse solver with a four node quadrilateral element. The mesh size used in the axisymmetric model 30x30 with 900 elements for air cooling and 4x30 with 120 elements for furnace cooling. The convergence limit used during the inverse simulation was 1E-6. Two sets of experiments based on air and furnace cooling were performed. The boundary conditions in both cases are shown in Table 4.3.

Table 4.3: Boundary Conditions of Air cooled and Furnace cooled steel mold

Boundaries	Air cooled	Furnace cooled
R1	Unknown heat flux "q"	Unknown heat flux "q"
R2 and R3	q=0, insulated	q=0, insulated
R4	h=10 W/m^{2}K,T_o=Ambient temperature (°C)	Thermal boundary using T2 thermocouple data

A schematic representation of the inverse solver model of the steel mold used for the approximation of the heat flux is shown in Figure 4.7.
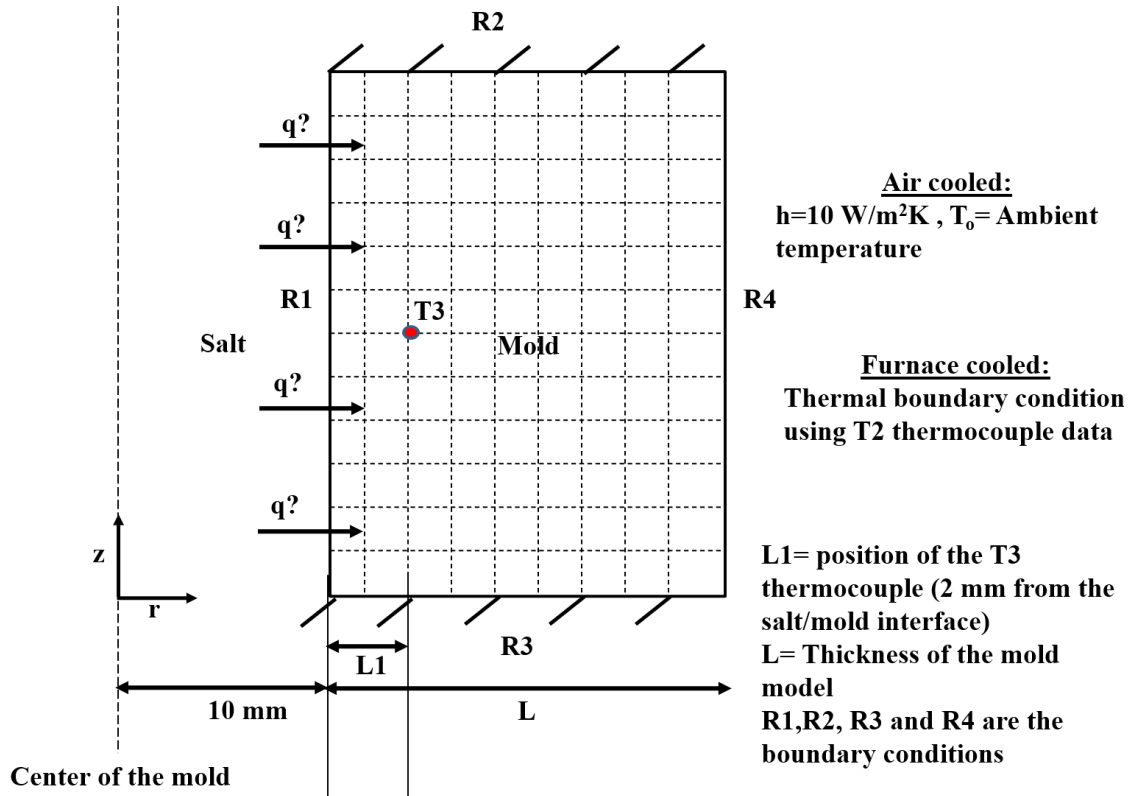
Figure 4.7: Schematic drawing illustrating the inverse solver model of the steel mold

Using the estimated heat flux (q) data obtained from the inverse solver, the net heat liberated from the sample into the mold (Q) was determined by multiplying the heat flux (q) with the heat transfer area (A). The energy balance equation 4.15 was employed at the inner surface of the mold and the rate of heat liberated at each time interval during the phase change (Q_{inst}) was calculated.

$$Q_{inst} = q \times A - m \times c_p \times \frac{dT}{dt} \tag{4.15}$$

The rate of heat liberated during solidification (Q_{inst}) was integrated over the solidifying range to obtain the total heat released during the phase change (Q_{total}). During the calculation of Q_{total} for KNO_3, the area under the curve in the artificial solidification range was considered as the interfacial heat flux curve did not significantly reflect the phase transformation of the salt. In the solar salt sample, the solidification of the salt was significantly reflected on the heat flux curve at the mold /salt interface. Therefore, for the solar salt, the absolute area under the curve with end points of solidification as baseline was considered for the estimation of Q_{total} as per equation 4.16. This Q_{total} was divided by the

mass of the sample to obtain the phase change enthalpy per unit mass (H_f) as per the equation 4.17.

$$Q_{total} = \int_{t_{e'}}^{t_{s'}} Q_{inst} \qquad (4.16)$$

$$H_f = \frac{Q_{total}}{m} \qquad (4.17)$$

Where, ts' and te' represents the time corresponding to the temperatures T_l+5 and T_s-5 respectively, m= sample mass (kg), A= heat transfer area (m^2), c_p= Average specific heat of the salt (J/kgK), dT/dt= cooling rate (°C/sec) and H_f = phase change enthalpy/latent heat (J/kg).

The major source of error while determining the latent heat is the choice of a start and end temperature of solidification used for integrating the heat flow peak (Q_{inst}). To alleviate this problem, an artificial mushy zone with an initial temperature of 5 °C before the start of solidification temperature (T_l) and 5 °C after the end of solidification temperature (T_s) was chosen.

The T2 thermocouple data is used to calculate the error between the estimated and measured temperature at 2 mm from the outer surface of the mold where the T2 thermocouple was placed. This will help to check the reliability of the estimated heat flux and also help in the validating the boundary condition used. The error was calculated using equation 4.18.

$$Error\% = (\frac{T_{measured} - T_{estimated}}{T_{measured}}) \times 100 \qquad (4.18)$$

The % error estimated for KNO_3 and solar salt was 0.4 and 0.02, respectively. This shows that the difference between the measured and estimated temperatures was significantly less and therefore, the heat flux obtained and chosen boundary conditions were quite reliable.

The wettability of the salts was studied on a polished mild steel surface using the Drop shape analyzer (DSA100, Kruss, Germany). The contact angle of the salts was measured and tabulated.

4.4. A quantitative approach for thermal characterization of phase change materials

Salts such as potassium nitrate (KNO_3), sodium nitrate ($NaNO_3$), and solar salt mixture (60wt% $NaNO_3$+40wt% KNO_3) were used for this method. The salt material was taken and melted in the same steel mold which was used for the modified IHCP- energy balance combined technique. An electric resistance furnace was used for salt melting. The melt was then allowed to cool. Both furnace and air cooling were used. The steel mold used has a mass of 1.731 kg, and the dimensions of the mold were the same as shown in Figure 4.5.

The length to diameter ratio of steel mold was maintained at greater than 5 to ensure heat transfer in the radial direction. The mass and thermophysical properties of the salts used in this approach are tabulated in Table 4.4.

Table 4.4: Mass, Specific heat capacity and thermal conductivity values of the samples

Materials / Properties	KNO_3	$NaNO_3$	60wt%$NaNO_3$ +40wt%KNO_3
Mass(kg)	0.62	0.64	0.65
Average Specific heat capacity(kJ/kgK)	1.20 (Sudheer and Prabhu 2016)	1.725 (Roget et al. 2013a)	1.485 (Cáceres et al. 2017)
Thermal conductivity(W/mK)	0.45 (Zhao et al. 2015)	0.55 (Cáceres et al. 2017)	0.615 (Cáceres et al. 2017)

The experimental set-up was instrumented with two K-type thermocouples. One was placed at the center of the sample to assess the thermal behavior of the salt (T1), and another thermocouple T3 was placed at a distance of 2 mm from the inner surface of the mold. The

top and bottom parts of the mold were insulated to avoid any heat loss in the axial direction. K type Inconel sheathed 1mm diameter calibrated thermocouples were used for measuring the temperature. NI USB 9213 data acquisition system was used to process and acquire the temperature data. The scanning frequency used was 2 Hz.

In this approach, Fourier's law of conduction is used to determine the enthalpy of phase change. The only assumption being that the T3 thermocouple data is considered as the temperature data of the inner surface of the mold.

R1= 0 as T1 is measured at the center of the sample

R2= 0.01 m as it is measured at the inner surface of the mold.

The rate at which heat is released at the inner surface of the mold (Q) is calculated using equations 4.19, 4.20, and 4.21

$$Q = -kA\frac{dT}{dr} \tag{4.19}$$

$$\frac{dT}{dr} = \frac{T1 - T3}{R2 - R1} \tag{4.20}$$

$$A = 2\pi r H' \tag{4.21}$$

where k = thermal conductivity (W/mK), A= surface area of the mold (m^2), dT/dr= thermal gradient across the salt (°C/m), H'= height of the mold (m),

The rate of heat released during solidification (Q$_{inst}$) is calculated using equation 4.22.

$$Q_{inst} = Q - mC_p\frac{dT}{dt} \tag{4.22}$$

where C$_p$ = average specific heat of the sample (J/kgK), m is the mass of the sample (kg), dT/dt= cooling rate (°C/s)

The Q$_{inst}$ is integrated between the start and end time of the cooling process to obtain the total heat released during solidification (Q $_{total}$), which is then divided by mass (m) to obtain the phase change enthalpy of the salt sample (H$_f$) by using equations 4.23 and 4.24.

$$Q_{total} = \int_{te\prime}^{ts\prime} Q_{inst} \qquad (4.23)$$

$$H_f = \frac{Q_{total}}{m} \qquad (4.24)$$

Solidification characteristics of the salt sample can be assessed from the cooling behavior of salt. The flowchart depicting the entire method is shown in Figure 4.8.
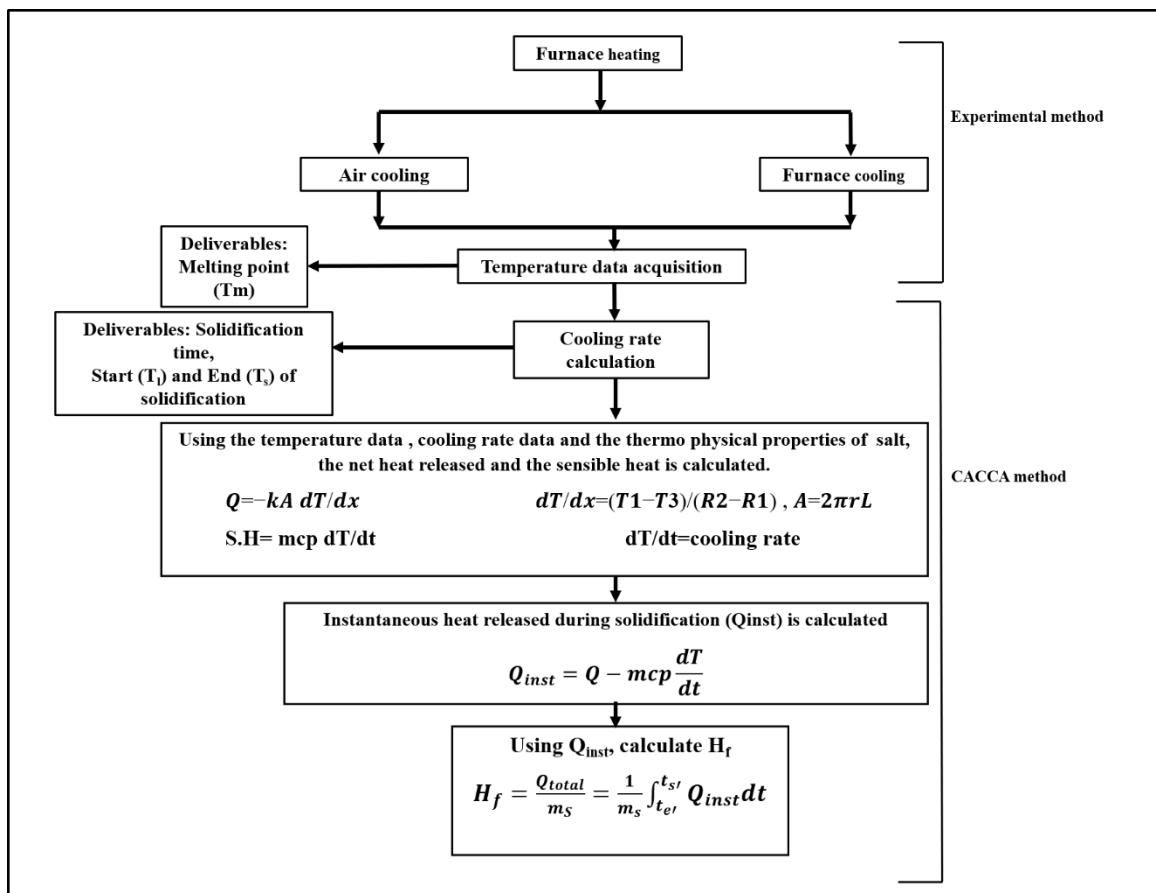
Figure 4.8: Flowchart depicting the experimental method used for the quantitative approach

4.5. Characterization of base and MWCNT enhanced Lithium-based eutectic salts

4.5.1. Salt Preparation

4.5.1.1. Binary eutectic mixtures (Li-K)

Li-K nitrate eutectic salt preparation: In this, the eutectic composition of 33 wt. % of $LiNO_3$ and 67 wt. % KNO_3 was used. $LiNO_3$ was procured from Nice chemicals, Kerela. For 1 kg of eutectic salt 330 gms of $LiNO_3$ was taken in a 116 gm steel container and heated at 350°C. This was done to remove any absorbed moisture from the salt. To this, 666 gms of KNO_3 was added and was allowed to melt at 300°C. The molten mixture was then mixed well. It was then allowed to solidify. To obtain a homogenous eutectic salt, this molten mixture was kept in the muffle furnace at a temperature of 200 °C for around two days. This process was adopted to obtain a well homogenized and moisture-free eutectic salt.

4.5.1.2.   Ternary eutectic mixtures (Li-T)

Li-Na-K nitrate ternary salt: The eutectic weight composition of the salt used in this work is 26 wt. % $LiNO_3$-20 wt. % $NaNO_3$ -54% wt. % KNO_3. For 1 kg of the salt, 260 gms of $LiNO_3$ was taken in a 116 gms steel container and heated at 350°C to remove any absorbed moisture from the salt. To this, 198 gms of $NaNO_3$ and 534 gms of KNO_3 were added and were melted at 300°C. The salt melt was mixed well and was allowed to then solidify. To produce a homogenous eutectic mixture, the salt mixture was kept in a muffle furnace for three days at 180 °C.

4.5.1.3.   Quaternary eutectic mixtures (Li-Q)

$LiNO_3$- $NaNO_3$- KNO_3- $NaNO_2$ salt: The eutectic weight composition of the salt used in this work is 17.5 wt. % $LiNO_3$-14.2 wt. % $NaNO_3$ -50.5% wt. % KNO_3-17.8 wt. % $NaNO_2$. For 1 kg of the salt 175 gms of $LiNO_3$ was taken in a 117 gms steel container and heated at 300°C. To this, 140 gms of $NaNO_3$ and 499 gms of KNO_3 and 176 gms of $NaNO_2$ were added and was allowed to melt at 300°C. The $NaNO_2$ was procured from Molychem chemicals, Mumbai. The salt mixture was mixed well and was allowed to then solidify. For the production of a homogenous eutectic mixture, the salt mixture was kept in a muffle furnace for four days at 200 °C.

A flowchart depicting the salt preparation procedure is shown in Figure 4.9.

Eutectic Salt Preparation
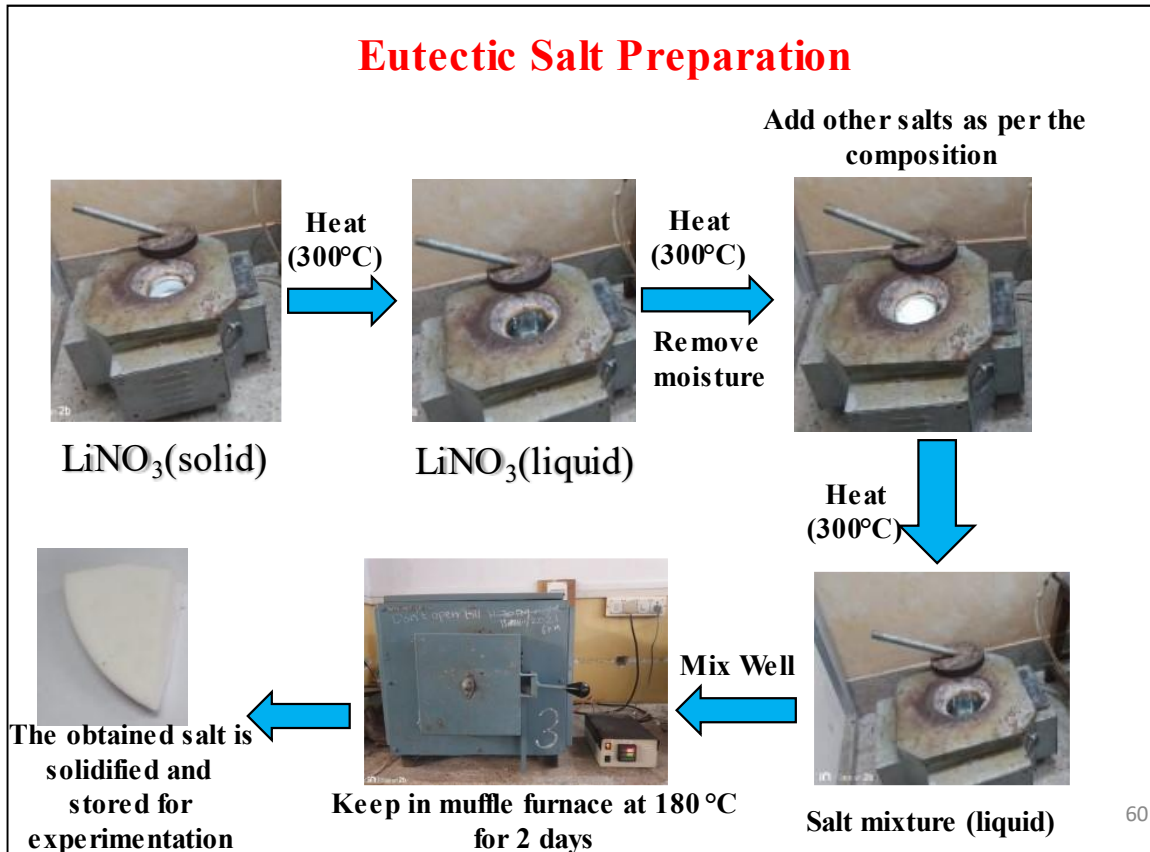
Figure 4.9: A flowchart depicting the process of salt preparation

4.5.2. Nano salt preparation

80gms of the salt was taken in a glass beaker and melted on a hot plate maintained at a temperature above the melting temperature of the salt. Once melted, 0.1 wt. % MWCNT was added to it. The salt with nanoparticles was continuously stirred to avoid any agglomeration maintaining the melting temperature. The nano salt was directly poured into the mold for experimentation. The same procedure was also adopted for 0.5 % and 1% weight concentration of MWCNT. The MWCNT used had an outer diameter of 20-30nm, length of 10-20 μm and purity of MWCNT was higher than 95%.

A flowchart depicting the Nano enhanced salt preparation procedure is shown in Figure 4.10.

Nano Salt Preparation
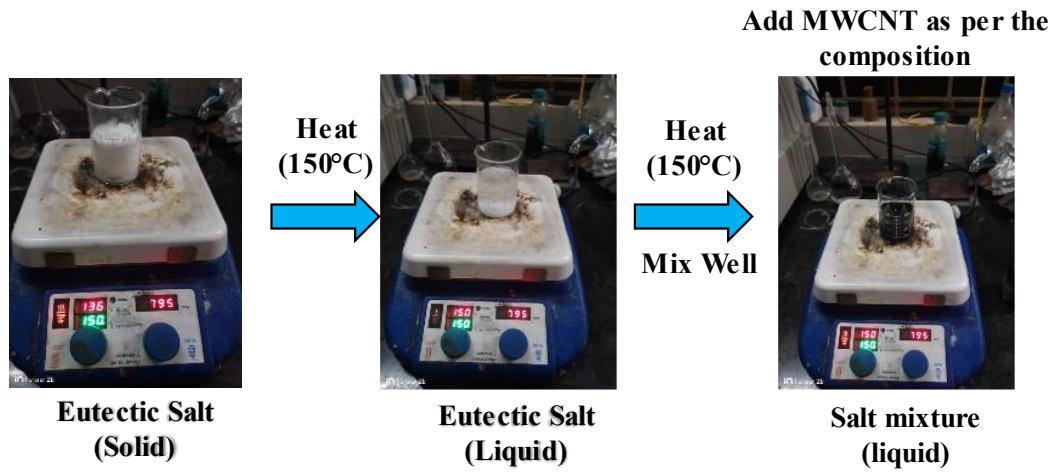
Figure 4.10: A flowchart depicting the process of Nano enhanced salt preparation

4.5.3. Thermal characterization of lithium-based eutectic salts

The modified IHCP- energy balance method in steel mold with furnace cooling was used for the thermal characterization of these lithium-based salts. In this technique, the heat flux transients between the mold and the salt using the steel mold model are estimated using Tmmfe software using the IHCP problem. Using the estimated interfacial heat flux, the net heat liberated from the salt into the mold (Q) is calculated by multiplying the estimated heat flux (q) with the heat transfer area (A), as shown in equation 4.25.

$$Q = q \times A \qquad \qquad \textbf{(4.25)}$$

This heat comprises both sensible and latent heat in the solidification range. The effective specific heat capacity during solidification (c_{peff}) is calculated using this net heat liberated (Q) as per equation 4.26.

$$c_{peff} = \frac{Q}{m \dfrac{dT}{dt}} \qquad \qquad \textbf{(4.26)}$$

Where m is the mass of the salt sample used in kg and dT/dt is the rate of cooling during solidification.

This effective specific heat capacity during solidification can also be represented by equation 4.27.

$$c_{peff} = c_{pavg} + \frac{H_f}{T_l - T_s} \tag{4.27}$$

where c_{pavg} is the average specific heat capacity of the salt and is given by equation 4.28.

$$c_{pavg} = \frac{c_{pl} + c_{ps}}{2} \tag{4.28}$$

H_f is the phase change enthalpy or the latent heat of the salt sample. T_l and T_s are the temperatures corresponding to the start of solidification +5°C and end of solidification -5°C respectively. This ±5°C was incorporated to avoid any errors associated with the selection of the beginning and end of solidification points.

Hence H_f in J/Kg can be calculated by rearranging equation 4.27 into equation 4.29.

$$H_f = (c_{peff} - c_{pavg})T_l - T_s \tag{4.29}$$

Using the post-processing feature in the TmmFe solver, the inner surface temperature (Ts) of the mold was estimated. Using this temperature and the center temperature, the thermal diffusivity of the salt in the liquid and solid phase was calculated.

For cylindrical one-dimensional heat conduction equation in no phase change region, thermal diffusivity (α) can be given as equation 4.30.

$$\alpha = \frac{dT/dt}{\frac{4(T1 - Ts)}{R_2^2 - R_1^2}} \tag{4.30}$$

Using the α_l and α_s obtained α_{avg} was estimated as equation 4.31.

$$\alpha_{avg} = \frac{\alpha_l + \alpha_s}{2} \tag{4.31}$$

Using the value of α_{avg} and c_{pavg}, k_{avg} was estimated from equation 4.32.

$$\alpha_{avg} = \frac{k_{avg}}{\rho c_{pavg}} \qquad\qquad \textbf{(4.32)}$$

Using the obtained k_{avg} and c_{pavg} the thermal effusivity (e) of the salt can also be calculated as per equation 4.34.

$$e = \sqrt{k_{avg}\rho c_{pavg}} \qquad\qquad \textbf{(4.33)}$$

4.6.   Selection of PCMs:

In the first section of the work, salts of known thermal parameters were selected for the development of thermal characterization method for salt-based phase change materials.

In the second section of the work, the salts selected were based on $LiNO_3$ which are used for low temperature applications (Melting temperature range of 100-120 degrees). $LiNO_3$ is considered to be a critical material in the field of energy storage. In the present work, lithium nitrate-based binary, ternary and quaternary eutectic salts are characterized to analyze the thermophysical parameters of these salts.

The following are the key reasons for selecting salts based on $LiNO_3$:

1. To improve the thermal performance of the molten salt.
2. To reduce the melting temperature and provide a wider operating temperature range.
3. To enhance the energy storage density of the PCMs.
4. To improve the thermal stability
5. To reduce the operational and maintenance cost of the energy system due to the low melting temperature of the salt.

All the salts selected were of laboratory grade with minimum assay ranging between 97% to 99%.

4.7. Micrographic Studies

The specimens for the micrographic study were prepared from sections of solidified PCM samples. The microstructures of each specimen at different locations were then examined by JEOL JSM 6380LA analytical scanning electron microscope at different magnifications.

4.8. Wettability studies of the base and nanoenhanced lithium-based salts

The wettability of the base salts and nano-enhanced salts was studied on a mild steel surface using the Drop shape analyzer (DSA100, Kruss, Germany). The contact angle of the salts was measured and tabulated. The test sample was prepared by dropping a drop of molten salt on the mild steel surface manually using a spatula. The contact angle of the solidified drop on the steel substrate was then studied. The photograph of the drop shape analyzer is shown in Figure 4.11.
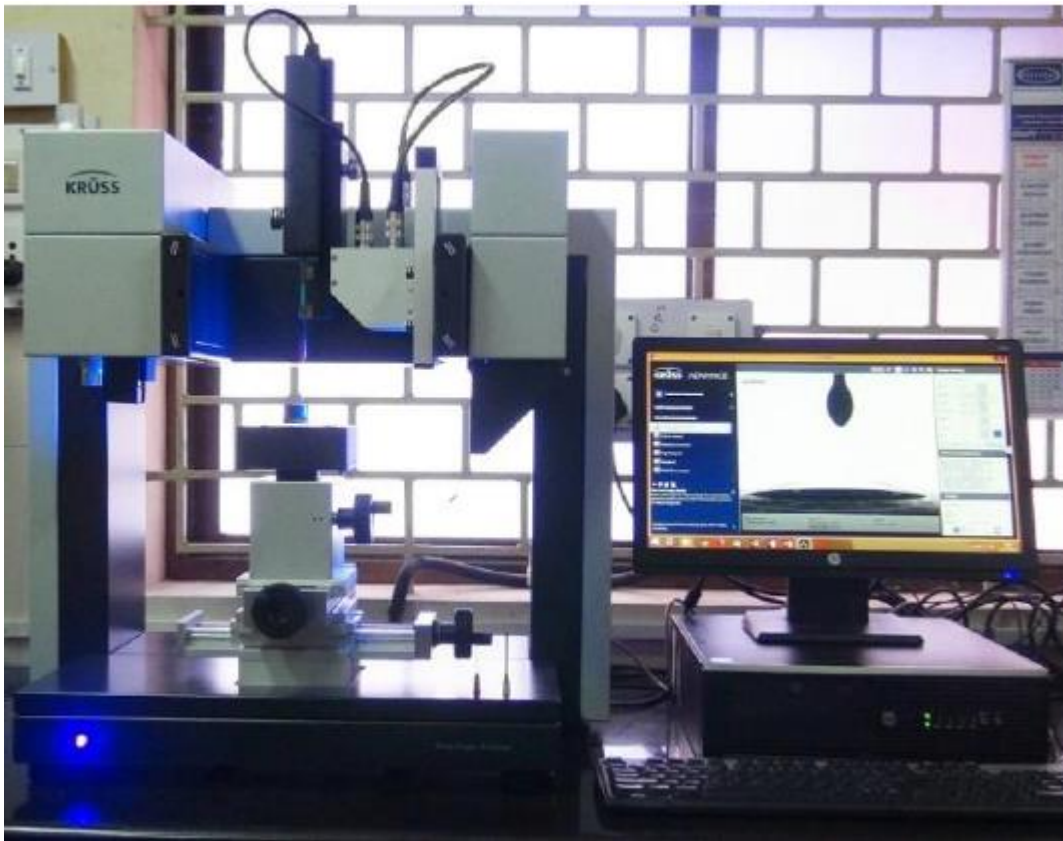
Figure 4.11: Photograph of the drop shape analyzer

Chapter 5 RESULTS AND DISCUSSIONS

5.1. Energy Balance Cooling Curve Analysis Technique

5.1.1. Results

The solidification parameters of pure metal tin (Sn), potassium nitrate (KNO_3), and sodium nitrate ($NaNO_3$) were obtained using the simplified energy conservation equation in CACCA analysis. The path of solidification for Sn, KNO_3, and $NaNO_3$ samples in the stainless-steel cups was obtained. The basic information obtained from the solidification path is the phase transition temperature. The first derivative curves or the cooling rate curves were superimposed on the thermal history curve or the cooling curves. These cooling curves and their first derivative curves for Sn, KNO_3, and $NaNO_3$ are represented in Figures 5.1, 5.3, and 5.5. respectively. The liquidus and solidus points were marked as E1 and E2 respectively on the first derivative curves.
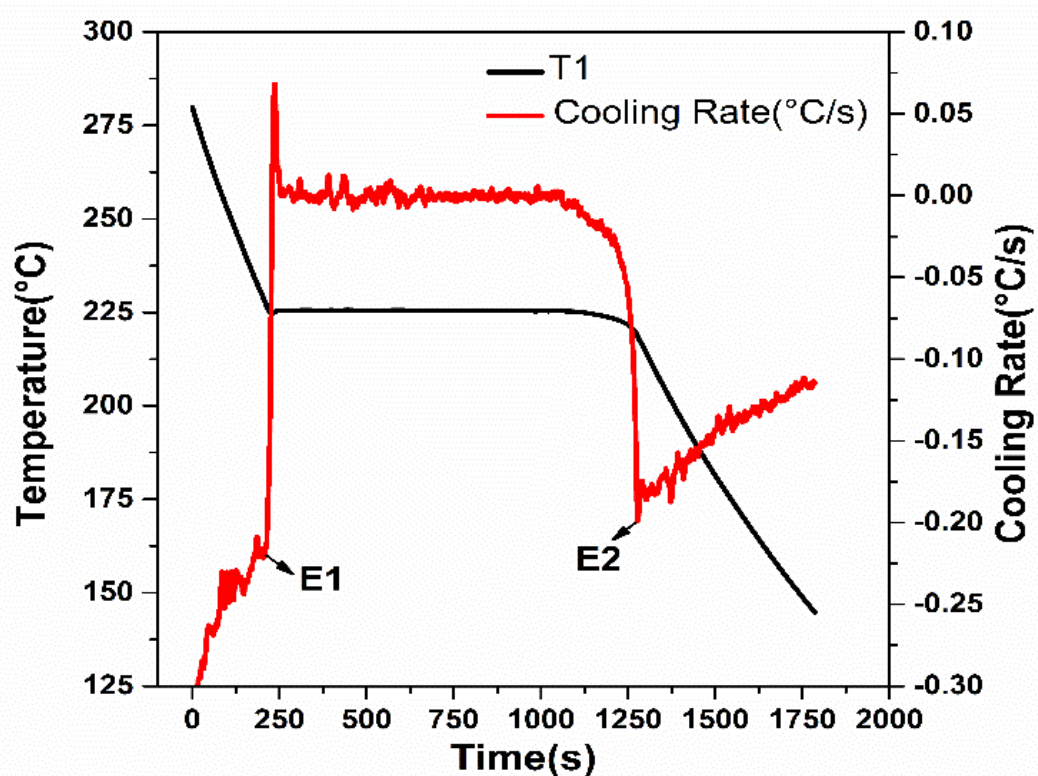
Figure 5.1: Cooling curve and the 1st derivative curve of tin in stainless steel cups
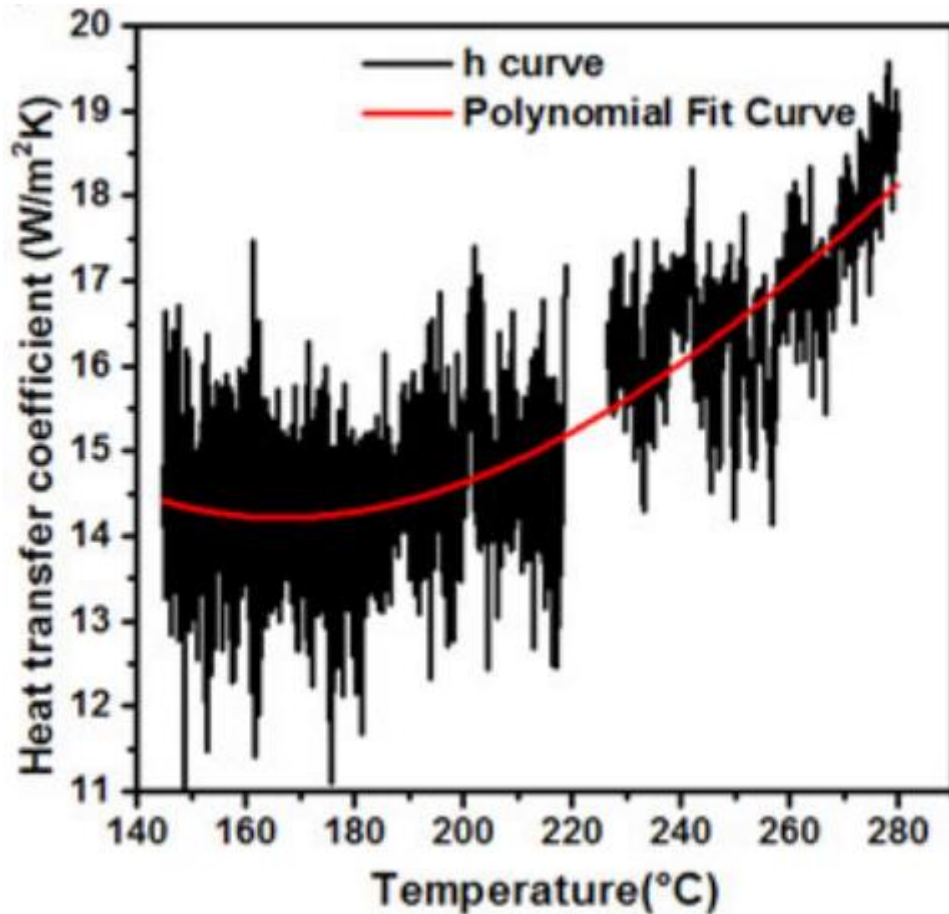
Figure 5.2: Variation of heat transfer coefficient with the temperature for tin

The variation of heat transfer coefficient with temperature in the no phase transformation region is represented in Figure 5.2. The estimated heat transfer coefficient for the phase change region obtained after the polynomial fitting of third order in the case of Sn is also shown in the same Figure.

The variation of heat transfer coefficient with temperature in the no phase change region for KNO_3 and $NaNO_3$ are represented in Figures 5.4 and 5.6 respectively.
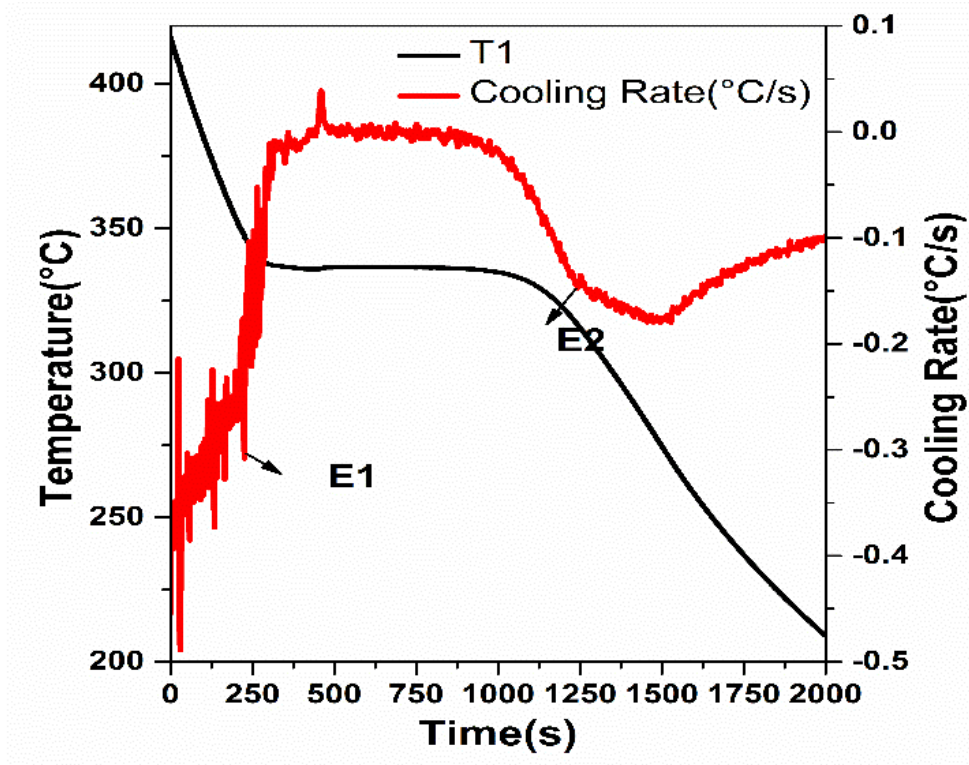
Figure 5.3: Cooling curve and the first derivative curve of potassium nitrate (KNO₃)
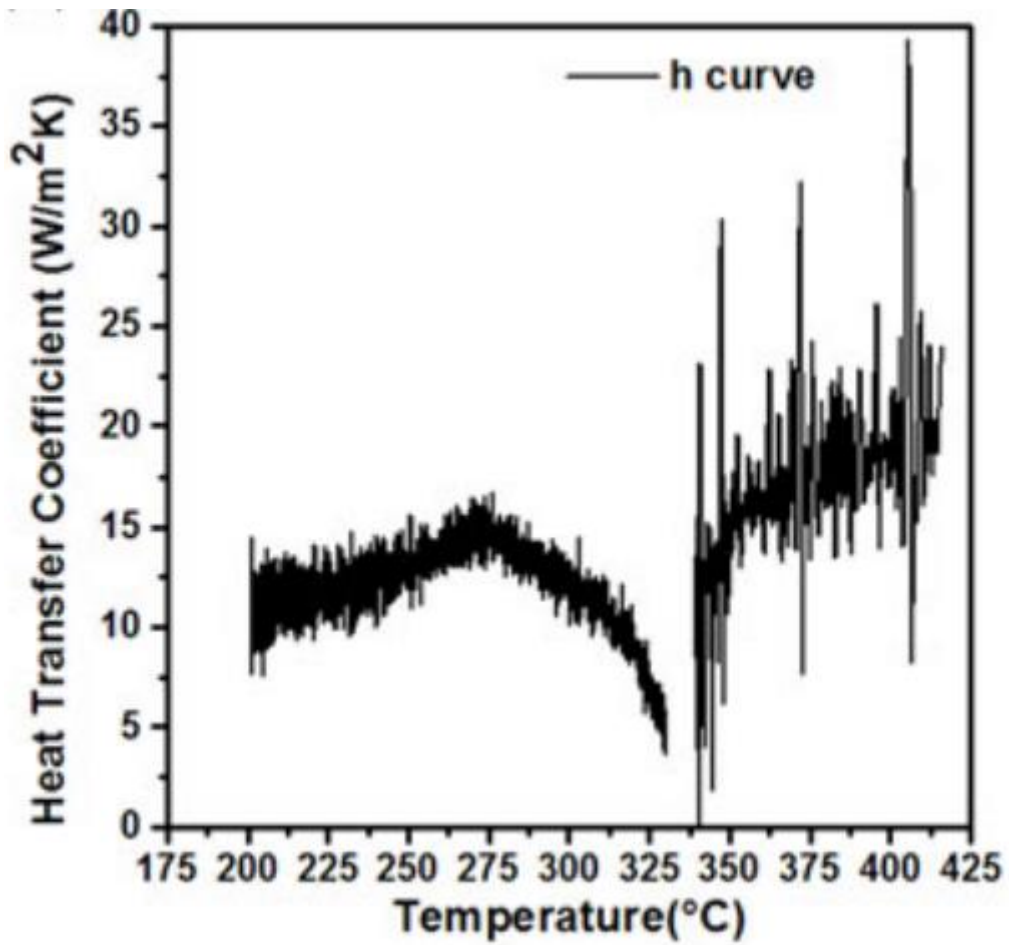
Figure 5.4: The variation of heat transfer coefficient with the temperature for potassium nitrate (KNO₃)
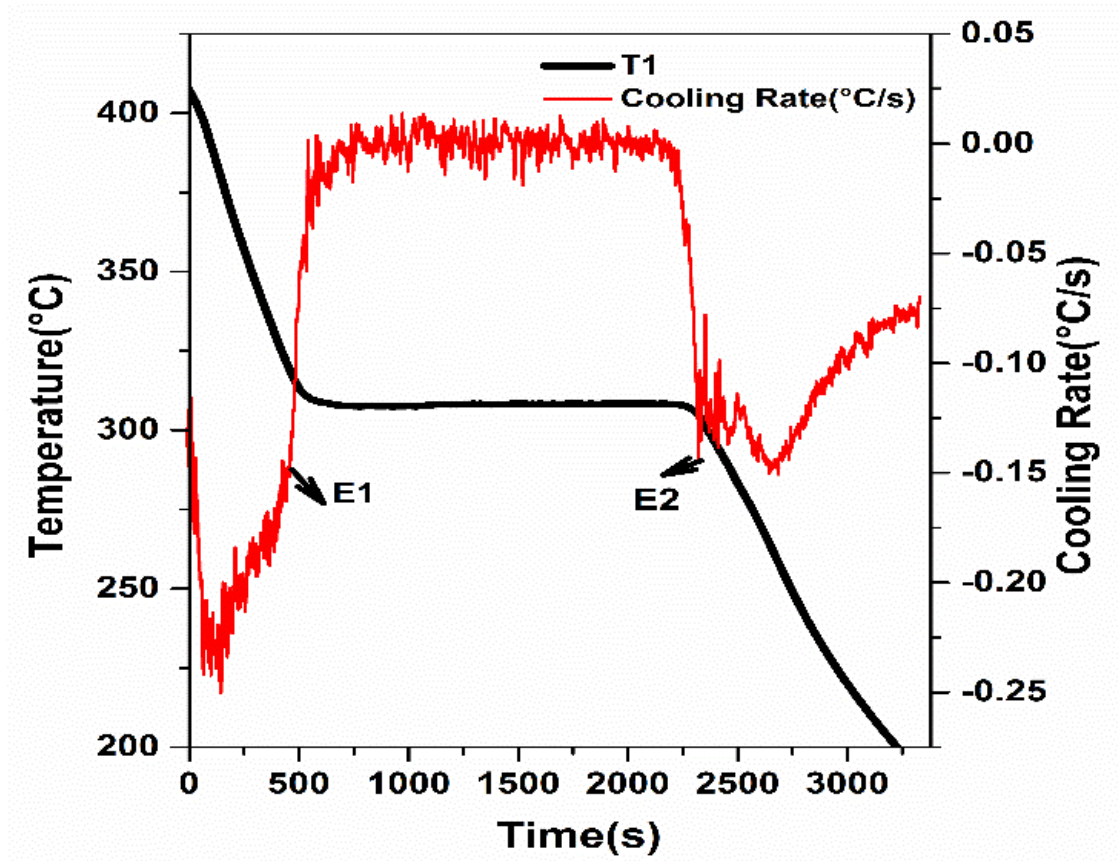
Figure 5.5: Cooling curve and the first derivative curve for sodium nitrate (NaNO₃)
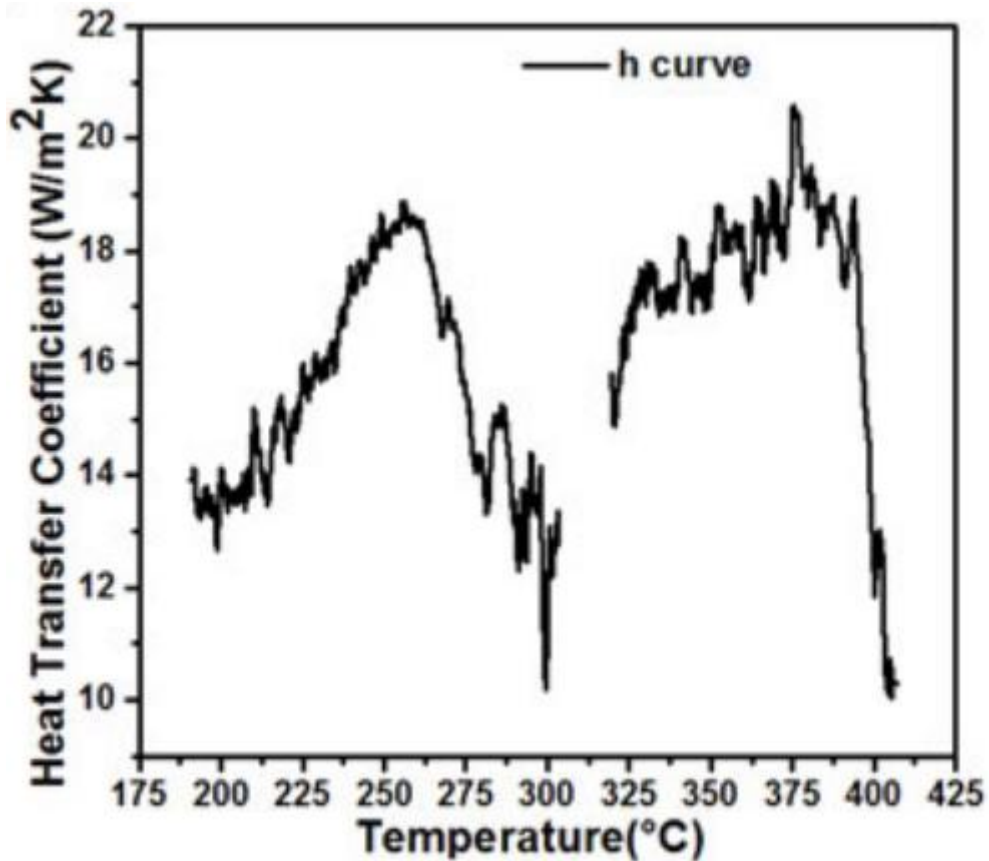
Figure 5.6: Variation of heat transfer coefficient with the temperature for sodium nitrate (NaNO₃)

5.1.2. Discussion

As per the thermal history and the cooling rate curves of Sn shown in the Figure 5.1, the solidification of the metal starts at around 214.8 s at a temperature of 226.3°C. This point is referred to as the liquidus point (E1). The end of solidification was observed at 1276.2 s at a temperature of 218.8°C. This point marks the end of solidification and is called the solidus point (E2). The melting point of Sn is at 225.5°C, which is the phase change temperature for Sn. The time taken for complete solidification of the metal was about 1061.4 s.

Similarly, in the case of salts (KNO₃), as shown in Figure 5.3, the phase change temperature was found to be 336°C. The liquidus point (E1) from the cooling rate curves was found to be 276 s and was recorded at a temperature of 339.5°C. The solidus point (E2) of the salt was found to be 1114 s and was recorded at a temperature of 330.3°C. KNO₃ took about

86

838 s for its complete solidification. The onset and the end of solidification were represented by a sharp change of slope in the first derivative curve.

In the case of $NaNO_3$, as shown in Figure 5.5, the phase change temperature was measured to be 308.2°C. The start and end of solidification (E1 and E2) was found to be at 475.5 s and 2340.5 s, respectively. The recorded temperatures at those points were 316.4°C and 302.5°C, respectively. The total time taken for solidification in case of $NaNO_3$ was about 1865 s.

The phase change characteristics of metal, as well as salts used in this work, is tabulated in Table 5.1

Table 5.1: Phase change characteristics of tin, potassium nitrate and sodium nitrate

Materials / Parameters		Sn	KNO_3	$NaNO_3$
Melting point (°C)		225.6	336	308.25
Solidification time (s)		1061.4	838	1865
E₁: Liquidus point	T_1 (°C)	226.3	339.5	316.4
	t_1 (s)	214.8	276	475.5
E2: Solidus point	T_s (°C)	218.8	330.3	302.5
	t_s (s)	1276.2	1114	2340.5

The latent heat values of Sn calculated using this method was 59.7 kJ/kg which is in agreement with the reported literature data of 60 kJ/kg (González-Rivera et al. 2017). However, the estimation of heat transfer coefficient 'h' values during the phase change period in the case of salts (KNO_3 and $NaNO_3$) was found to be cumbersome. The 'h' values as a function of temperature in no phase change region did not follow the fitting trend of polynomial third order, as shown in Figures 5.4 and 5.6. Thus the 'h' values in the region of phase change of the salts could not be estimated correctly.

The latent heat values calculated using the third-order polynomial fitting were approximately 87% higher than the reported literature values in the case of KNO_3 whereas,

for NaNO$_3$, the measured phase change enthalpy was 107% higher than reported literature data. The reason for such behavior in the case of salts was due to the non-fulfillment of the Biot number (Bi) criterion for the lumped thermal distribution system. To ensure uniform thermal distribution within the sample, the Bi should be less than 0.1(Sudheer and Prabhu 2016).

In the case of Sn, the Bi criterion was satisfied ensuring that the temperature distribution is same at all points within the sample but the same was not satisfied in the case of salts. This meant a thermal gradient within the salt sample, which was not considered in this method. It clearly showed that the heat transfer coefficient did not follow the exact best fit before and after solidification. It was affected by the latent heat released during solidification. Therefore, the characterization method fails in the case of salts. Hence, further experimental modifications are needed to use this technique for salts.

5.2. IHCP-Energy Balance Combined Technique

5.2.1. Results

The computer-aided cooling curve analysis (CACCA) analysis for potassium nitrate (KNO$_3$) and sodium nitrate (NaNO$_3$) was carried out using the inverse heat conduction problem (IHCP) -energy balance method to obtain the solidification parameters of the thermal parameters of the salt sample in a graphite crucible. The solidification path of both the salts and the thermal history of the mold were obtained. These are shown in Figures 5.7 and 5.8 where T1 represents the center thermocouple data, and T2 and T3 represent the graphite mold temperature near the outer surface and the inner surface respectively.
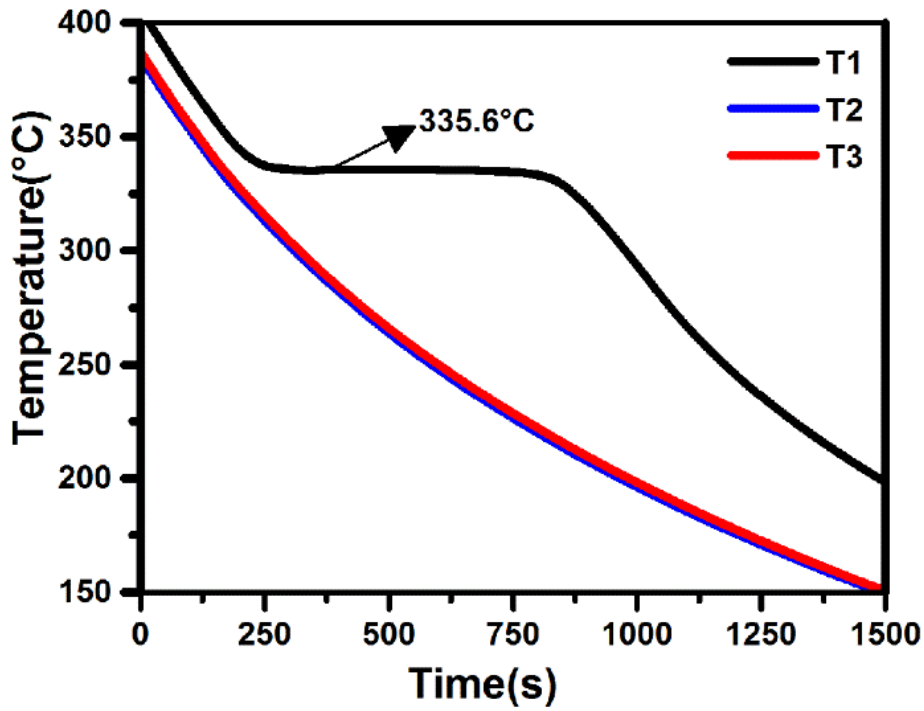
Figure 5.7: Thermal history during cooling of the salt potassium nitrate (KNO₃) and the mold
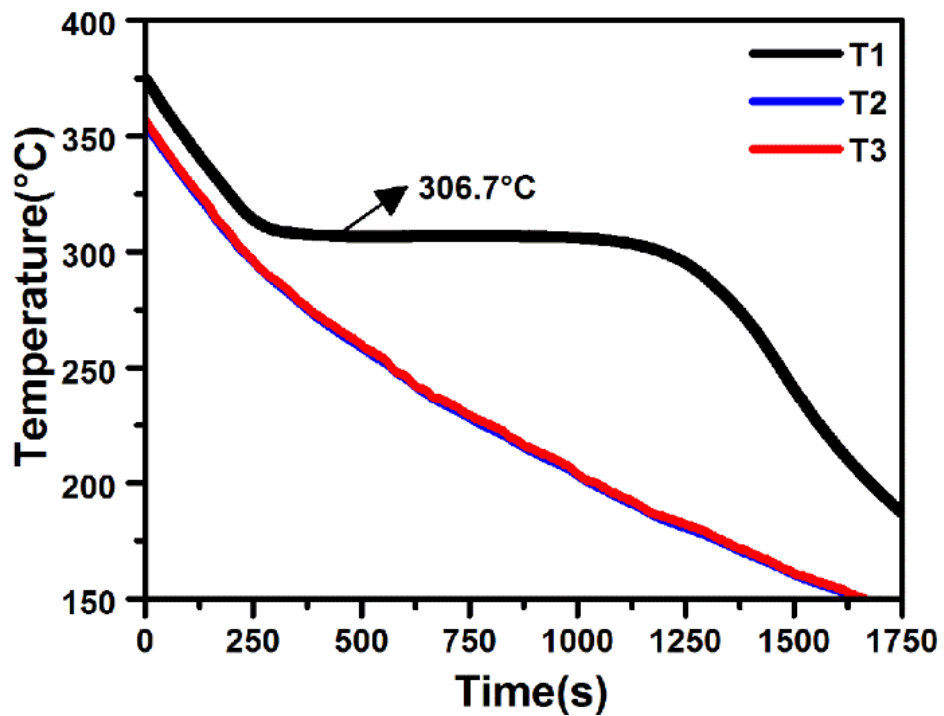
Figure 5.8: Thermal history during cooling of the salt sodium nitrate (NaNO₃) and the mold

89

The cooling rate curves were superimposed on the cooling curves for KNO_3 and $NaNO_3$ in Figures 5.9 and 5.10, respectively. The liquidus and solidus points are marked as E1 and E2 respectively on the cooling rate curves of the salts.
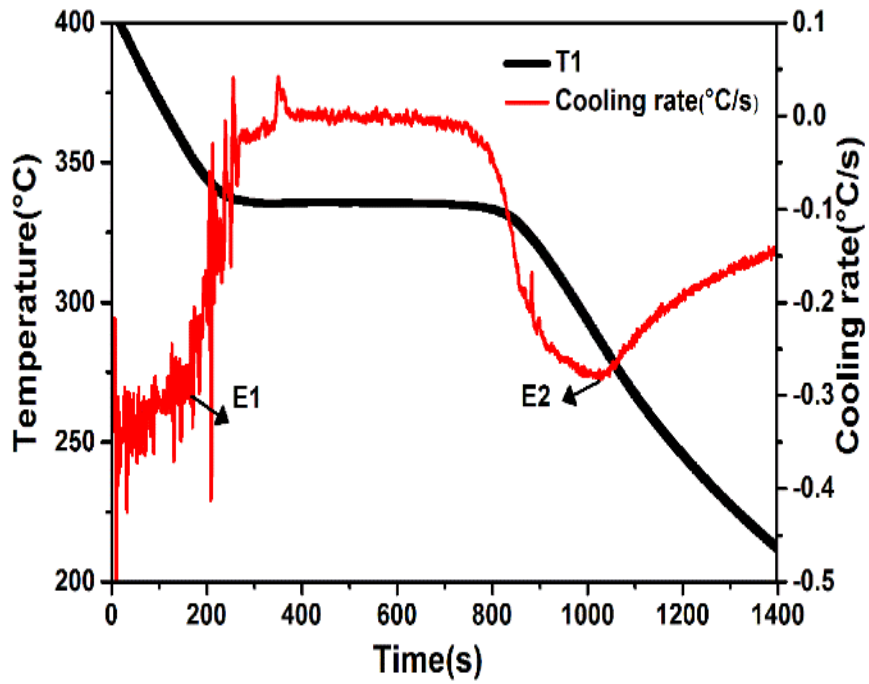
Figure 5.9: The cooling curve and the cooling rate curves for potassium nitrate (KNO_3)
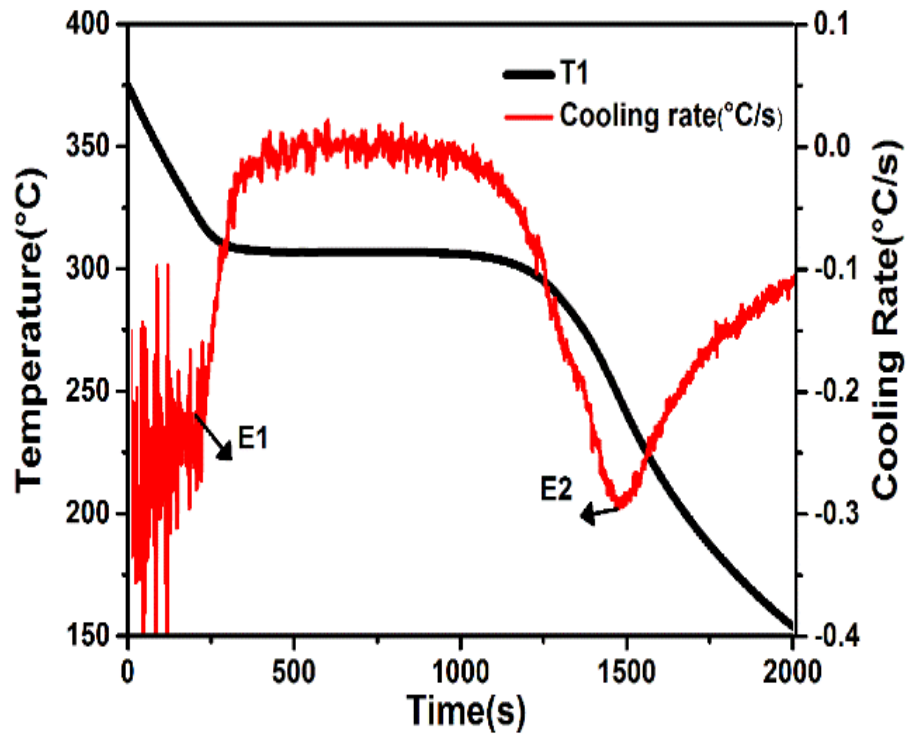
Figure 5.10: The cooling curve and the cooling rate curves for sodium nitrate (NaNO$_3$)

In the inverse analysis, the input given was the data file of the measured temperature data of the T3 thermocouple. The heat flux at the inner surface was estimated for both the salts KNO$_3$ and NaNO$_3$ as shown in Figure 5.11.
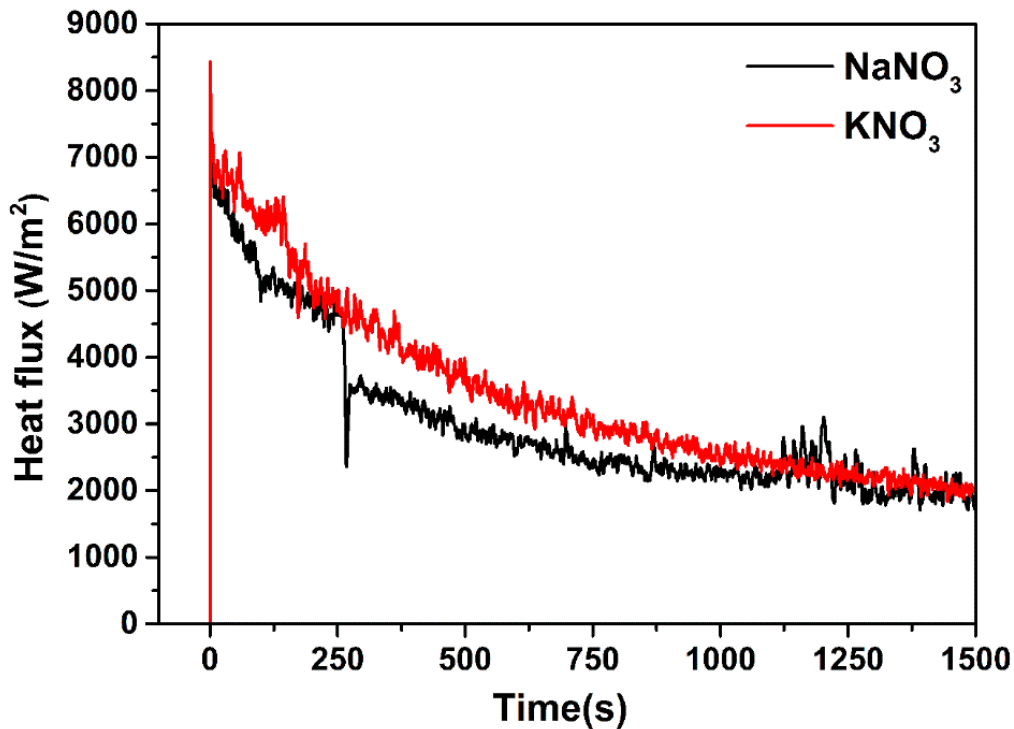
Figure 5.11: Estimated heat flux transients for the salts

5.2.2. Discussion

In the case of KNO_3, as per the solidification path shown in Figure 5.7, the solidification of the salt starts at around 173.5 s at a temperature of 350.57 °C. This point is referred to as the liquidus point (E1). The solidification ends at 1030.5 s at a temperature of 285.1 °C. This point reflects the complete solidification of the salt and is called solidus point (E2). This salt melts at a nearly constant temperature of 335.6 °C reflecting the phase change temperature of the salt. KNO_3 takes around 857 s for complete solidification. The liquidus and solidus points are selected from the cooling rate curve rather than the cooling curves for a more accurate selection of the liquidus and solidus points. It is represented as sharp peaks in the cooling rate curves.

Similarly, in the case of $NaNO_3$ as shown in Figure 5.8, the melting temperature from the cooling curve is measured to be 306.7°C. The solidification of this salt starts at 211 s and at a temperature of 321.1 °C. This liquidus point is represented by a change in slope on the cooling rate curve. The solidus point of the salt was at 1468 s at a temperature of 250.2 °C. $NaNO_3$ took around 1257 s for complete solidification.

The phase change parameters for both the salt samples obtained using IHCP- Energy balance combined technique are given below in Table 5.2

Table 5.2: Phase change characteristics of KNO_3 and $NaNO_3$

Materials / Parameters		KNO_3	$NaNO_3$
Melting point (°C)		335.6	306.7
Solidification time (s)		857	1257
E_1: Liquidus point	T_l(°C)	350.57	321.1
	t_l(s)	173.5	211
E2: Solidus point	T_s(°C)	285.1	250.2
	t_s(s)	1030.5	1468

The average specific heat value used for latent heat calculations was 1.2 kJ/kg K for KNO_3 (Sudheer and Prabhu 2016) and 1.11 kJ/kg K for $NaNO_3$ (Tooklang et al. 2014). The latent heat values for KNO_3 using this method during cooling were calculated to be 112 kJ/kg, comparable to the reported literature values of 91 kJ/kg and 102 kJ/kg (Sudheer and Prabhu 2016)(Roget et al. 2013b).

The phase change enthalpy for $NaNO_3$ was calculated to be 161 kJ/kg, where the literature data reports the values of 172 kJ/kg and 177kJ/kg (Tooklang et al. 2014). It can be seen that the values of the enthalpy of solidification obtained using this method were nearly close to the reported values of literature.

The error percentage values calculated using the measured and estimated temperature data for the T2 thermocouple near the mold's outer surface were ±0.88% for KNO_3 and ±0.42% for $NaNO_3$.These error values show the reliability of this method and the selection of parameters in the inverse analysis and the energy balance calculations.

5.3. IHCP-Energy Balance Combined Technique Using Steel Mold

5.3.1. Results

The solidification process of the pure salt potassium nitrate (KNO_3) and the solar salt, along with the cooling history of the mold in both the cases of air and furnace cooling, is shown in Figures 5 and 6, where T1, T2, and T3 represent the center thermocouple data and the temperature data near the outer and inner surface of the mold respectively.
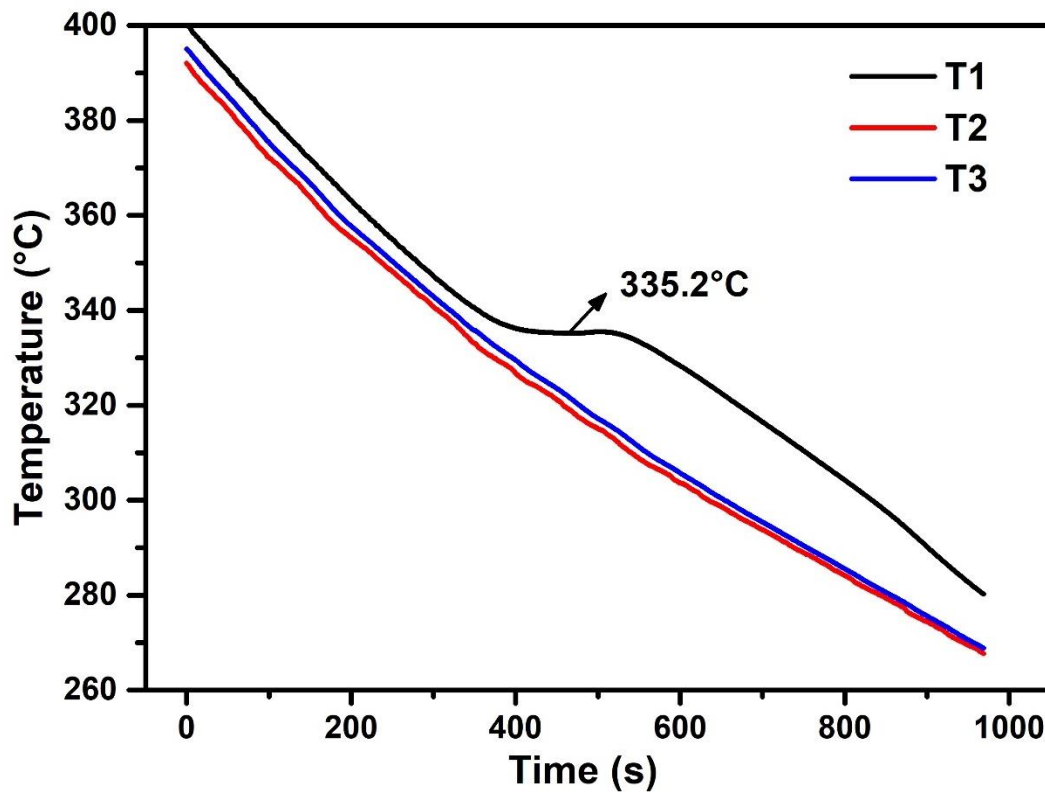
Figure 5.12: Thermal history obtained with KNO₃ and steel mold with Air cooling
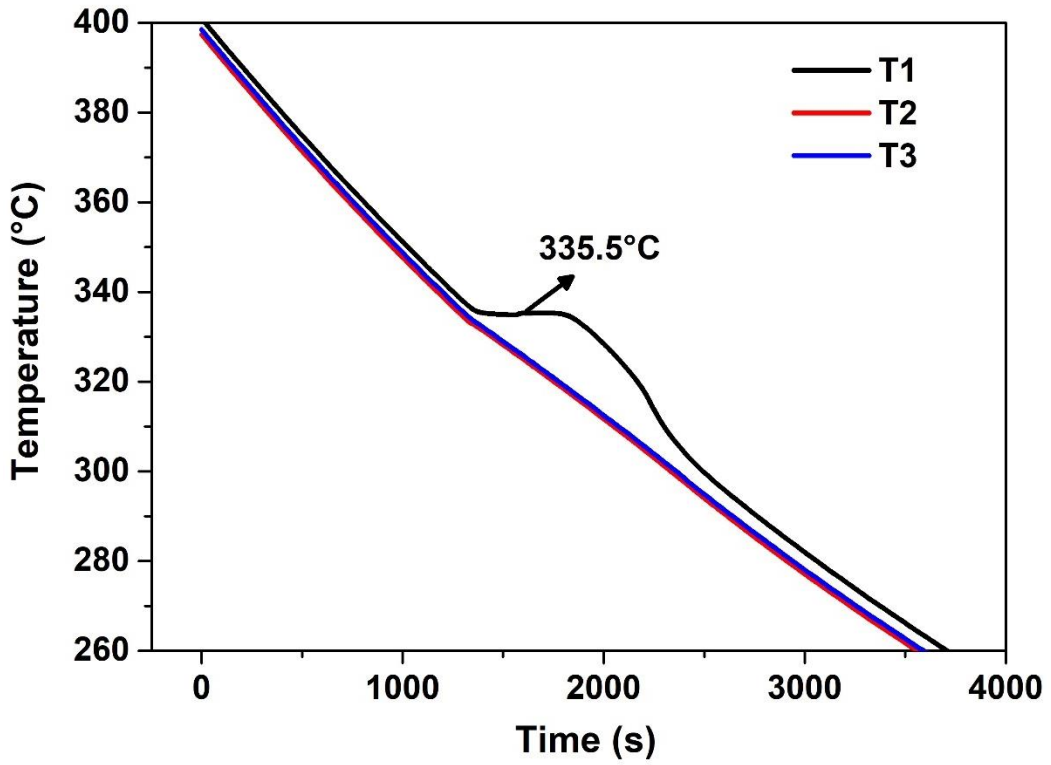
Figure 5.13: Thermal history obtained with KNO₃ and steel mold with furnace cooling
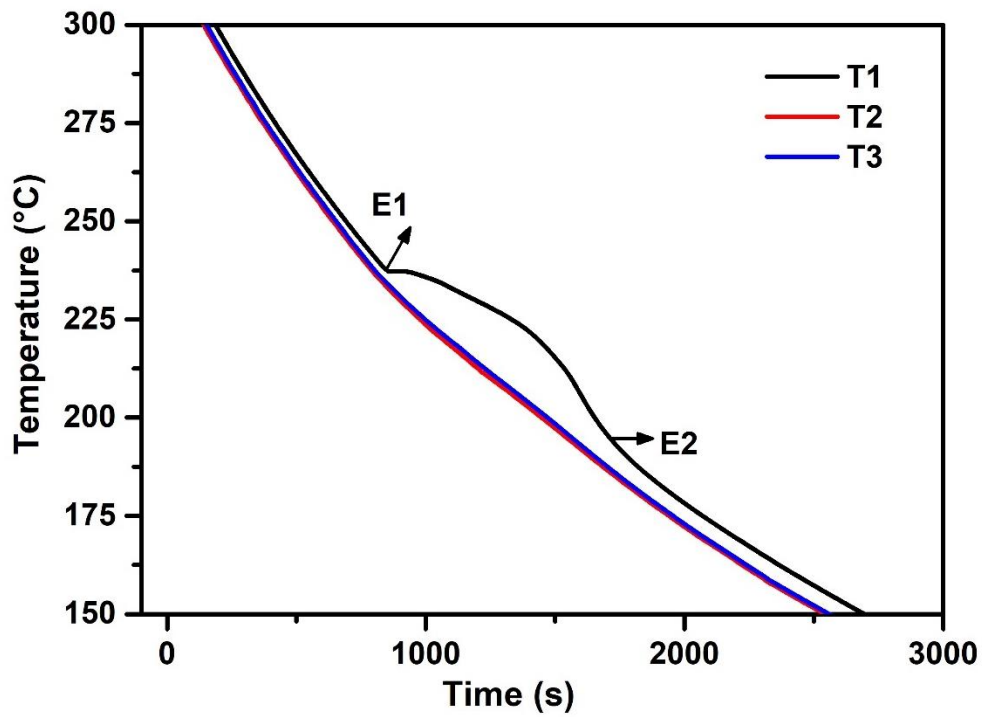
Figure 5.14: Thermal history obtained with 60wt% NaNO₃ and 40wt% KNO₃ solar salt and steel mold with air cooling
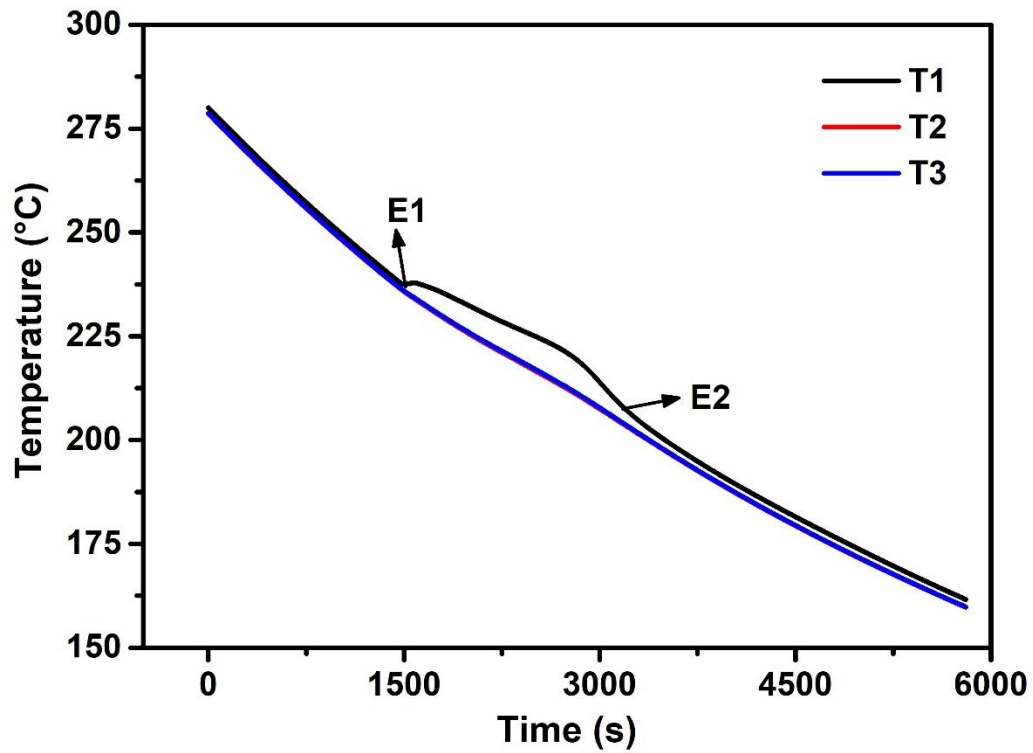
Figure 5.15: Thermal history obtained with 60wt% NaNO₃ and 40wt% KNO₃ solar salt and steel mold with furnace cooling

The cooling rate curve or the 1st derivative curve obtained from thermal history was superimposed on the cooling curve of KNO_3 and 60 wt.% $NaNO_3$ and 40 wt.% KNO_3 solar salt as shown in Figures 5.16 and 5.17.
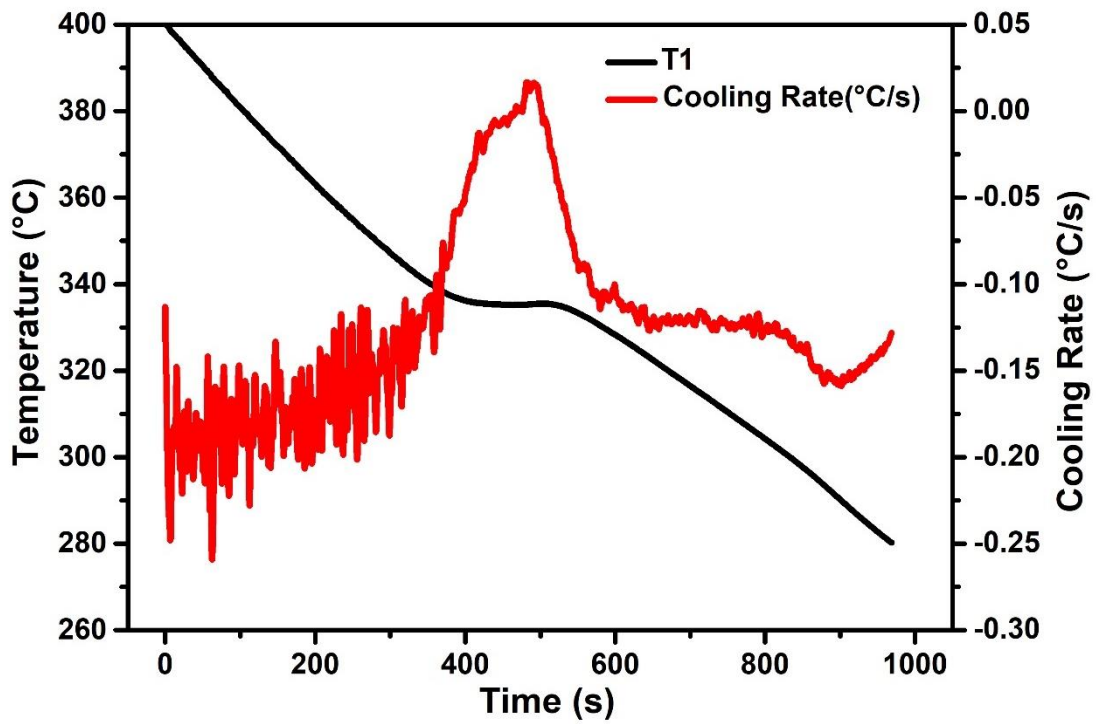
Figure 5.16: The cooling curve and the cooling rate curves of KNO₃ with Air cooling
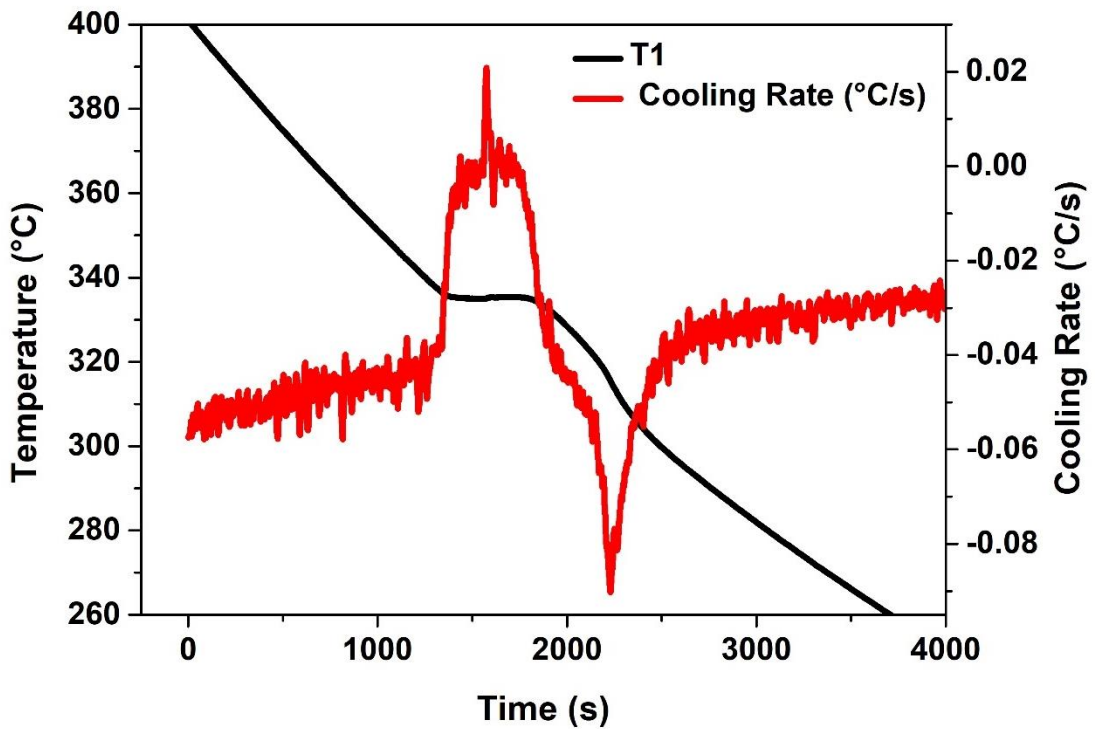
Figure 5.17: The cooling curve and the cooling rate curves of KNO₃ with furnace cooling
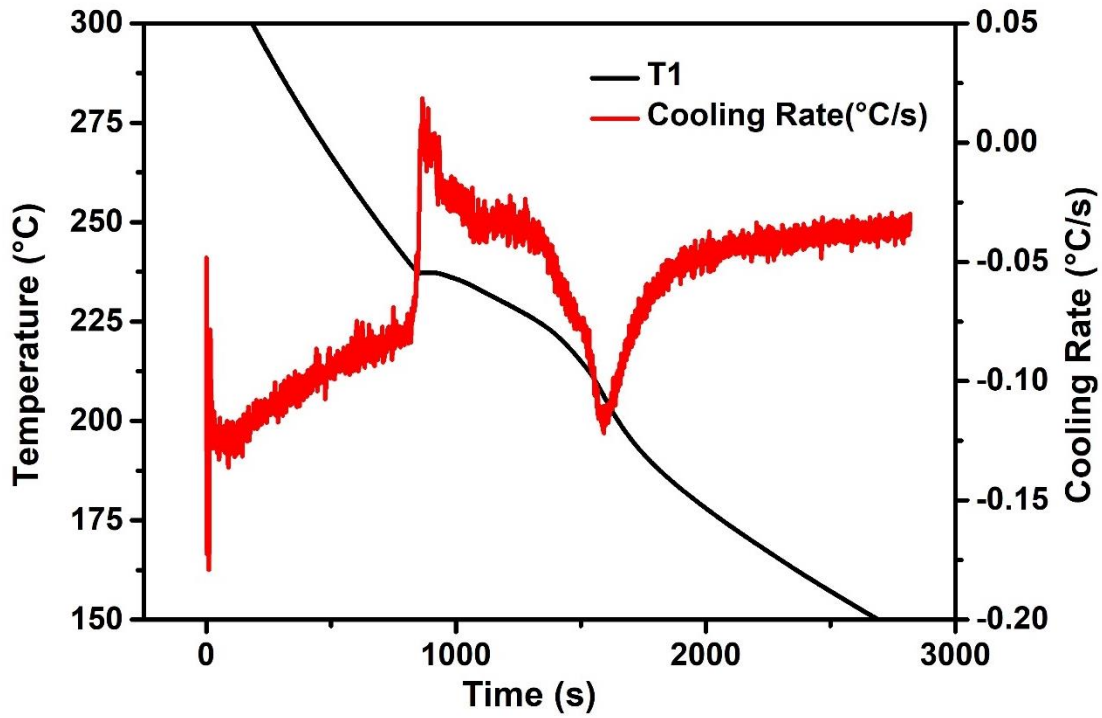
Figure 5.18: The cooling curve and the cooling rate curves of 60wt% NaNO₃ and 40wt% KNO₃ solar salt with Air cooling
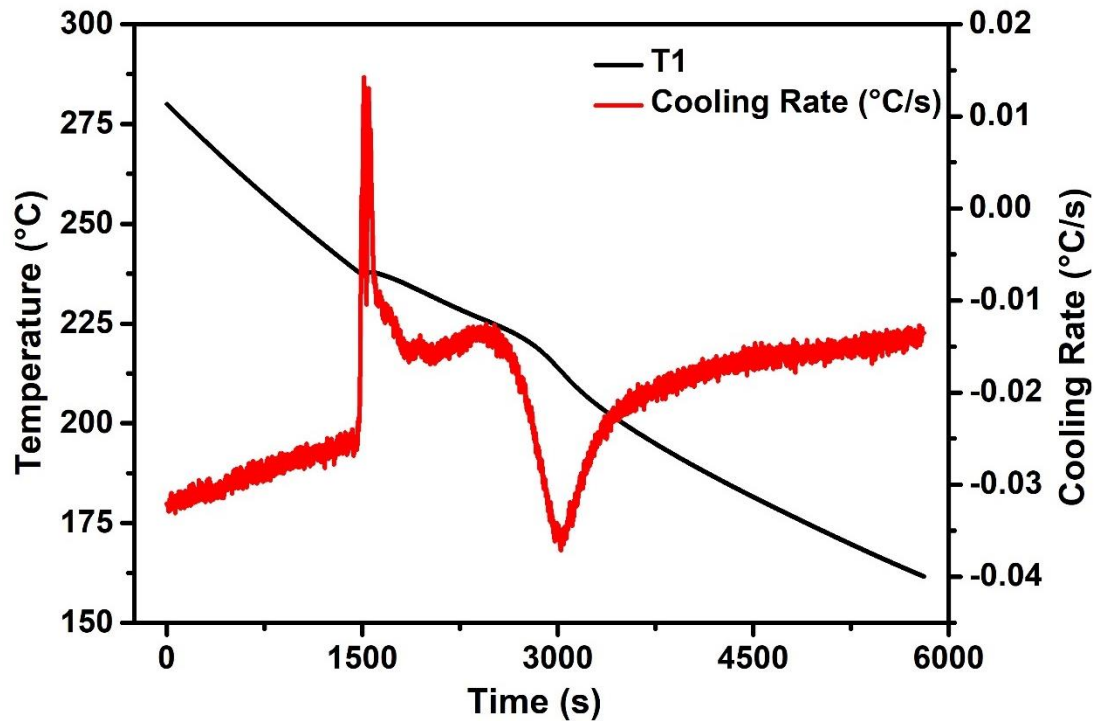
Figure 5.19: The cooling curve and the cooling rate curves of 60wt% NaNO₃ and 40wt% KNO₃ solar salt with Furnace cooling

The estimated heat flux at the salt and the mold interface for KNO_3 and 60wt% $NaNO_3$ and 40wt% KNO_3 solar salt are shown in Figures 5.20 and 5.21.
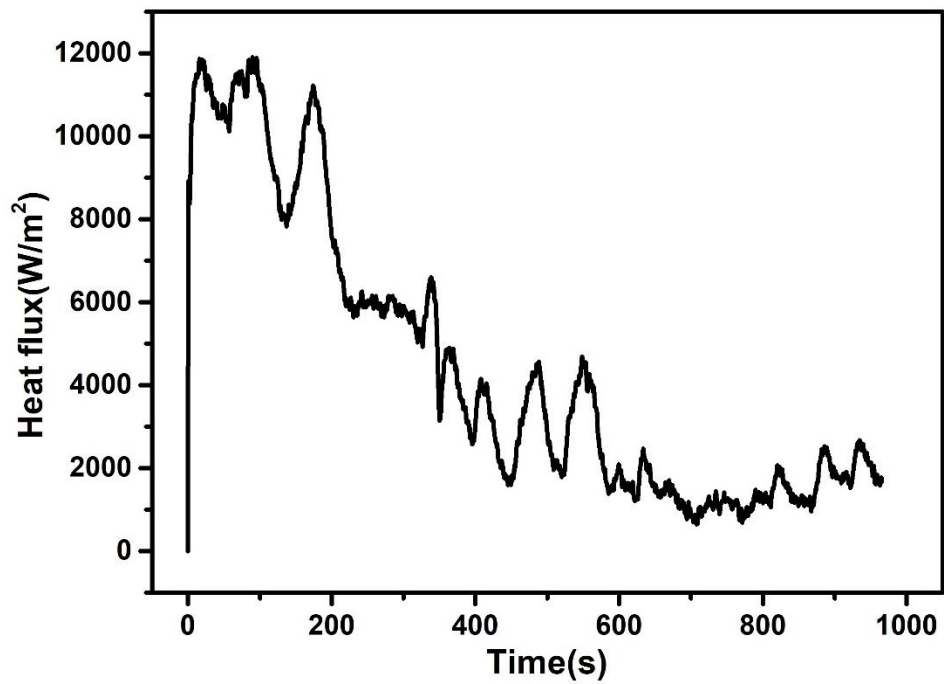
Figure 5.20: Estimated heat flux transients for the salt KNO_3 with Air cooling
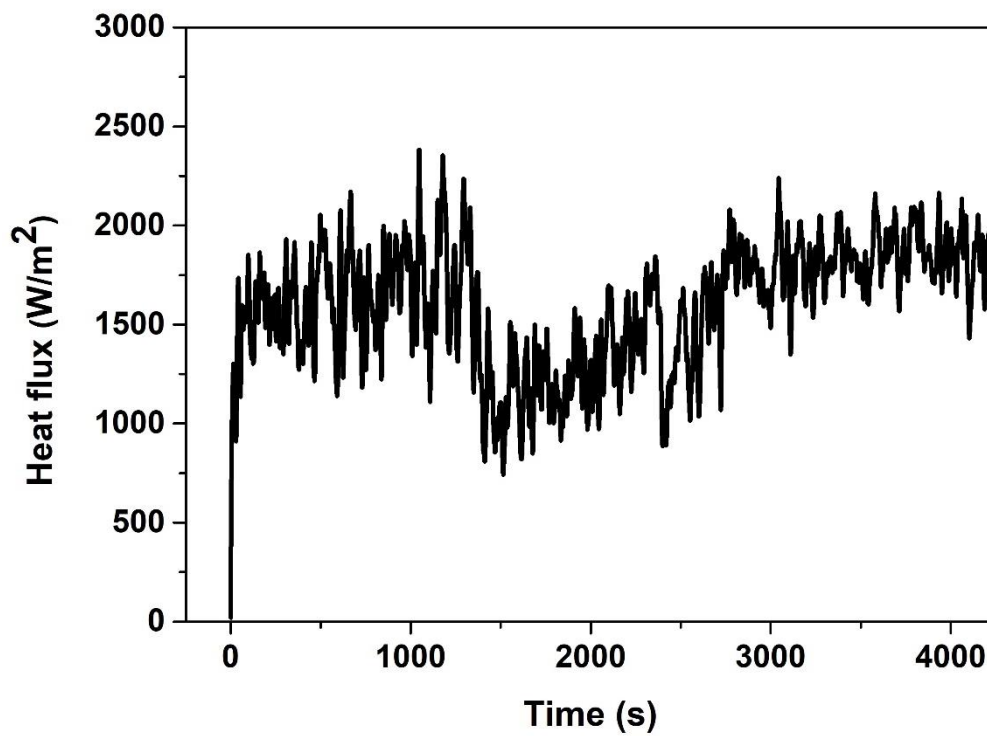
Figure 5.21: Estimated heat flux transients for the salt KNO_3 with Furnace cooling
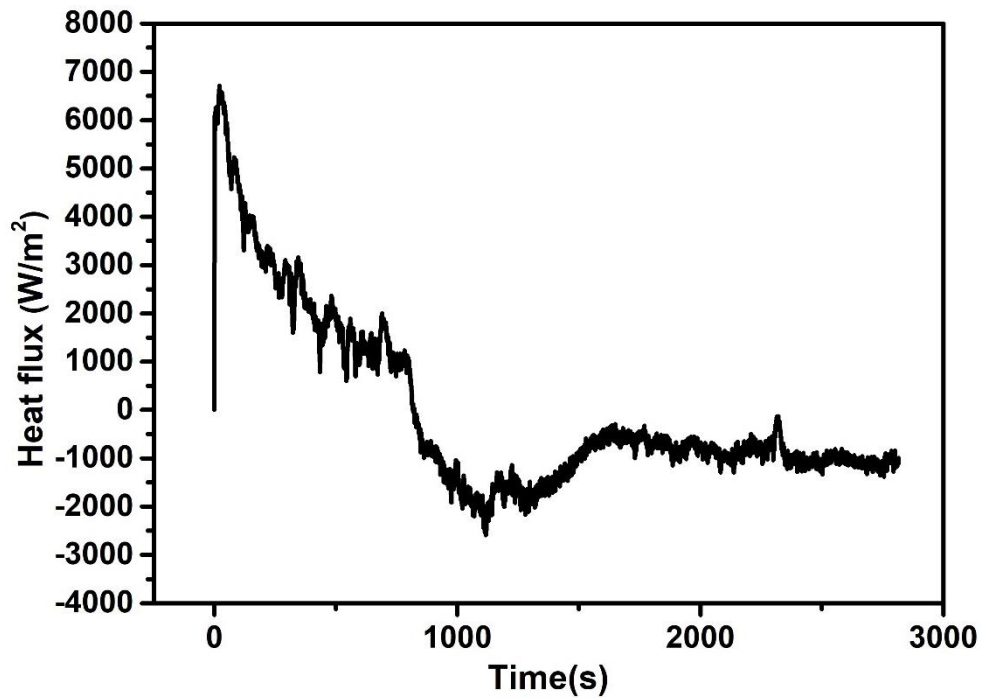
Figure 5.22: **Estimated heat flux transients for the 60wt% NaNO₃ and 40wt% KNO₃ solar salt with Air cooling**
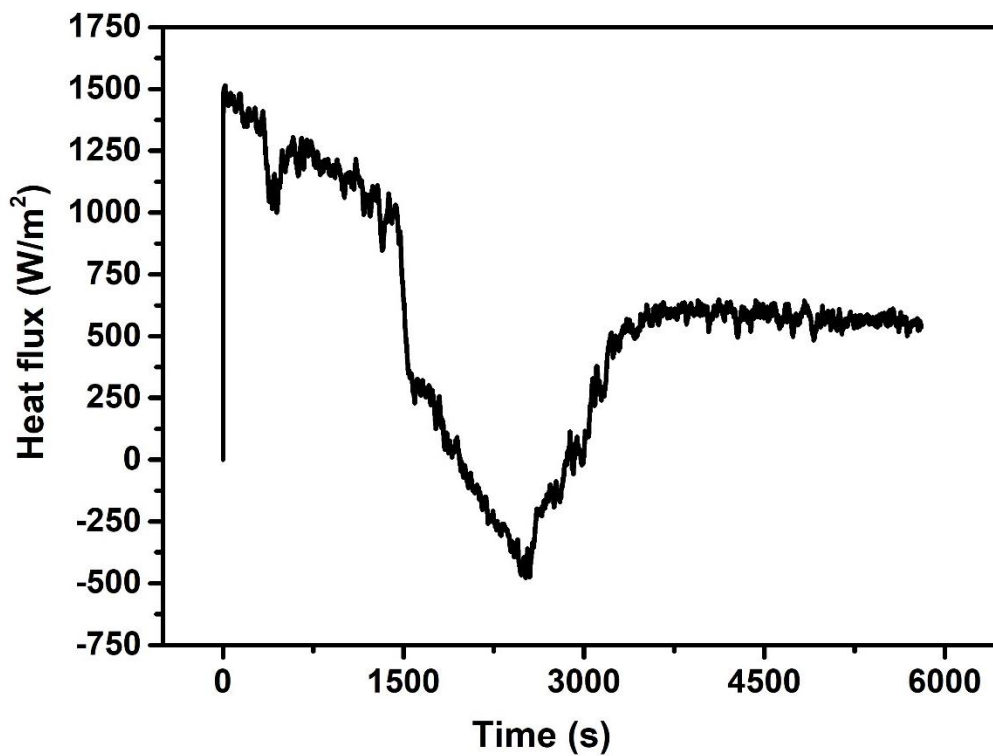
Figure 5.23: **Estimated heat flux transients for the 60wt% NaNO₃ and 40wt% KNO₃ solar salt with furnace cooling**

The wetting behavior of the KNO_3 and solar salt on the mild steel surface is shown in Figures 5.24 and 5.25, respectively.
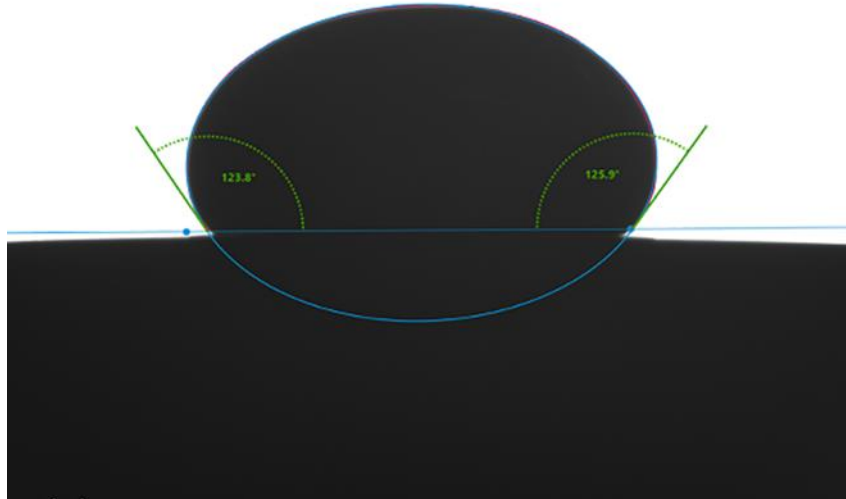
Figure 5.24: Wetting behavior of the solar salt sample on the mild steel surface
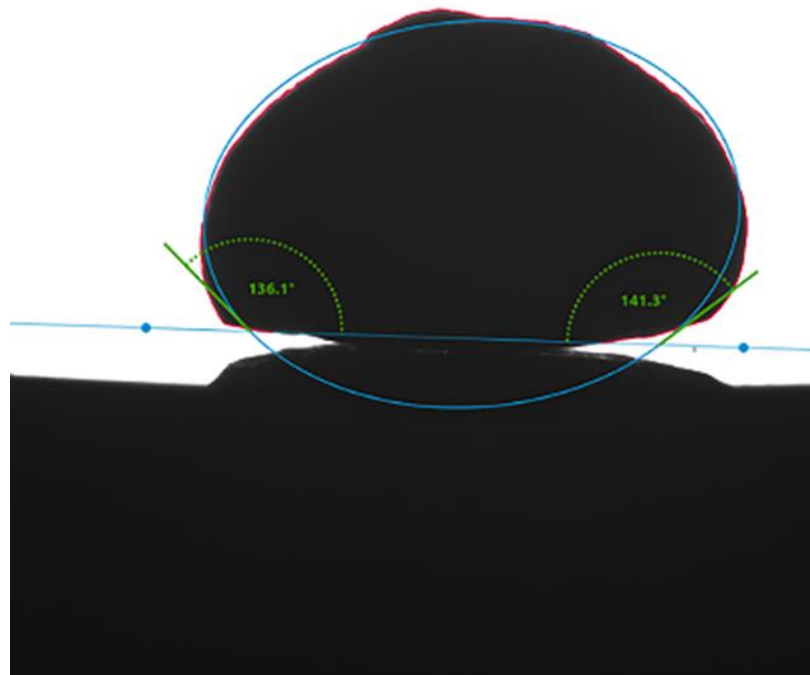
Figure 5.25: Wetting behavior of the KNO_3 salt sample on the mild steel surface

The contact angle between the salts and the mild steel surface is measured and given in Table 5.3.

Table 5.3: Contact angle data for both the salt samples on the mild steel surface

Salt sample	Mean contact angle	Contact angle (left)	Contact angle (right)
Solar salt	124.88°	123.8°	125.9°
KNO₃	138.69°	136.1°	141.3°

5.3.2. Discussion

In the case of air-cooled Potassium Nitrate (KNO$_3$), as per the cooling process shown in Figure 5.12, the salt changes its phase at a temperature of 335.2 °C representing its melting temperature. KNO$_3$ took a total of 229 s for complete phase change considering the ±5 range.

In the case of furnace cooling of KNO$_3$ represented in Figure 5.13, the phase change temperature was 335.5 °C, and the salt took 711 s for its complete solidification.

For solar salt, considering the ±5 range, the solidification starts at 242 °C and ends at 205 °C for both the cooling processes. The total time taken for complete solidification is 817 s and 1993.5 s for air cooling and furnace cooling, respectively, as shown in Figures 5.14 and 5.15.

The ±5 range was considered in selecting the start and end of solidification points to avoid any errors in the selection of solidification points which may affect the results obtained.

It can also be observed that the cooling rate had no significant effect on the phase change parameters of the salt samples.

The phase change enthalpy values for KNO$_3$ in this method was calculated to be 88.85 kJ/kg and 108.9 kJ/kg during air cooling and furnace cooling respectively while the reported literature values are 91 kJ/kg and 102 kJ/kg (Sudheer and Prabhu 2016)(Roget et al. 2013b). It can be observed that the latent heat values obtained using this method were nearly close to the reported values of the literature.

The phase change enthalpy calculated using this method for the solar salt was 92 kJ/kg and 104.1 kJ/kg for air cooling and furnace cooling, respectively. The values calculated were in agreement with the data reported (98 kJ/kg) in the literature (Lasfargues et al. 2015).

A drop in the heat flux curve in the solidification range was observed for solar salt as shown in Figure 5.22 and 5.23 which was due to the phase transformation of the salt. Such a drop was not significantly observed in KNO_3 heat flux data in Figures 5.20 and 5.21. To study this more, the wetting behavior or the contact angle analysis of both the salts on a mild steel substrate was studied.

From the wetting behavior, as shown in Figures 5.24 and 5.25 and contact angle analysis data as shown in Table 5.3, it was observed that the contact angle of the solar salt on the mild steel surface was lower than KNO_3, indicating better wettability of the solar salt.

The lower wettability of KNO_3 on mild steel surface leads to the formation of air pockets at the interface which acts as a barrier to the heat transfer from the salt to the mold. Therefore, the salt/ mold interfacial heat flux data did not capture the phase transformation during the solidification of the salt. However, in solar salt, the wetting tendency is higher, leading to a conforming contact at the salt/ mold interface and lower resistance to interfacial heat transfer. Therefore, the heat flux transients reflect the phase transformation of the solar salt as indicated by a sharp drop during the solidification range.

5.4. A quantitative approach for thermal characterization of phase change materials

5.4.1. Results

The CACCA analysis was done on the salt samples of KNO_3 and $NaNO_3$ and solar salt and the thermal behavior of the samples on cooling was recorded. The thermal history of salts and temperature data of the mold for both the cooling techniques (air and furnace) were measured. The cooling rate curves of the salt samples were superimposed on the cooling curves of the samples under both cooling conditions and are depicted in Figures 5.26- 5.31.
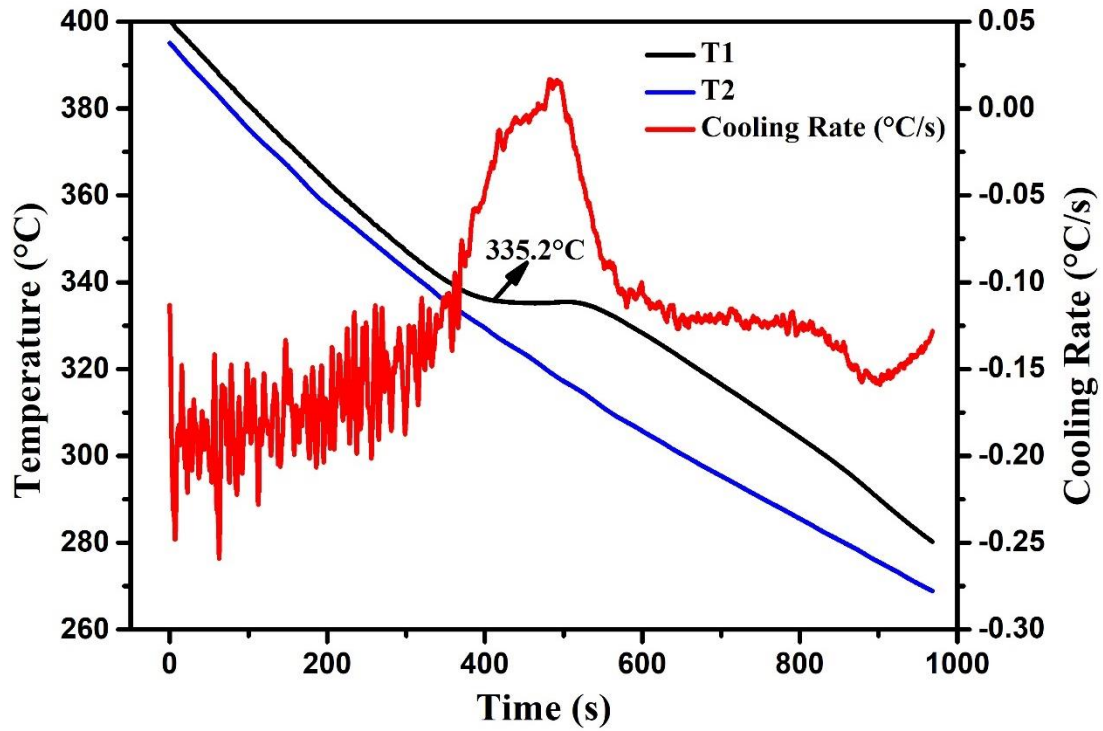
Figure 5.26: Temperature history of KNO₃ and mold with the superimposed first derivative curve with air cooling
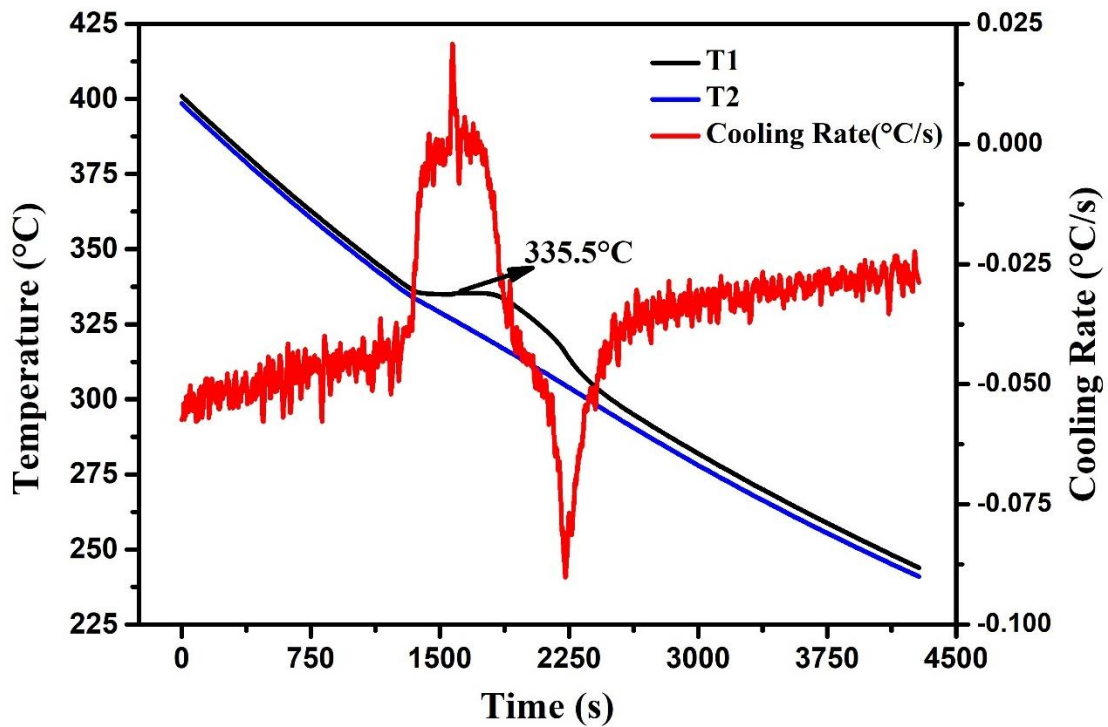
Figure 5.27: Temperature history of KNO₃ and mold with the superimposed first derivative curve with Furnace cooling

104
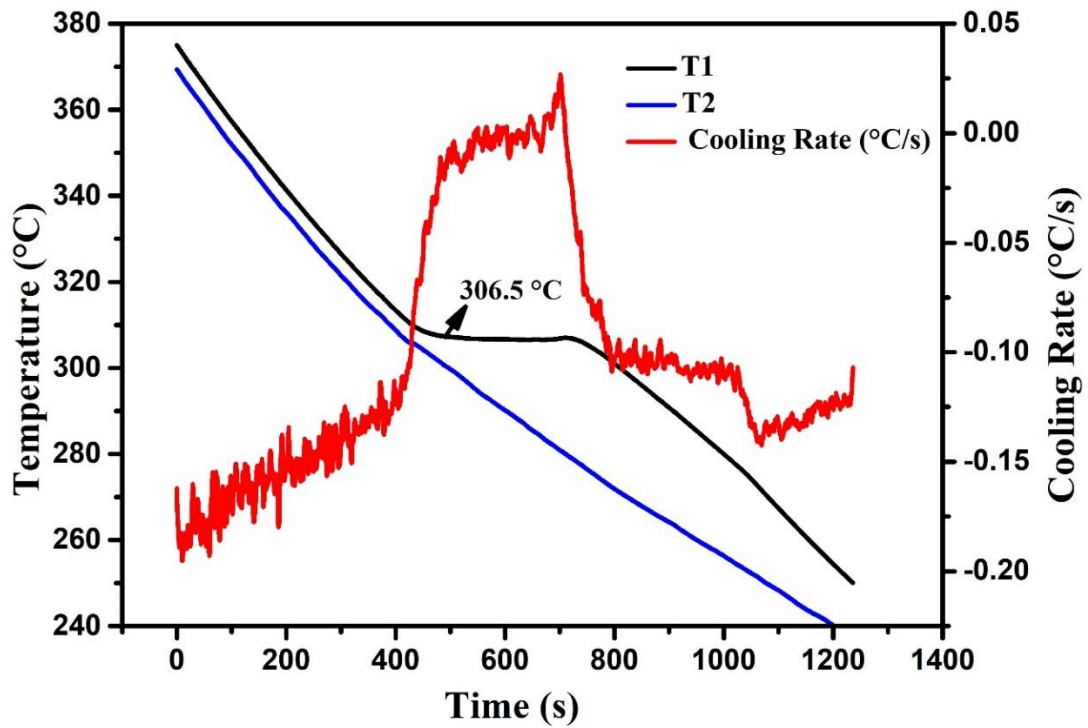
Figure 5.28: Temperature history of NaNO₃ and mold with the superimposed first derivative curve with air cooling
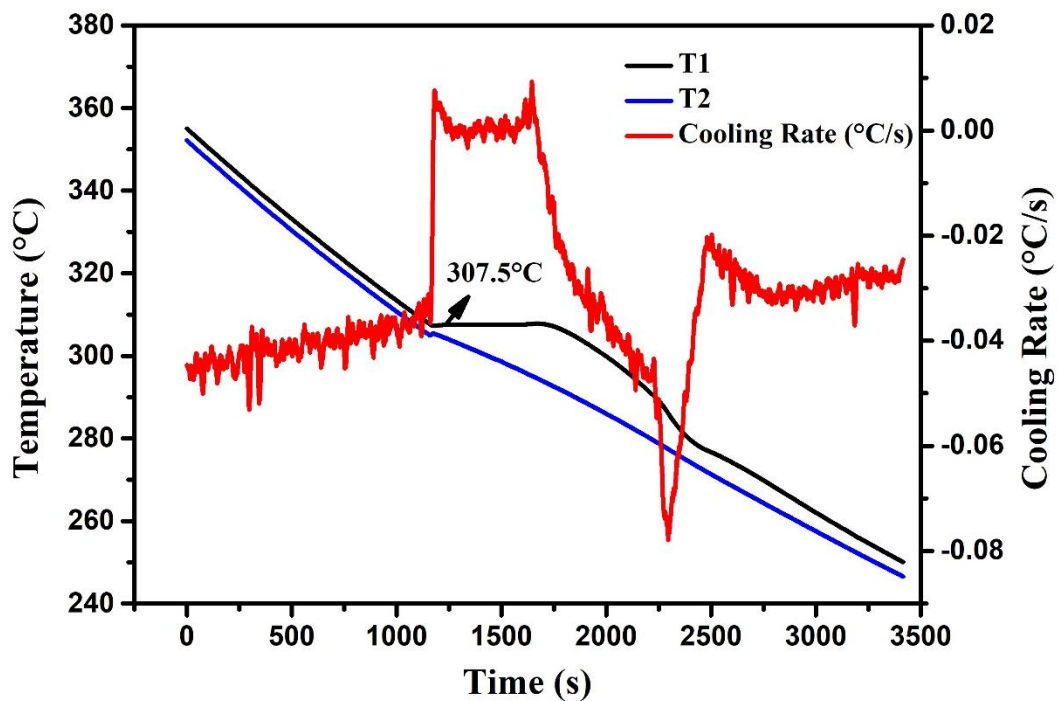
Figure 5.29: Temperature history of NaNO₃ and mold with the superimposed first derivative curve with furnace cooling
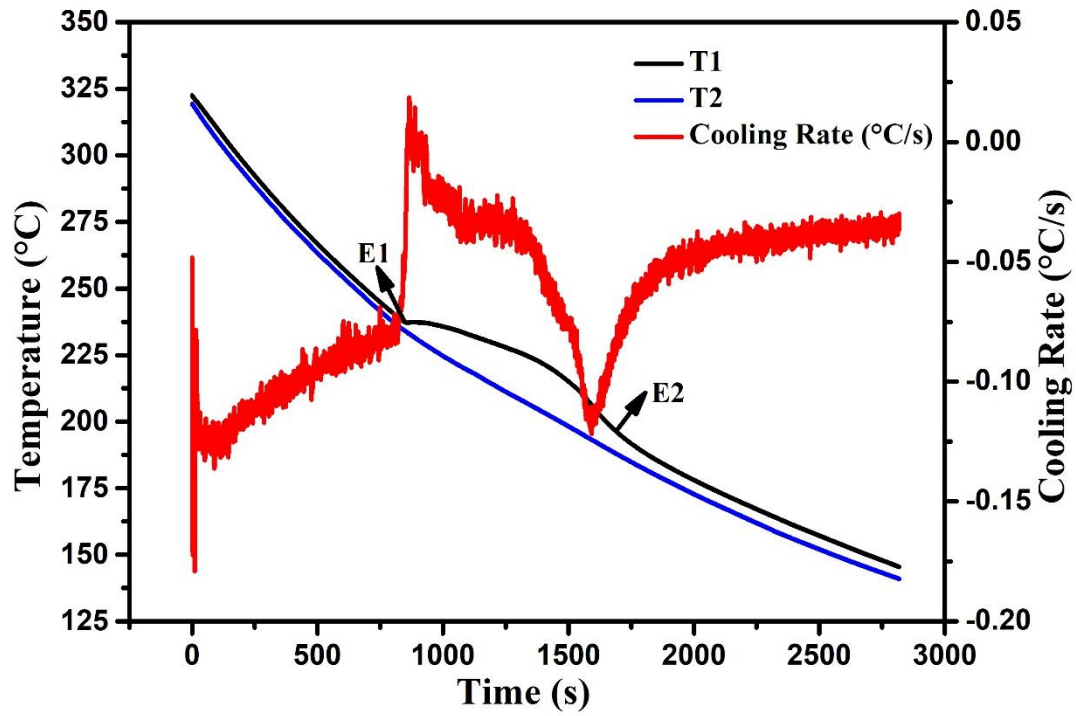
Figure 5.30: Temperature history of solar salt and mold with the superimposed first derivative curve with air cooling
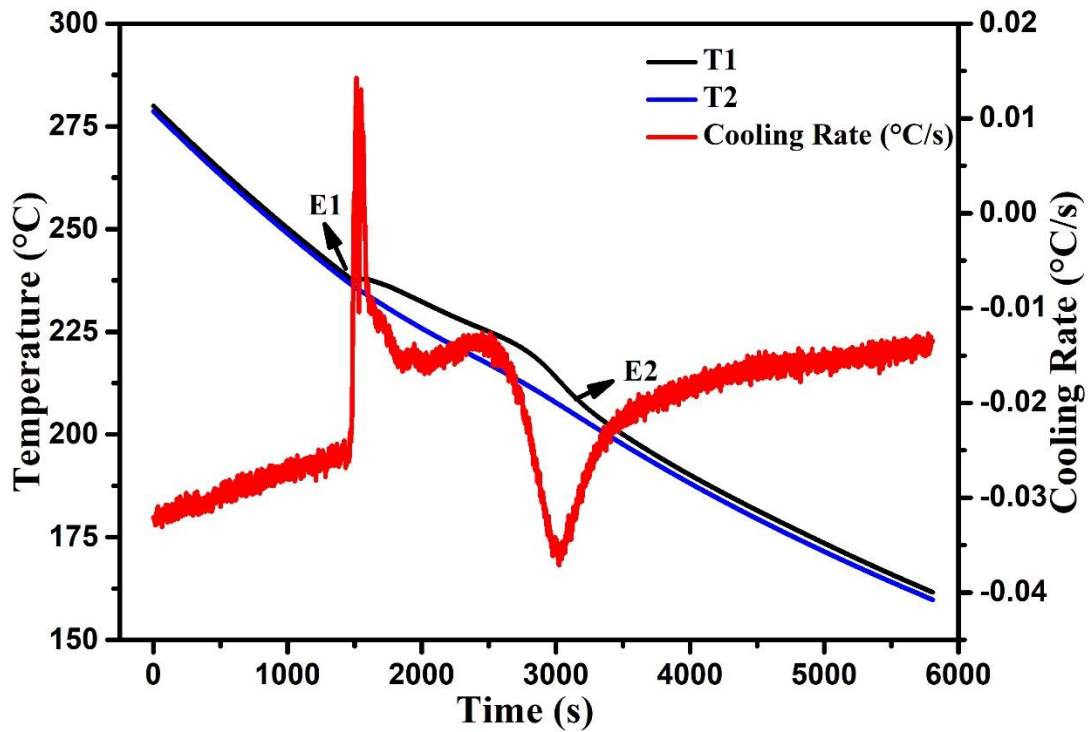
Figure 5.31: Temperature history of solar salt and mold with the superimposed first derivative curve with furnace cooling

5.4.2. Discussions

The phase change characteristics of the salt samples such as solidification temperature, solidification time, start and end of solidification temperatures, and the phase change enthalpy of the salt samples under both the cooling conditions are given in Table 5.4

Table 5.4: Phase change characteristics of salts under both cooling conditions

Materials / Properties	KNO$_3$		NaNO$_3$		Solar salt	
	Air-cooled	Furnace cooled	Air-cooled	Furnace cooled	Air-cooled	Furnace cooled
Melting temperature (°C)	335.2	335.5	306.5	307.5	221	221
Start of solidification temperature (°C) (E1)	340.2	340.5	311.5	312.5	242	242
End of solidification temperature (°C) (E2)	330.2	330.5	301.5	302.5	205	205
Solidification time (s)	229	711	379.5	886	817	1993.5
Latent heat (kJ/kg)	99.58	95.93	185.28	161.58	109.83	106.06

In the case of air-cooled KNO$_3$, the measured melting temperature was 335.2 °C with ± 0.5 °C standard deviations assuming ±5 of the melting temperature as the solidification range. Similarly, in the case of the furnace cooled this temperature was measured to be 335.5 °C ± 0.5°C.

The total solidification time depends on the cooling method; thus, air-cooled sample solidified in 229 s, whereas the furnace cooled sample took 711 s for complete solidification.

The phase change enthalpy of the KNO_3 sample calculated was 99.58 ± 5 kJ/kg and 95.93 ± 5 kJ/kg for both air-cooled and furnace-cooled samples. The values obtained are in close accordance with the reported literature values of 91 kJ/kg and 102 kJ/kg (Sudheer and Prabhu 2016) (Roget et al. 2013b). We can see that the cooling rate did not affect the phase change characteristics of the sample except the solidification time.

In the case of $NaNO_3$, the melting temperature measured for the air-cooled sample was $306.5 \pm 1°C$, and furnace cooled sample was $307.5 \pm 1°C$. The total time of solidification for the air-cooled sample was 379.5 s and 886 s for the furnace-cooled sample.

The latent heat calculated for $NaNO_3$ sample was 185.28 ± 10 kJ/kg and 161.58 ± 10 kJ/kg for both air-cooled and furnace-cooled samples. The latent heat values reported in the literature are about 172 kJ/kg and 177 kJ/kg. (Tooklang et al. 2014)(Zhao et al. 2015)

Similarly, for the solar salt sample, the start and the end of the solidification temperature were measured as 242 °C and 205 °C for both the cooling methods. The time taken for solidification was calculated to be 817 s and 1993.5 s in air-cooled and furnace-cooled samples, respectively. The estimated phase change enthalpy values were 109.83 kJ/kg, and 106.06 kJ/kg for air-cooled samples and furnace cooled samples, respectively. The calculated values were in close accordance with the literature. (Lasfargues et al. 2015)

5.5. Thermal characterization of Lithium binary, Lithium ternary, and Lithium quaternary nitrate eutectic salts enhanced with nanoparticles:

Temperature measurements during cooling were used to obtain the cooling curve/thermal history of the salt and the mold. The start and end solidification temperature was estimated using the cooling rate curve, which is nothing but the 1st derivative curve of the thermal history of the salt. The solidification time was calculated using the start and the end of the solidification temperature. The thermal characterization of the salt was done using the IHCP-energy balance method in steel mold with furnace cooling.

The base salts and the enhanced salts melt over a range of temperatures rather than at a single temperature as they are not pure materials. The thermal parameters analyzed for all the base salts and nanoenhanced salts are the start and end of solidification temperatures, solidification time, effective specific heat capacity, average specific heat capacity, latent

heat, thermal diffusivity, thermal conductivity, and thermal effusivity. The results of the average solidification points and solidification time are given in Table 5.5.

Table 5.5: The solidification temperatures, melting range, and solidification time of lithium-based PCMs and Ne-PCMs

	MWCNT concentration	Start of solidification temperature (°C)	End of solidification temperature (°C)	Melting range	Solidification time (s)
LiK	0%	121.74 ± 1.35	92.48 ± 2.78	29.25	5001±346
	0.1%	123.66 ± 2.47	92.5 ± 1.9	29.94	5132±436
	0.5%	122.58 ± 1.84	92.9 ± 1.98	30.24	4843±288
	1%	124.88 ± 0.83	92.57 ± 1.79	32.31	5021±183
LiT	0%	117.41 ± 1.33	96.64 ± 1.87	20.77	3293±289
	0.1%	122.58 ± 0.75	103.80 ± 0.63	18.78	3022±205
	0.5%	124.68 ± 1.23	104.41 ± 1.86	20.26	3203±173
	1%	123.33 ± 2.37	103.11 ± 1.18	19.74	3165±278
LiQ	0%	101.59 ± 2.8	86.65 ± 2.33	14.94	2806±286
	0.1%	96.09 ± 2.27	83.21 ± 3.1	13.31	2746±321
	0.5%	96.11 ± 1.86	83.66 ± 1.99	12.45	2697±236
	1%	95.64 ± 2.65	81.98 ± 3.34	13.63	2780±201

It was observed that the addition of any weight concentration of nanoparticles to the lithium base salts did not affect the start and end of the solidification point and the solidification time, but a significant effect was observed in other parameters, which are discussed below.

5.5.1. Latent heat

The phase change materials have high energy storage capacity because of the latent heat involved in their phase change. The latent heat value of the base salt was calculated and

compared to the literature values to assess the reliability of the method and the salt produced. The latent heat values of the base salts obtained and the literature values were in close agreement with each other.

The latent heat value was affected by the addition of nanoparticles. It was observed that 0.1% MWCNT produced the highest enhancement, followed by 0.5% and then 1%.

This trend was observed both in LiK and LiT salts. LiQ enhanced salts showed no or a minimal effect on the phase change enthalpy of the system.

An enhancement in the value means that the energy storage capacity of the base salts is increased, which will, in turn, improve the efficiency and effectiveness of the TES.

In the case of NePCMs, the intimate inclusion of nanoparticles in salt PCMs can change the van der walls forces when the concentration of nanoparticles is high. If the salt and nanoparticle's interaction potential is higher than that between the salt molecules themselves, an increase in the latent heat is expected. This could be a reason for the increase in the value of latent heat obtained. (Shaikh et al. 2008)(Hamdy et al. 2017).

Sometimes these nanoparticles agglomerate and form small agglomerates which entrap some nanoparticles. This agglomerate also entraps some solid PCM. Therefore, more energy is required to melt the entrapped salt, causing an increase in the latent heat value. (Chieruzzi et al. 2015)

The decrease in the latent heat observed at higher concentrations is attributed to the addition of a high concentration of nanoparticles. Under these conditions, the nanoparticles get trapped and form agglomerates which affect the latent heat by altering the entropy of the system. (Hamdy et al. 2017).

5.5.2. Average specific heat capacity

The energy storage density of the PCM is governed by two forms of heat, namely sensible heat and latent heat. For sensible heat, the SHC is a significant parameter. The addition of nanoparticles affects the SHC values and, in turn, affects the energy storage capacity of the material. The specific heat capacity obtained for the base salt was in close accordance with literature data. A significant increase in the value was obtained at 0.1% MWCNT while 0.5

and 1% showed less increment in the case of LiK and LiT salts. In LiQ salts, not much influence was observed due to nanoparticle addition.

The nanoparticles possess high surface energy owing to their high surface area to volume ratio. Due to this high surface energy, they adsorb the salt ions onto their surface to form nanolayers. These nanolayers/ semisolid layers are considered to possess enhanced thermal properties and chemical properties, thus leading to an increase in the specific heat capacity of the PCM. The nanoparticles due to their high surface area and high surface energy, lead to an increase in the thermal resistance between the nanoparticles and the bulk salt molecules. This interfacial interaction can also lead to a rise in SHC and act as an additional thermal storage factor (Chieruzzi et al. 2015).

With a further increase in the concentration, a decrease in average SHC was observed. This decrease can be due to the agglomeration of nanoparticles at higher concentrations. The nanoparticles cluster together and settle down due to agglomeration. Therefore, the surface energy decreases, and also, they do not participate in the enhancement process.

5.5.3. Effective specific heat capacity

To represent the storage capacity of the PCM, a parameter that involves the cumulative effect of the specific heat and the latent heat is the effective specific heat capacity of the material. A similar trend was observed for this parameter too. A similar trend as average SHC was observed in the case of LiT and LiK salts. The effect of nanoparticles addition to LiQ had an insignificant impact on the latent heat and average SHC. Therefore, the impact on effective SHC was also negligible. The effective specific heat capacity includes both the average specific heat capacity and the phase change enthalpy. So, a similar trend was observed with nanoparticle addition.

The effect of various concentrations of Nanoparticles on the above three parameters is tabulated in Table 5.6.

Table 5.6: Latent heat, solidification temperature, and solidification time for various MWCNT concentrations

Salt	MWCNT concentration	Latent heat (kJ/kg)		Effective specific heat capacity (kJ/kgK)		Average specific heat capacity (kJ/kgK)	
		Average value	%age enhancement	Average value	%age enhancement	Average value	%age enhancement
LiK	0%	176	-	7.4	-	1.3	-
	0.1%	225	27.6	10.1	36.6	2.6	92.05
	0.5%	196	11.4	8.8	19.5	2.3	68.5
	1%	185	4.97	7.9	6.58	1.8	34.3
LiT	0%	97	-	7.3	-	2.7	-
	0.1%	116	19.28	9.7	31.98	3.4	26.21
	0.5%	115	18.27	9.1	24.47	3.1	16.98
	1%	107	10.3	8.7	19.54	2.8	6.10
LiQ	0%	59	-	8.0	-	3.9	-
	0.1%	64	9.4	8.2	2.07	3.4	-12.63
	0.5%	60	1.62	8.7	9.31	4.0	0.57
	1%	51	-13.45	7.3	-9.11	3.3	-15.41

The effect of nanoparticles on various other parameters like thermal diffusivity, thermal conductivity, and thermal effusivity was also studied.

5.5.4. Thermal diffusivity

It is a significant parameter that includes the cumulative effect of both thermal conductivity and average SHC, keeping the density of the material constant. The thermal diffusivity value is directly proportional to the thermal conductivity and inversely proportional to the

average SHC. Therefore, the net effect of both thermal conductivity and SHC is reflected in the value of thermal diffusivity. The effect produced by the addition of nanoparticles followed the same trend in this property too. The value of the thermal parameter increased with 0.1% addition of nanoparticles reflecting the higher increase in thermal conductivity than SHC. This value slightly decreased by 0.5% and then reduced by 1% for LiK and LiT salts. LiQ showed no such trend or increment.

5.5.5.   Thermal conductivity

Inorganic salt-based PCMs have a limitation of low thermal conductivity due to which the charging and the discharging time of the PCM are high. To alleviate this limitation, high thermal conductivity nanoparticles are introduced into the base PCMs. MWCNT due to their columnar structure, forms fractal-like long-range dendritic nanostructures that form the heat conduction links to enhance the heat transfer and the thermal conductivity. (Hamdy et al. 2017)The addition of 0.1% MWCNT showed a rise in the value, while the value did not significantly increase at a higher concentration of MWCNT. This can be due to the formation of agglomerate clusters of nanoparticles leading to their settling. Once settled, the nanoparticles do not contribute to the improvement of the thermal characteristics.

5.5.6.   Thermal effusivity

It is a very significant, key performance parameter associated to analyse the performance of the PCM. It defines the ability of the PCM to exchange heat with the surroundings. Therefore, PCMs with higher effusivity can absorb or release more thermal energy and at a faster rate. It includes the net effect of thermal conductivity and average specific heat capacity in its value. The addition of nanoparticles had a positive impact on the thermal effusivity value. A significant increase was observed with the addition of 0.1 to 0.5% MWCNT. Beyond this concentration, the effect was reduced.

The values obtained for the above parameters in NePCM and base PCMs are given in Table 5.7.

Table 5.7: Thermal Diffusivity, Conductivity and effusivity values of PCMs and NePCMs

Salt	MWCNT concentration	Thermal diffusivity (m²/s)		Thermal conductivity (W/mK)		Thermal effusivity (Ws$^{1/2}$/m²K)	
		Average value	%age enhancement	Average value	%age enhancement	Average value	%age enhancement
LiK	0%	3E-07	-	0.6	-	1196.18	-
	0.1%	5E-07	52.1	2.5	290.5	3309.17	176.6
	0.5%	4E-07	33.2	1.8	185.7	2449.50	104.8
	1%	2E-07	-25.1	0.9	46	1487.61	24.4
LiT	0%	2E-07	-	0.8	-	1723.89	-
	0.1%	4E-07	115.8	1.4	69.8	2657.56	54.2
	0.5%	3E-07	70.9	1.0	26.5	2498.29	44.9
	1%	2E-07	-9.2	1.0	21.1	2258.07	30.9
LiQ	0%	2E-07	-	0.9	-	2859.29	-
	0.1%	2E-07	6.1	1.2	32.9	2741.55	-4.1
	0.5%	2E-07	-16.6	0.9	5.5	2449.64	-14.3
	1%	2E-07	-8.9	1.2	28	2539.78	-11.2

The results obtained for the basic parameters were selected by maximizing the number of trials and by maintaining the minimum standard deviation. The average value of these basic parameters for lithium-based PCMs and NePCMs, along with the standard deviation is shown in Figure 5.32 below.
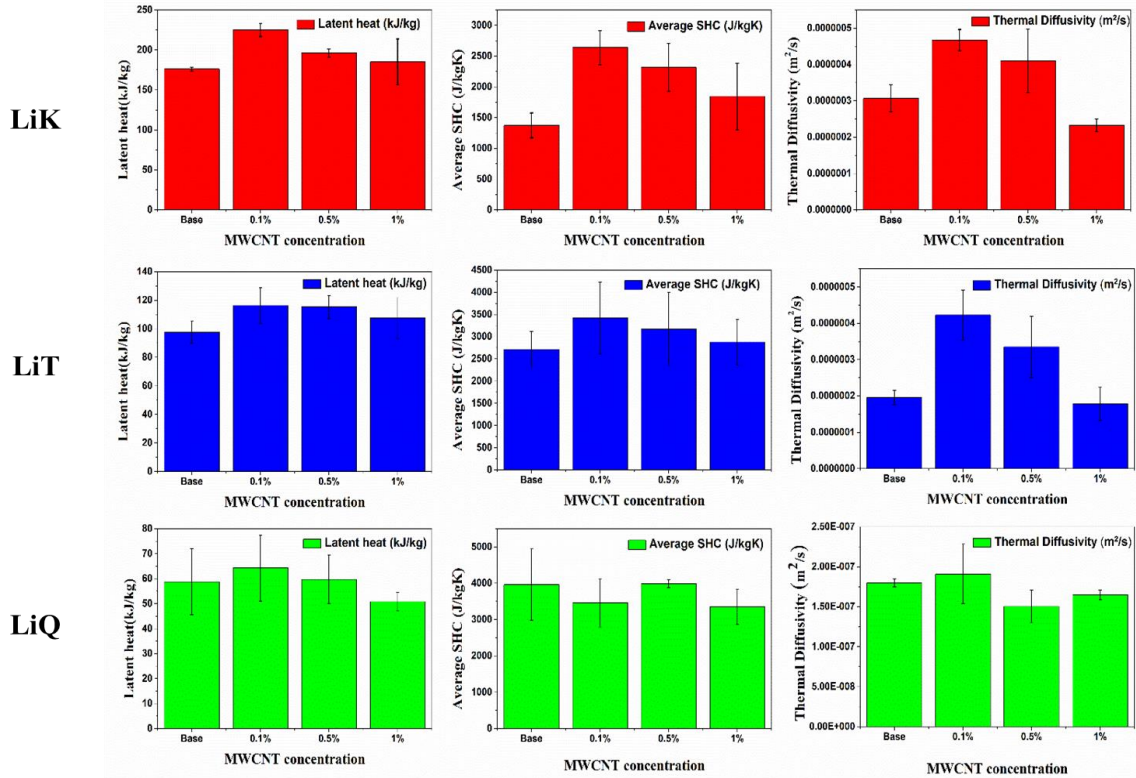
Figure 5.32: The average values with their corresponding error values of PCMs and NePCMs

To summarize, the nanoparticles between the ranges of 0.1% -0.5% showed a significant positive impact on all the thermophysical parameters of the PCMs. With 1 % nanoparticles, agglomeration, clustering, and settling reduced the effectiveness of the nanoparticles added. Such a trend was not observed in LiQ salts. The addition of MWCNT nanoparticles had no significant effect on the thermal parameters of the salt. The reason can be that being a multi-component system, the stability of the salt is relatively less. Degradation of the salt can also be a reason.

5.6. Measurement Uncertainty analysis

Tables showing the standard deviation, and the sample errors with 95% confidence for the calculated thermal parameters such as latent heat, specific heat capacity and thermal diffusivity are given in tables 5.8, 5.9 and 5.10 respectively. Three trials were performed for each experiment.

Table 5.8: The values of latent heat with the standard deviation values and sample error values (95% confidence)

Salts		Latent heat (kJ/kg)	Standard deviation	Sample error (95% confidence)
LiK	Base	176	4.5	5
	0.1%	224	18	20
	0.5%	196	10	12
	1%	185	53	60
LiT	Base	97	8	9
	0.1%	116	12	14
	0.5%	115	8	9
	1%	107	14	16
LiQ	Base	59	13	15
	0.1%	64	13	15
	0.5%	60	10	11
	1%	51	3	4

Table 5.9: The values of average specific heat capacity with the standard deviation values and sample error values (95% confidence)

Salts		Average SHC (kJ/kgK)	S.D.	Sample error (95% confidence)
LiK	Base	1.3	0.2	0.2
	0.1%	2.6	0.3	0.3
	0.5%	2.3	0.4	0.4

	1%	1.8	0.5	0.6
LiT	Base	2.7	0.4	0.4
	0.1%	3.4	0.8	0.9
	0.5%	3.1	0.8	0.9
	1%	2.8	0.5	0.5
LiQ	Base	3.9	0.9	1.1
	0.1%	3.4	0.6	0.7
	0.5%	4.00	0.1	0.1
	1%	3.35	0.5	0.5

Table 5.10: The values of thermal diffusivity with the standard deviation values and sample error values (95% confidence)

Salts		Thermal diffusivity (m^2/s)	S.D.	Sample error (95% confidence)
LiK	Base	3E-7	4E-8	4E-08
	0.1%	5E-7	3E-8	3E-08
	0.5%	4E-7	9E-8	10E-08
	1%	2E-7	2E-8	2E-08
LiT	Base	2E-7	2E-8	2E-08
	0.1%	4E-7	7E-8	8E-08
	0.5%	3E-7	8E-8	9E-08

	1%	2E-7	5E-8	5E-08
LiQ	Base	2E-7	5E-9	5E-09
	0.1%	2E-7	4E-8	4E-08
	0.5%	2E-7	2E-8	2E-08
	1%	2E-7	6E-9	7E-09

5.7. Micrographic studies of the nano-enhanced salts:

When salts are doped with nanoparticles, these nanoparticles form an interconnected network which provides an easy path for effective heat transfer. Nanoparticles themselves have a higher value of thermal conductivity as compared to salt. Therefore, the addition of nanoparticles leads to an increase in the rate of heat transfer through conduction.

At higher concentrations of nanoparticles in the base salt, they tend to form clusters and agglomerate reducing the quantity of effective nanoparticles available for improvement of thermal properties. To analyze the agglomeration of nanoparticles, micrographic studies of NePCMs were performed.

The SEM micrographs of base salt and nano-enhanced salts with MWCNT concentrations of 0.1, 0.5, and 1% are shown in Figure 5.33-5.36
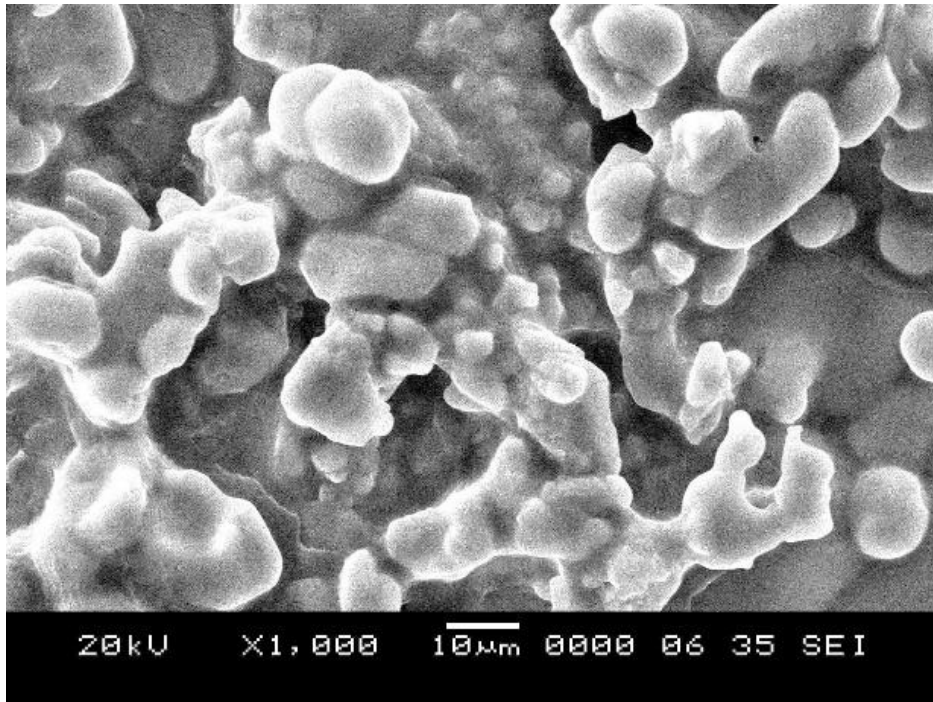
Figure 5.33: The SEM micrographs of nano-enhanced lithium binary Base salt
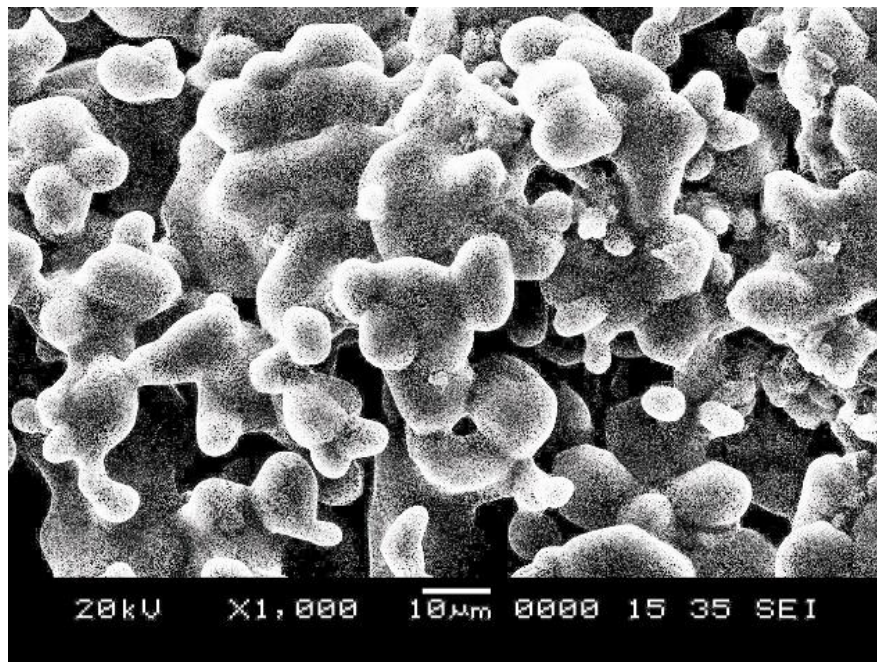
Figure 5.34: The SEM micrographs of nano-enhanced lithium binary salt with 0.1 % MWCNT
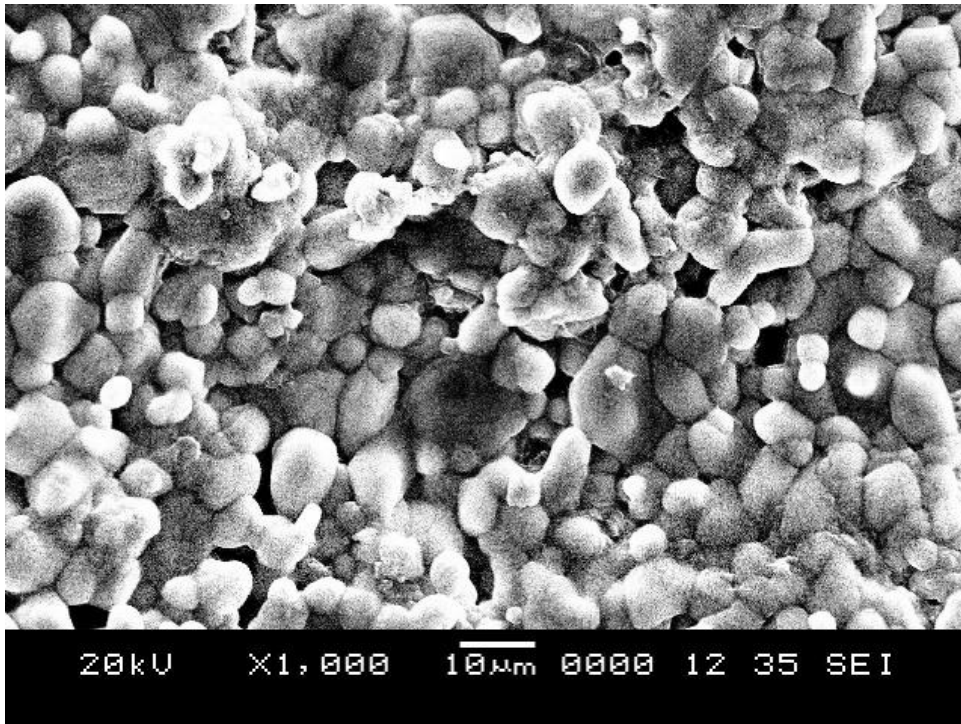
Figure 5.35: The SEM micrographs of nano-enhanced lithium binary salt with 0.5 % MWCNT
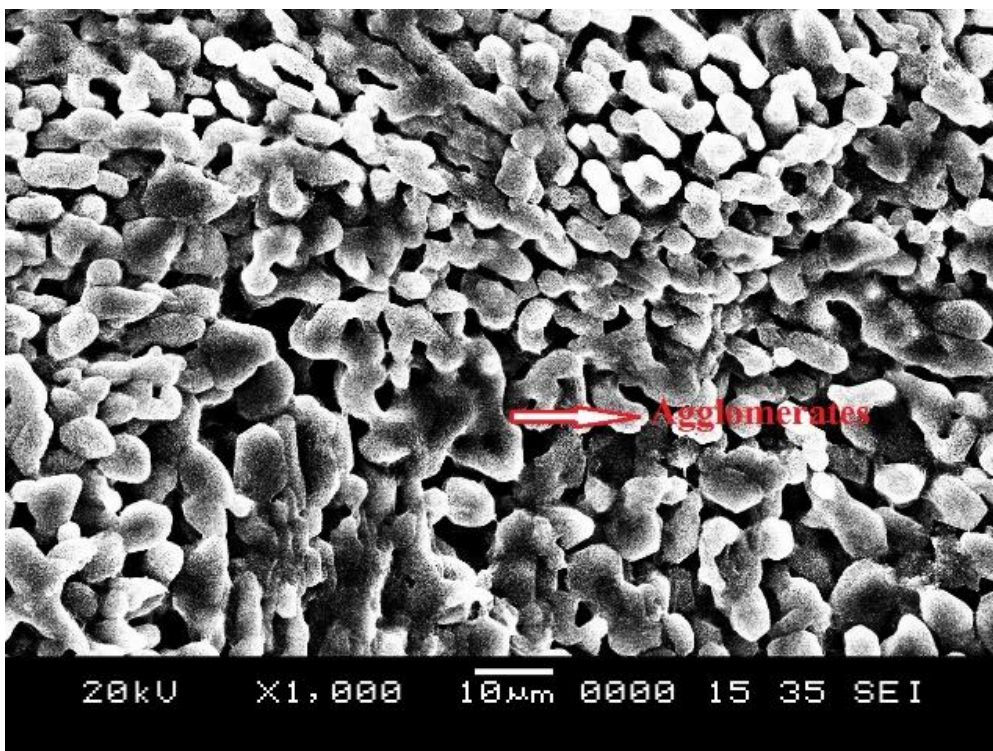
Figure 5.36: The SEM micrographs of nano-enhanced lithium binary salt with 1% MWCNT

120

The agglomeration of nanoparticles can be seen in a higher concentration of nanoparticles which reduces its efficiency to improve the thermal parameters of base salt.

5.8. Wettability studies of the base and nano-enhanced lithium-based salts

The wettability of base salts and nano-enhanced salts was studied on a mild steel surface using the Drop shape analyzer (DSA100, Kruss, Germany). The contact angle of the salts was measured and tabulated. The test sample was prepared by manually using a spatula by impinging a drop of molten salt on the mild steel surface. The contact angle of the solidified drop on the steel substrate was then studied. The contact angles for all lithium based PCMs and nanoenhanced PCMs are shown in figure 5.37-5.39.
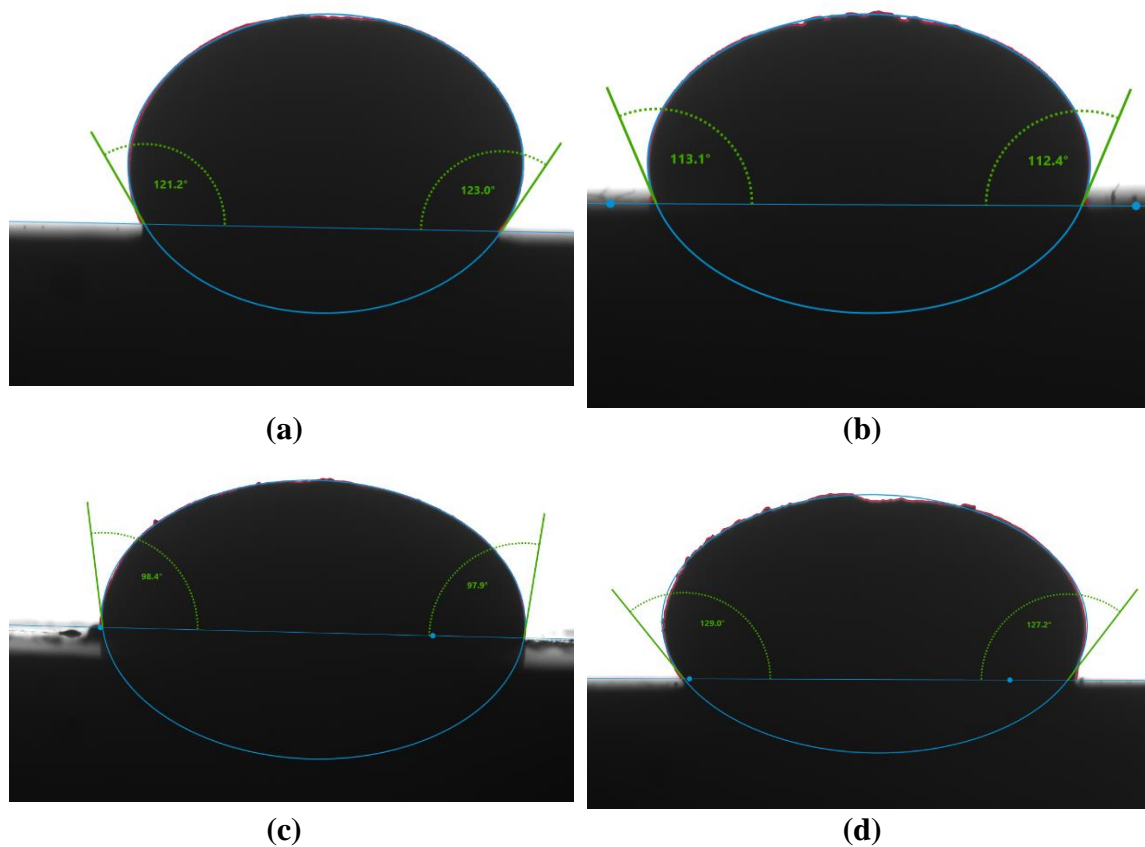
Figure 5.37: Contact angle measurement of LiK (a) Base salt (b) 0.1 wt. % (c) 0.5 wt. % (d) 1wt.%

(a)

/

(b)

(c)

(d)
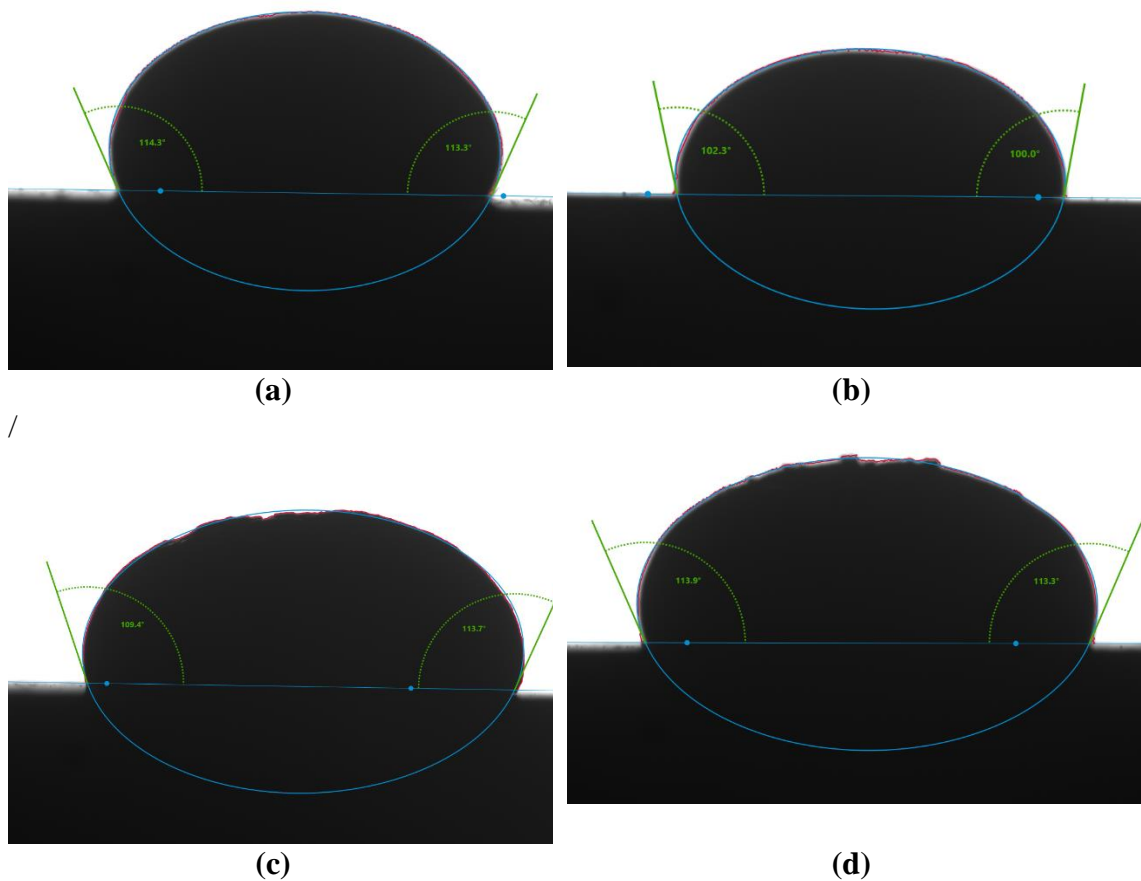
Figure 5.38: Contact angle measurement of LiT (a) Base salt (b) 0.1 wt. % (c) 0.5 wt. % (d) 1 wt.%
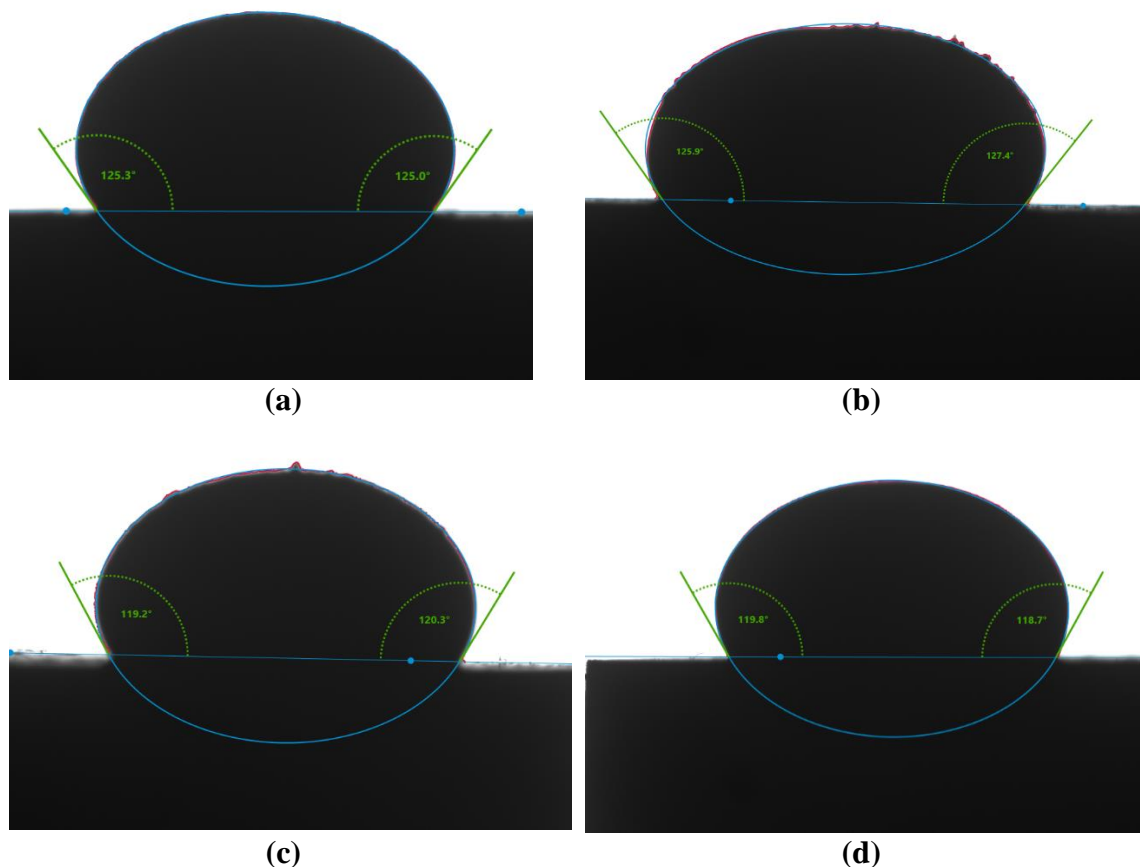
Figure 5.39: Contact angle measurement of LiQ (a) Base salt (b) 0.1 wt. % (c) 0.5 wt. % (d) 1 wt.%

The average contact angle along with their standard deviation for all the lithium-based salts, is listed in Table 5.11.

Table 5.11: The average contact angle of all lithium-based PCMs and NePCMs.

	Base	**0.1**	**0.5**	**1**
LiK	121.57 ± 1.47	112.97 ± 0.83	97.92 ± 0.39	129.46 ± 2.14
LiT	112.31 ± 1.99	100.5 ± 0.92	110.41 ± 0.02	114.81 ± 1.41
LiQ	126.46 ± 1.48	125.42 ± 0.99	121.15 ± 1.85	118.92 ± 0.27

In LiK and LiT salts with 0.1 and 0.5 %, the contact angles showed a lower value than the base salt, which means an improvement in wetting characteristics. In the case of 1%, the contact angle had a higher value owing to the agglomeration and reduction in the

availability of effective nanoparticles. Insignificant or significantly less effect was observed in the case of LiQ salts.

This can be because of the low stability due to the multicomponent system and degradation of the salt which can affect the interaction of the salt with the nanoparticles and in turn affect the wetting behavior of the nano salts.

Chapter 6 CONCLUSIONS

The following conclusions were drawn based on the results and discussion of the present work.

1. The energy balance method is a simple and inexpensive technique to determine the phase change characteristics of metal-based energy storage materials. It provides a good approximation of the phase change enthalpy without any baseline calculations. However, its applicability was limited only to metal-based energy storage materials. and could not characterize salts accurately.

2. The IHCP- Energy balance method eliminated the limitation of fitting the base-line accurately. The phase change characteristics obtained using this method were nearly close to the values reported in the literature. However, the usage of graphite crucible had severe limitations like frequent cracking, moisture absorption, and non-reusability.

3. The modified IHCP- Energy balance method using steel mold offered an inexpensive and straightforward technique to study and assess the solidification parameters of thermal energy storage materials. This method eliminates limitations due to fitting in baseline calculations and errors due to the choice of points for integrating the heat flow peak for latent heat calculations. The phase change parameters and the calculated latent heat values of the KNO_3 and solar salt samples were found to be in good agreement with the reported literature data. The thermal characterization results show that the modified IHCP-energy balance method is promising for the thermal characterization of salt-based phase change materials.

4. The effect of both air cooling and furnace cooling of salt samples in the steel mold was investigated. It was observed that the cooling rate has no significant impact on the solidification characteristics of salt samples.

5. The wettability of the solar salt was higher than KNO_3. The solar salt offers lower resistance to heat flow at the interface, whereas KNO_3 offers more heat flow resistance with non-conforming interfacial contact.

6. A quantitative method based on Fourier's law of conduction of heat transfer was proposed to characterize TES materials. The technique is devoid of sample size limitations, reference materials, baseline calculations, and improper selection of solidification points. The phase change parameters and the latent heat calculated using the quantitative technique were in close accordance with the reported literature data.

7. As LiK has a melting enthalpy higher than Li-T and LiQ and therefore the net heat energy storage capacity of LiK is higher than the other salts.

8. The addition of $LiNO_3$ reduces the melting temperature and thus improves the overall effectiveness of the TES system. Upon improvements in the manufacturing process of $LiNO_3$, low cost, and availability, this critical material can be a crucial component of PCMs for enhanced energy storage of the PCMs.

9. The addition of MWCNT had no significant effect on the solidification temperatures and solidification time for all lithium-based salts.

10. In LiK and LiT salts, the addition of the nanoparticles in the range of 0.1% to 0.5 % showed a significant positive impact on the thermophysical parameters like latent heat, specific heat capacity, thermal conductivity, thermal diffusivity and thermal effusivity. Beyond this, the effect starts to diminish owing to the agglomeration and settling of the nanoparticles. The enhancement in latent heat for LiK and LiT with 0.1 % observed was 27.6% and 19.28% respectively. These values decreased with an increase in the MWCNT weight fractions.

11. The addition of nanoparticles to LiQ salts showed no significant effect on the various thermophysical parameters such as phase change enthalpy, specific heat capacity, thermal diffusivity etc. This can be due to the low stability and the degradation of the salt.

12. In LiK and LiT salts, an improvement in wetting characteristics was observed in 0.1 and 0.5% nanoparticle concentrations. At 1% nanoparticle concentration, the contact angle had a higher value owing to the agglomeration and reduction in the

availability of effective nanoparticles. The effect of the addition of nanoparticles on contact angle was negligible in the case of LiQ salts.

This page intentionally left blank

Chapter 7 REFERENCES

Acem, Z., Lopez, J., and Palomo Del Barrio, E. (2010). "KNO3/NaNO3-Graphite materials for thermal energy storage at high temperature: Part I.-Elaboration methods and thermal properties." *Appl. Therm. Eng.*, 30(13), 1580–1585.

Agarwala, S., and Prabhu, K. N. (2018). "Assessment of Solidification Parameters of Salts and Metals for Thermal Energy Storage Applications Using IHCP-Energy Balance Combined Technique." *Trans. Indian Inst. Met.*, 71(11), 2677–2680.

Agarwala, S., and Prabhu, K. N. (2020). "An experimental approach based on inverse heat conduction analysis for thermal characterization of phase change materials." *Thermochim. Acta*, 685(February), 178540.

Agarwala, S., and Prabhu, K. N. (2021). "A Quantitative Approach for Thermal Characterization of Phase Change Materials." 10, 166–172.

Agarwala, S., and Prabhu, N. K. (2019). "Characterization of metals and salts-based thermal energy storage materials using energy balance method." *Heat Transf. - Asian Res.*, 48(5), 1889–1898.

Alva, G., Lin, Y., and Fang, G. (2018). "An overview of thermal energy storage systems." *Energy*.

Andreu-Cabedo, P., Mondragon, R., Hernandez, L., Martinez-Cuenca, R., Cabedo, L., and Julia, J. (2014). "Increment of specific heat capacity of solar salt with SiO2 nanoparticles." *Nanoscale Res. Lett.*, 9(1), 582.

Badenhorst, H., and Cabeza, L. F. (2017). "Critical analysis of the T-history method: A fundamental approach." *Thermochim. Acta*, 650, 95–105.

Barlow, J. O., and Stefanescu, D. M. (2002). *Computer-Aided Cooling Curve Analysis Revisited*.

Barreneche, C., Solé, A., Miró, L., Martorell, I., Fernández, A. I., and Cabeza, L. F. (2013). "Study on differential scanning calorimetry analysis with two operation modes and organic and inorganic phase change material (PCM)." *Thermochim. Acta*, 553, 23–26.

Bauer, T., Odenthal, C., and Bonk, A. (2021). "Molten Salt Storage for Power Generation." *Chemie-Ingenieur-Technik*.

Bauer, T., Tamme, R., Christ, M., and Öttinger, O. (2006). "PCM-Graphite Composites for High Temperature Thermal Energy Storage." *ECOSTOCK, 10th Int. Conf. Therm. Energy Storage*, (June), 19.

Cáceres, G., Fullenkamp, K., Montané, M., Naplocha, K., and Dmitruk, A. (2017). "Encapsulated nitrates phase change material selection for use as thermal storage and heat transfer materials at high temperature in concentrated solar power plants." *Energies*.

Carlson, K. D., and Beckermann, C. (2012). "Determination of solid fraction-temperature relation and latent heat using full scale casting experiments: Application to corrosion resistant steels and nickel based alloys." *Int. J. Cast Met. Res.*, 25(2), 75–92.

Chieruzzi, M., Cerritelli, G. F., Miliozzi, A., and Kenny, J. M. (2013). "Effect of nanoparticles on heat capacity of nanofluids based on molten salts as PCM for thermal energy storage." *Nanoscale Res. Lett.*, 8(1), 448.

Chieruzzi, M., Miliozzi, A., Crescenzi, T., Torre, L., and Kenny, J. M. (2015). "A New Phase Change Material Based on Potassium Nitrate with Silica and Alumina Nanoparticles for Thermal Energy Storage." *Nanoscale Res. Lett.*, 10(1), 273.

Coscia, K., Oztekin, A., and Mohapatra, S. (2011). "Imece2011-6 4465." 1–6.

Djurdjevic, M. B., Odanovic, Z., and Talijan, N. (2011). "Characterization of the solidification path of AlSi5Cu(1-4 wt.%) alloys using cooling curve analysis." *Jom*, 63(11), 51–57.

E. Günther, S. Hiebler, H. M. (2004). "Function of Temperature." *Bavar. Cent. Appl. Energy Res. (ZAE Bayern)*, 1–7.

Farid, M. M., Khudhair, A. M., Razack, S. A. K., and Al-Hallaj, S. (2004). "A review on phase change energy storage: Materials and applications." *Energy Convers. Manag.*, 45(9–10), 1597–1615.

Fernández, A. G., Ushak, S., Galleguillos, H., and Pérez, F. J. (2014). "Development of new molten salts with LiNO3 and Ca(NO3)2 for energy storage in CSP plants." *Appl.*

Energy, 119(3), 131–140.

Ferrer, G., Barreneche, C., Solé, A., Martorell, I., and Cabeza, L. F. (2017). "New proposed methodology for specific heat capacity determination of materials for thermal energy storage (TES) by DSC." *J. Energy Storage*, 11, 1–6.

Fras, E., Kapturkiewicz, W., Burbielko, A., and Lopez, H. F. (1993). "A new concept in thermal analysis of castings." 101(January), 505–511.

Frazzica, A., and Cabeza, L. F. (2019). *Recent Advancements in Materials and Systems for Thermal Energy Storage — An Introduction to Experimental Characterization Methods*. Springer International Publishing.

Gao, J. W., Zheng, R. T., Ohtani, H., Zhu, D. S., and Chen, G. (2009). "Experimental Investigation of Heat Conduction Mechanisms in Nanofluids . Clue on Clustering." 1–5.

Ge, Z., Ye, F., Cao, H., Leng, G., Qin, Y., and Ding, Y. (2014). "Carbonate-salt-based composite materials for medium- and high-temperature thermal energy storage." *Particuology*, 15, 77–81.

Gibbs, J. W., and Mendez, P. F. (2008). "Solid fraction measurement using equation-based cooling curve analysis." *Scr. Mater.*

Glatzmaier, G. (2011). "Summary Report for Concentrating Solar Power Thermal Storage Workshop: New Concepts and Materials for Thermal Energy Storage and Heat-Transfer Fluids, May 20, 2011." *Natl. Renew. Energy Lab.*, (May 2011).

González-Rivera, C., Amaro-Villeda, A., and Ramírez-Argáez, M. (2017). "Conference Paper Cooling Curve Analysis Method using a Simplified Energy Balance." 2018.

Günther, E., Hiebler, S., Mehling, H., and Redlich, R. (2009). "Enthalpy of phase change materials as a function of temperature: Required accuracy and suitable measurement methods." *Int. J. Thermophys.*, 30(4), 1257–1269.

Hamdy, E., Ebrahim, S., Abulfotuh, F., and Soliman, M. (2017). "Effect of multi-walled carbon nanotubes on thermal properties of nitrate molten salts." *Proc. 2016 Int. Renew. Sustain. Energy Conf. IRSEC 2016*, 317–320.

Hentschke, R. (2016). "On the specific heat capacity enhancement in nanofluids." *Nanoscale Res. Lett.*, 11(1), 88.

Herrmann, U., Kelly, B., and Price, H. (2004). "Two-tank molten salt storage for parabolic trough solar power plants." *Energy*, 29(5–6), 883–893.

Hoshi, A., Mills, D. R., Bittar, A., and Saitoh, T. S. (2005). "Screening of high melting point phase change materials (PCM) in solar thermal concentrating technology based on CLFR." *Sol. Energy*, 79(3), 332–339.

Huang, Z., Gao, X., Xu, T., Fang, Y., and Zhang, Z. (2014). "Thermal property measurement and heat storage analysis of LiNO3/KCl - expanded graphite composite phase change material." *Appl. Energy*, 115, 265–271.

Ihsan-ul-haq, Shin, J.-S., and Lee, Z.-H. (2004). "Computer-aided cooling curve analysis of A356 aluminum alloy." *Met. Mater. Int.*, 10(1), 89–96.

Jansone, D., Dzikevics, M., and Veidenbergs, I. (2018). "Determination of thermophysical properties of phase change materials using T-History method." *Energy Procedia*, 147, 488–494.

Jin, Z., Tian, Y., Xu, X., Cui, H., Tang, W., Yun, Y., and Sun, G. (2018). "Experimental Investigation on Graphene Oxide/SrCl2·6H2O Modified CaCl2·6H2O and the Resulting Thermal Performances." *Materials (Basel).*, 11(9), 1507.

Jo, B., and Banerjee, D. (2015). "Enhanced specific heat capacity of molten salt-based carbon nanotubes nanomaterials." *J. Heat Transfer*, 137(9), 1–7.

Kant, K., Shukla, A., Sharma, A., and Henry Biwole, P. (2017). "Heat transfer study of phase change materials with graphene nano particle for thermal energy storage." *Sol. Energy*, 146, 453–463.

Kardam, A., Narayanan, S. S., Bhardwaj, N., Madhwal, D., Shukla, P., Verma, A., and Jain, V. K. (2015). "Ultrafast thermal charging of inorganic nano-phase change material composites for solar thermal energy storage." *RSC Adv.*, 5(70), 56541–56548.

Kaviarasu, C., and Prakash, D. (2016). "Review on phase change materials with nanoparticle in engineering applications." *J. Eng. Sci. Technol. Rev.*, 9(4), 26–386.

Kenisarin, M. M. (2010). "High-temperature phase change materials for thermal energy storage." *Renew. Sustain. Energy Rev.*, 14(3), 955–970.

Khanafer, K., Tavakkoli, F., Vafai, K., and AlAmiri, A. (2015). "A critical investigation of the anomalous behavior of molten salt-based nanofluids." *Int. Commun. Heat Mass Transf.*, 69, 51–58.

Kibria, M. A., Anisur, M. R., Mahfuz, M. H., Saidur, R., and Metselaar, I. H. S. C. (2015). "A review on thermophysical properties of nanoparticle dispersed phase change materials." *Energy Convers. Manag.*, 95, 69–89.

Laing, D., Bahl, C., Bauer, T., Lehmann, D., and Steinmann, W. D. (2011). "Thermal energy storage for direct steam generation." *Sol. Energy*, 85(4), 627–633.

Lasfargues, M., Bell, A., and Ding, Y. (2016). "In situ production of titanium dioxide nanoparticles in molten salt phase for thermal energy storage and heat-transfer fluid applications." *J. Nanoparticle Res.*, 18(6), 1–11.

Lasfargues, M., Geng, Q., Cao, H., and Ding, Y. (2015). "Mechanical dispersion of nanoparticles and its effect on the specific heat capacity of impure binary nitrate salt mixtures." *Nanomaterials*, 5(3), 1136–1146.

Liao, Z., Li, X., Wang, Z., Chang, C., and Xu, C. (2014). "Phase change of molten salt during the cold filling of a receiver tube." *Sol. Energy*, 101, 254–264.

Lin, Y., Alva, G., and Fang, G. (2018). "Review on thermal performances and applications of thermal energy storage systems with inorganic phase change materials." *Energy*, 165, 685–708.

Liu, M., Belusko, M., Steven Tay, N. H., and Bruno, F. (2014). "Impact of the heat transfer fluid in a flat plate phase change thermal storage unit for concentrated solar tower plants." *Sol. Energy*, 101, 220–231.

Liu, M., Gomez, J. C., Turchi, C. S., Tay, N. H. S., Saman, W., and Bruno, F. (2015). "Determination of thermo-physical properties and stability testing of high-temperature phase-change materials for CSP applications." *Sol. Energy Mater. Sol. Cells*, 139, 81–87.

Liu, M., Steven Tay, N. H., Bell, S., Belusko, M., Jacob, R., Will, G., Saman, W., and

Bruno, F. (2016). "Review on concentrating solar power plants and new developments in high temperature thermal energy storage technologies." *Renew. Sustain. Energy Rev.*, 53(October), 1411–1432.

Malekan, M., and Shabestari, S. G. (2011). "Computer-aided cooling curve thermal analysis used to predict the quality of aluminum alloys." *J. Therm. Anal. Calorim.*, 103(2), 453–458.

Marín, J. M., Zalba, B., Cabeza, L. F., and Mehling, H. (2003). "Determination of enthalpy-temperature curves of phase change materials with the temperature-history method: Improvement to temperature dependent properties." *Meas. Sci. Technol.*, 14(2), 184–189.

Mehling, H., and Cabeza, L. F. (2008). *Heat and cold storage with PCM*. *Heat cold storage with PCM*.

Michels, H., and Pitz-Paal, R. (2007). "Cascaded latent heat storage for parabolic trough solar power plants." *Sol. Energy*, 81(6), 829–837.

Mohammad, R., and Saeed, R. (2016). "Scholars' Mine Thermal characterization of phase change materials for thermal energy storage."

Mondragón, R., Juliá, J. E., Cabedo, L., and Navarrete, N. (2018). "On the relationship between the specific heat enhancement of salt-based nanofluids and the ionic exchange capacity of nanoparticles." *Sci. Rep.*, 8(1).

Morisson, V., Rady, M., Palomo, E., and Arquis, E. (2008). "Thermal energy storage systems for electricity production using solar energy direct steam generation technology." *Chem. Eng. Process. Process Intensif.*, 47(3), 499–507.

Munyalo, J. M., Zhang, X., and Xu, X. (2018). "Experimental investigation on supercooling, thermal conductivity and stability of nanofluid based composite phase change material." *J. Energy Storage*, 17, 47–55.

Myers, P. D., Alam, T. E., Kamal, R., Goswami, D. Y., and Stefanakos, E. (2016). "Nitrate salts doped with CuO nanoparticles for thermal energy storage with improved heat transfer." *Appl. Energy*, 165, 225–233.

Oh, A. S. H., Kauffmann, Y., Scheu, C., Kaplan, W. D., and Rühle, M. (2016). "Ordered

Liquid Aluminum at the Interface with Sapphire Published by : American Association for the Advancement of Science Stable URL : http://www.jstor.org/stable/3842710 Linked references are available on JSTOR for this article : Stem-Cell Homeostasis an." 310(5748), 661–663.

Palkowski, H., and Günther, L. (2005). "Association of Metallurgical Engineers Serbia and Montenegro." *Metal. 11*, 3, 215–224.

Paola, M. G. De, Arcuri, N., Calabrò, V., and Simone, M. De. (2017). "Thermal and stability investigation of phase change material dispersions for thermal energy storage by T-history and optical methods." *Energies*, 10(3).

Pedrosa, F., Marcelo, T., Nogueira, C. A., Gomes, A., and Diamantino, T. (2018). "Molten nitrate salts containing lithium as thermal energy storage media: A short review." *ECOS 2018 - Proc. 31st Int. Conf. Effic. Cost, Optim. Simul. Environ. Impact Energy Syst.*

Peng, Q., Ding, J., Yang, X., Wei, X., and Yang, J. (2009). "Performance of Molten Salts Phase Change Materials." *… ISES World Congr. 2007 (Vol. I …*, (135), 1–5.

Pielichowska, K., and Pielichowski, K. (2014). "Phase change materials for thermal energy storage." *Prog. Mater. Sci.*, 65, 67–123.

Prabhu, K. N., and Ashish, A. A. (2002). "Inverse modeling of heat transfer with application to solidification and quenching." *Mater. Manuf. Process.*, 469–481.

Raam Dheep, G., and Sreekumar, A. (2014). "Influence of nanomaterials on properties of latent heat solar thermal energy storage materials - A review." *Energy Convers. Manag.*, 83, 133–148.

Rathod, M. K., and Banerjee, J. (2013). "Thermal stability of phase change materials used in latent heat energy storage systems: A review." *Renew. Sustain. Energy Rev.*, 18, 246–258.

Riazi, H., Mesgari, S., Ahmed, N. A., and Taylor, R. A. (2016). "The effect of nanoparticle morphology on the specific heat of nanosalts." *Int. J. Heat Mass Transf.*, 94, 254–261.

Rizvi, S. M. M., and Shin, D. (2020). "Mechanism of heat capacity enhancement in molten salt nanofluids." *Int. J. Heat Mass Transf.*, 161.

Roget, F., Favotto, C., and Rogez, J. (2013a). "Study of the KNO3-LiNO3 and KNO3-NaNO3-LiNO3 eutectics as phase change materials for thermal storage in a low-temperature solar power plant." *Sol. Energy*, 95, 155–169.

Roget, F., Favotto, C., and Rogez, J. (2013b). "Study of the KNO3-LiNO3and KNO3-NaNO3-LiNO3eutectics as phase change materials for thermal storage in a low-temperature solar power plant." *Sol. Energy*.

Romanin, V. D., and Fereres, S. (2017). "Based Carbon Nanotube Suspensions Used As Phase Change." 1–5.

Sarbu, I., and Sebarchievici, C. (2018). "A comprehensive review of thermal energy storage." *Sustain.*, 10(1).

Seo, J., and Shin, D. (2014). "Enhancement of specific heat of ternary nitrate (LiNO3-NaNO3-KNO3) salt by doping with SiO2 nanoparticles for solar thermal energy storage." *Micro Nano Lett.*, 9(11), 817–820.

Shaikh, S., Lafdi, K., and Hallinan, K. (2008). "Carbon nanoadditives to enhance latent energy storage of phase change materials." *J. Appl. Phys.*, 103(9).

Sharma, A., Tyagi, V. V., Chen, C. R., and Buddhi, D. (2009). "Review on thermal energy storage with phase change materials and applications." *Renew. Sustain. Energy Rev.*, 13(2), 318–345.

Shin, D., and Banerjee, D. (2010). *Effects of silica nanoparticles on enhancing the specific heat capacity of carbonate salt eutectic (work in progress). Int. J. Struct. Chang. SOLIDS-Mechanics Appl.*

Shin, D., and Banerjee, D. (2011a). "Enhanced Specific Heat of Silica Nanofluid." *J. Heat Transfer*.

Shin, D., and Banerjee, D. (2011b). *AJTEC2011-44375 EXPERIMENTAL INVESTIGATION OF MOLTEN SALT NANOFLUID FOR SOLAR THERMAL ENERGY APPLICATION*.

Shin, D., and Banerjee, D. (2014). "Specific heat of nanofluids synthesized by dispersing alumina nanoparticles in alkali salt eutectic." *Int. J. Heat Mass Transf.*, 74, 210–214.

Shin, D., Jo, B., Kwak, H., and Banerjee, D. (2010). "Investigation of High Temperature Nanofluids for Solar Thermal Power Conversion and Storage Applications." *2010 14th Int. Heat Transf. Conf. Vol. 7*.

Shin, D., Tiznobaik, H., and Banerjee, D. (2014). "Specific heat mechanism of molten salt nanofluids." *Appl. Phys. Lett.*, 104(12).

Shukla, A., Buddhi, D., and Sawhney, R. L. (2008). "Thermal cycling test of few selected inorganic and organic phase change materials." *Renew. Energy*, 33(12), 2606–2614.

Shukla, J. P. (2018). "Mechanical Engineering Department at Birla Vishwakarma Mahavidyalaya, Vallabh Vidyanagar, Gujarat (India)." *Int. J. Glob. Energy Issues*, 41(2003), 108–127.

Solé, A., Miró, L., Barreneche, C., Martorell, I., and Cabeza, L. F. (2013). "Review of the T-history method to determine thermophysical properties of phase change materials (PCM)." *Renew. Sustain. Energy Rev.*, 26(Supplement C), 425–436.

Stefanescu, D. M. (2015). "Thermal analysis-theory and applications in metalcasting." *Int. J. Met.*, 9(1), 7–22.

Sudheer, R., and Prabhu, K. N. (2015). "Characterization of Metal-PCMs for Thermal Energy Storage Applications." *Mater. Sci. Forum*, 830–831, 505–508.

Sudheer, R., and Prabhu, K. N. (2016). "A Computer Aided Cooling Curve Analysis method to study phase change materials for thermal energy storage applications." *Mater. Des.*, 95, 198–203.

Sudheer, R., and Prabhu, K. N. (2017a). "Cooling Curve Analysis of Micro- and Nanographite Particle-Embedded Salt-PCMs for Thermal Energy Storage Applications." *J. Mater. Eng. Perform.*, 26(Ref 4), 4040–4045.

Sudheer, R., and Prabhu, K. N. (2017b). "Cooling Curve Analysis of Micro- and Nanographite Particle-Embedded Salt-PCMs for Thermal Energy Storage Applications." *J. Mater. Eng. Perform.*, 26(Ref 4), 4040–4045.

Tan, Z. C., Wang, L., and Shi, Q. (2009). "Study of Heat capacity enhancement in some nanostructured materials." *Pure Appl. Chem.*, 81(10), 1871–1880.

Tao, Y. B., Lin, C. H., and He, Y. L. (2015). "Preparation and thermal properties characterization of carbonate salt/carbon nanomaterial composite phase change material." *Energy Convers. Manag.*, 97, 103–110.

Thakare, K. A., and Bhave, A. . (2015). "Review on Latent Heat Storage and Problems Associated With Phase Change Materials." *IJRET Int. J. Res. Eng. Technol.*, 04(10), 2319–1163.

Tian, H., Wang, W., Ding, J., Wei, X., and Huang, C. (2016). "Preparation of binary eutectic chloride/expanded graphite as high-temperature thermal energy storage materials." *Sol. Energy Mater. Sol. Cells*, 149, 187–194.

Tian, H., Wang, W., Ding, J., Wei, X., Song, M., and Yang, J. (2015). "Thermal conductivities and characteristics of ternary eutectic chloride/expanded graphite thermal energy storage composites." *Appl. Energy*, 148, 87–92.

Tiznobaik, H., Banerjee, D., and Shin, D. (2015). "Effect of formation of 'long range' secondary dendritic nanostructures in molten salt nanofluids on the values of specific heat capacity." *Int. J. Heat Mass Transf.*, 91, 342–346.

Tiznobaik, H., and Shin, D. (2013a). "Enhanced specific heat capacity of high-temperature molten salt-based nanofluids." *Int. J. Heat Mass Transf.*, 57(2), 542–548.

Tiznobaik, H., and Shin, D. (2013b). "Experimental validation of enhanced heat capacity of ionic liquid-based nanomaterial." *Appl. Phys. Lett.*

Tooklang, P., Vaivudh, S., Sukchai, S., and Rakwichian, W. (2014). "Thermal Distribution Performance of NPCM: NaCl, NaNO<sub>3</sub> and KNO<sub>3</sub> in the Thermal Storage System." *Energy Power Eng.*, 06(07), 174–185.

Wang, B. X., Zhou, L. P., and Peng, X. F. (2006). "Surface and size effects on the specific heat capacity of nanoparticles." *Int. J. Thermophys.*, 27(1), 139–151.

Wei, G., Wang, G., Xu, C., Ju, X., Xing, L., Du, X., and Yang, Y. (2018). "Selection principles and thermophysical properties of high temperature phase change materials for thermal energy storage: A review." *Renew. Sustain. Energy Rev.*, 81(May), 1771–1786.

Wong-Pinto, L.-S., Milian, Y., and Ushak, S. (2020). "Progress on use of nanoparticles in salt hydrates as phase change materials." *Renew. Sustain. Energy Rev.*, 122, 109727.

Wu, T., Xie, N., Niu, J., Luo, J., Gao, X., fang, Y., and Zhang, Z. (2020). "Preparation of a low-temperature nanofluid phase change material: MgCl2–H2O eutectic salt solution system with multi-walled carbon nanotubes (MWCNTs)." *Int. J. Refrig.*, 113, 136–144.

Wu, Y., Li, J., Wang, M., Wang, H., Zhong, Y., Zhao, Y., Wei, M., and Li, Y. (2018). "Solar salt doped by MWCNTs as a promising high thermal conductivity material for CSP." *RSC Adv.*, 8(34), 19251–19260.

Xiao, J., Huang, J., Zhu, P., Wang, C., and Li, X. (2014). "Preparation, characterization and thermal properties of binary nitrate salts/expanded graphite as composite phase change material." *Thermochim. Acta*, 587, 52–58.

Xiao, X., Zhang, P., and Li, M. (2013). "Thermal characterization of nitrates and nitrates/expanded graphite mixture phase change materials for solar energy storage." *Energy Convers. Manag.*, 73, 86–94.

Xiao, X., Zhang, P., and Li, M. (2015). "Experimental and numerical study of heat transfer performance of nitrate/expanded graphite composite PCM for solar energy storage." *Energy Convers. Manag.*, 105, 272–284.

Xie, Q., Zhu, Q., and Li, Y. (2016). "Thermal Storage Properties of Molten Nitrate Salt-Based Nanofluids with Graphene Nanoplatelets." *Nanoscale Res. Lett.*, 11(1), 306.

Yang, L., Huang, J. nan, and Zhou, F. (2020). "Thermophysical properties and applications of nano-enhanced PCMs: An update review." *Energy Convers. Manag.*, 214(March), 112876.

Ye, F., Ge, Z., Ding, Y., and Yang, J. (2014). "Multi-walled carbon nanotubes added to Na2CO3/MgO composites for thermal energy storage." *Particuology*, 15, 56–60.

Yinping, Z., Yi, J., and Yi, J. (1999). "A simple method, the -history method, of determining the heat of fusion, specific heat and thermal conductivity of phase-change materials." *Meas. Sci. Technol.*, 10(3), 201–205.

Zalba, B., Marín, J. M., Cabeza, L. F., and Mehling, H. (2003). *Review on thermal energy*

storage with phase change: Materials, heat transfer analysis and applications. Appl. Therm. Eng.

Zhang, L. di, Chen, X., Wu, Y. ting, Lu, Y. wei, and Ma, C. fang. (2016). "Effect of nanoparticle dispersion on enhancing the specific heat capacity of quaternary nitrate for solar thermal energy storage application." *Sol. Energy Mater. Sol. Cells*, 157, 808–813.

Zhang, L., Reilly, C., Li, L., Cockcroft, S., and Yao, L. (2014). "Development of an inverse heat conduction model and its application to determination of heat transfer coefficient during casting solidification." *Heat Mass Transf. und Stoffuebertragung*, 50(7), 945–955.

Zhao, C. Y., Ji, Y., and Xu, Z. (2015). "Investigation of the Ca(NO3)2–NaNO3 mixture for latent heat storage." *Sol. Energy Mater. Sol. Cells*, 140, 281–288.

Zhong, L., Zhang, X., Luan, Y., Wang, G., Feng, Y., and Feng, D. (2014). "Preparation and thermal properties of porous heterogeneous composite phase change materials based on molten salts/expanded graphite." *Sol. Energy*, 107, 63–73.

Zhou, D., and Eames, P. (2016). "Thermal characterisation of binary sodium/lithium nitrate salts for latent heat storage at medium temperatures." *Sol. Energy Mater. Sol. Cells*, 157(3), 1019–1025.

Zhou, S. Q., and Ni, R. (2008). "Measurement of the specific heat capacity of water-based Al2O3 nanofluid." *Appl. Phys. Lett.*, 92(9), 093123.

LIST OF PUBLICATIONS

Journal Publications (Based on Ph.D. work)

1. Agarwala, S., and Prabhu, K. N. (2018). "Assessment of Solidification Parameters of Salts and Metals for Thermal Energy Storage Applications Using IHCP-Energy Balance Combined Technique." Trans. Indian Inst. Met., 71(11), 2677–2680. https://doi.org/10.1007/s12666-018-1407-8.

2. Agarwala, S., and Prabhu, N. K. (2019). "Characterization of metals and salts-based thermal energy storage materials using energy balance method." Heat Transf. - Asian Res., 48(5), 1889–1898. DOI: 10.1002/htj.21461

3. Agarwala, S., and Prabhu, K. N. (2020). "An experimental approach based on inverse heat conduction analysis for thermal characterization of phase change materials." Thermochim. Acta, 685(February), 178540. https://doi.org/10.1016/j.tca.2020.178540

4. Agarwala, S., and Prabhu, K. N. (2021). "A Quantitative Approach for Thermal Characterization of Phase Change Materials." 10, 166–172. DOI:10.1520/MPC20200031

This page is intentionally left blank

BIO-DATA

Name : SWATI AGARWALA

Date of Birth : 16-12-1987

Permanent Address : FF-3, Civil Township, Rourkela,

Dist.: Sundargarh, State: Odisha,769004 , India

Email : s.agarwala16@gmail.com

Academic qualifications and Work experience:

Bachelor of Technology (B.Tech) : Mechanical Engineering; (2010)

Odisha Engineering College, Bhubaneswar, Odisha.

Master of Technology (M.Tech) : Process Metallurgy; (2014)

National Institute of Technology, Karnataka.

Work Experience: Graduate Engineer Trainee (July 2010- July 2011), Ultratech Cement, Rawan, Raipur, Chattisgarh

Assistant Professor, (2014-2016)
Trident Academy of Technology, Bhubaneswar, Odisha